DIPLOMARBEIT

VERGLEICH VON QUENCHERSCHALTUNGEN UND SPADs

ausgeführt zum Zwecke der Erlangung des akademischen Grades eines

Diplom-Ingenieurs

eingereicht an der Technischen Universität Wien Fakultät für Elektrotechnik

und Informationstechnologie

am

Institute of Electrodynamics, Microwave and Circuit Engineering

unter der Leitung von

Univ.Prof. Dr.ing. Horst Zimmermann

Univ.Ass. Dipl.-Ing. Bernhard Steindl

durch

Samuel Gaspar

Mat. Nr.: 1428158

Wien, März 2018

Samuel Gaspar

TECHNISCHE UNIVERSITÄT WIEN

DIPLOMA THESIS

COMPARISON OF QUENCHING CIRCUITS AND SPADs

Institute: Institute of Electrodynamics, Microwave and Circuit Engineering

Supervisor: Univ.Prof. Dr.ing. Horst Zimmermann
Univ.Ass. Dipl.-Ing. Bernhard Steindl

Author: Samuel Gaspar
Mat. Nr. 1428158

Vienna, March 2018

Abstract

In the past years, there has been an increase of interest in the field of quantum information. Quantum objects, such as photons, are used to transfer or encode information in quantum information technologies. Single photon in the visible or near infrared range has extremely small energy, only around 10^{-19} J. To detect such a small amount of energy, detectors with high sensitivity need to be deployed. Initially, photomultiplier tubes have been used for this purpose, but new detectors and technologies emerged in the recent years, such as superconducting nanowires, frequency up-conversion, quantum-dot phototransistors and single photon avalanche diodes (SPADs). SPADs are probably the mostly used single photon detectors nowadays: they are reliable, offer great quantum efficiency, low dark count rate and high maximal counting rate. Si SPADs are used to detect photons in the visible or near infrared range and are more common, whereas SPADs fabricated from 3-5 semiconductors can be deployed for light detection in the telecommunication wavelength of 1.55 µm.

Detector device is, however, not the only component required for single photon light detection. These devices have to be connected to a quenching circuit that ceases the avalanche ignited by the photon and restores the bias voltage to ready the device for another detection. Some of the quenching circuit types are passive quenching circuits, passive quenching circuits with active reset and active quenching circuits, and these circuits can be integrated on a chip together with the SPAD, or produced from discrete components with discrete SPADs.

The choice of the detector type, circuit operating principle as well as the specific type of construction affect the performance of the device significantly. It is therefore of high importance to choose the right device and quenching circuit for the application to fulfil the required specifications.

In this work, two discrete Si SPADs from two different manufacturers will be compared together with 3 quenching circuits: two passive quenching circuits and one active. In the first chapter, most common detector types are introduced. Second chapter is dedicated to types of quenching circuits, both integrated and discrete. In the third chapter design and measurements of the SPADs and chosen circuits are presented and compared. Fourth chapter describes possible single photon detector applications.

Kurzfassung

In den letzten Jahren hat das Interesse auf dem Gebiet der Quanteninformation zugenommen. Quantenobjekte,wie Photonen werden verwendet, um Informationen in Quanteninformationstechnologien zu übertragen oder zu kodieren. Ein einzelnes Photon im sichtbaren oder nahen Infrarotbereich hat eine extrem kleine Energie von nur etwa 10-19 J. Um solch eine kleine Menge an Energie zu detektieren, müssen Detektoren mit hoher Empfindlichkeit eingesetzt werden. Für diesen Zweck wurden zunächst Photomultiplierröhren verwendet, aber in den letzten Jahren sind neue Detektoren und Technologien entstanden, wie supraleitende Nanodrähte, Frequenz-Up-Conversion, Quantenpunktphototransistoren und Einzelphoton-Lawinen-Dioden (SPADs). SPADs sind heutzutage wahrscheinlich die am häufigsten verwendeten Einzelphotonendetektoren: Sie sind zuverlässig, bieten eine große Quanteneffizienz, eine niedrige Dunkelzählrate und eine hohe maximale Zählrate. Si SPADs werden verwendet, um Photonen im sichtbaren oder nahen Infrarotbereich zu detektieren, wohingegen SPADs, die aus 3-5 Halbleitern hergestellt sind, zur Lichtdetektion in der Telekommunikationswellenlänge von 1,55 µm eingesetzt werden können.

Die SPAD ist jedoch nicht die einzige Komponente, die für die Detektion von Einzelphotonenlicht benötigt wird. Der gesamte Detektor besteht aus einer SPAD in Kombination mit einer Quencherschaltung, die die durch das Photon gezündete Lawine stoppt und die Vorspannung wiederherstellt. Das ist notwendig um die Vorrichtung für eine weitere Detektion sensitiv zu sein. Einige der Quencherschaltungsarten sind passive Quencherschaltungen, passive Quencherschaltungen mit aktiver Rücksetz und aktive Quencherschaltung. Diese Schaltungen können zusammen mit der SPAD auf einem Chip integriert oder aus diskreten Komponenten mit diskreten SPADs hergestellt werden.

Die Wahl des Detektortyps, des Schaltungsprinzips sowie der spezifischen Bauart beeinflusst die Leistungsfähigkeit des Gerätes erheblich. Um die erforderlichen Spezifikationen zu erfüllen, ist daher von großer Wichtigkeit die richtige Kombination aus SPAD und Quencherschaltung für die gewünschte Anwendung zu wählen.

In dieser Arbeit werden zwei diskrete Si SPADs von zwei verschiedenen Herstellern mit drei Quencherschaltungen verglichen: zwei passive Löschkreise und ein aktiver. Im ersten Kapitel werden die gebräuchlichsten Detektortypen vorgestellt. Das zweite Kapitel widmet sich den integrierten und diskreten Arten von Quencherschaltungen. Im dritten Kapitel werden Design und Messungen der

SPADs und ausgewählter Schaltungen vorgestellt und verglichen. Das vierte Kapitel beschreibt mögliche Anwendungen eines einzelnen Photonendetektors.

Acknowledgement

I would like to express my thanks to Univ.Prof. Mag.rer.nat. Dr.techn.Horst Zimmermann for allowing me to write this Diploma thesis at the Institute of Electrodynamics, Microwave and Circuit Engineering. I would also like to thank my colleagues from the institute, mainly Univ.Ass. Dipl.-Ing. Bernhard Steindl and Univ.Ass. Dipl.-Ing. Dr.techn. Michael Hofbauer for their support and help with the measurement setup.

Table of Contents

Abbreviations & Symbols

APD	avalanche photodiode
FET	Field effect transistor
Ge	Germanium
He	Helium
K	Kelvin
PMT	photomultiplier tube
PPLN	Periodically poled lithium niobite
QD	quantum dot
Si	Silicium
SNSPD	superconducting nanowire single-photon detector
SPAD	Single-photon Avalanche diode
V_E	Excess voltage
WDW	Wavelength-division multiplexer
η	detection efficiency
λ	wavelenght
τ_R	detector recovery time
In	Indium
Ga	Galium
As	Arsenic
P	Phosphorus
h	Planck's constant
υ	photon frequency
τ_D	detector dead time
C_D	SPAD junction capacitance
C_S	SPAD stray capacitance
Q_T	Total charge
T_{QD}	delay of active quenching
QRND	Quantum random number generator
Mb	Megabit
Kb	Kilobit
V_{BR}	breakdown voltage
IC	integrated circuit
MOS	metal oxide semiconductor
N-MOS	n-type metal oxide semiconductor
P-MOS	p-type metal oxide semiconductor

List of Figures

List of Tables

1. Single-photon detectors

1.1 Detector characteristics

Single- photon detector development has been driven mainly by the explosive growth of quantum information applications. They can be divided into two main groups [1]: detectors that can distinguish number of incoming photons and detectors that can be triggered by one or more photons but cannot identify their amount. In this work, the focus has been put on the latter. There is a number of attributes by which the detector can be characterized. Some of the most important ones are [2]:

Spectral range: Every photon counter is sensitive only for light with specific wavelength, which is determined by a detector material. For different applications different wavelengths are needed. For example, at a wavelength of 1,55 μm the losses are lowest in an optical fibre, so this wavelength is chosen for optical communication over long distances.

Detection efficiency (η): It is defined as a probability with which the photon that arrives to the detector is registered and counted. High η values are desired, however, it is not the only parameter that determines how many photons can be detected. Detection efficiency can be calculated as:

$$\eta = \frac{Number\ of\ photons\ sent}{Number\ of\ photons\ detected} \quad (1)$$

Dead time: It is the period of time after a successful photon absorption, during which the detector is unable to count any other photons. In many detectors the dead time value is given by the electronic circuits built around the detector, not the detector itself. This factor is limiting the highest count rate of the detector. Various techniques based on the detector type have been introduced to reduce this time interval.

Timing jitter: Every avalanche is a statistical process, which leads to different output waveforms of the SPAD for every photon detection. There will always be an uncertainty caused by various effects, for example the position of the carrier impact. Carriers that first have to diffuse to the depletion region will worsen the effect due to random delay introduced by the diffusion ([3]). Total uncertainty of the photon arrival time is called timing jitter. It is usually modelled as Gaussian curve together with the sum of a delta function and one or more exponential functions. The exponential functions represent the carriers which must diffuse to the depletion region, while the delta function models the carriers created directly in this region. The sum of these two components is the time

distribution for the carriers to reach the depletion region. The timing uncertainty is represented by the gaussian component and caused by the statistical nature of the ionization process [4].

Dark count rate (DCR): Ideally, the detector should not produce any current under dark conditions. In practice, carriers can be generated also by other mechanisms. Possible mechanisms that can generate a dark count are [5]: dark carriers primary injected or generated in the multiplication region during voltage pulse, dark carriers generated before the voltage pulse and dark carriers released from the traps that were captured during previous avalanche processes (afterpulse).

Afterpulsing probability (APP): During avalanche, carriers can be captured by the traps that allow energy levels close to energy bands [6]. After a delay time (usually below hundreds of nanoseconds at room temperature [7]), these carriers can be released and cause another output pulse. This imposes a limit on the dead time, as it cannot be too small, otherwise the APP will become very significant. Another factor that influences APP is the temperature- with lower temperature the trap lifetime increases. The biasing of the device can also have an impact on the afterpulsing, because with increasing bias voltage the probability that a trap will capture charge carrier rises.

Through these metrics, detectors can be compared and chosen according to the application.

1.2 Detector technologies

In this section, basic overview of the most frequently utilised sensing elements will be provided. In each case, performance, principle of operation, advantages and disadvantages will be discussed. These parameters will be summarized at the end of this chapter in Table 1-2. Figure of merit [2], will also be introduced to make the comparison easier.

1.2.1 Photomultiplier tubes

First photomultiplier tube was invented in 1930 by a Soviet-Russian physicist and engineer Kubetsky [8]. There are many commercially available on the market today and efforts are being made to improve these devices even further. PMT consists of a window, through which photons can enter the device, photocathode, focusing electronics, electron multipliers (dynodes) and an anode. Basic schematic picture of a photomultiplier tube is shown in Figure 1-1.

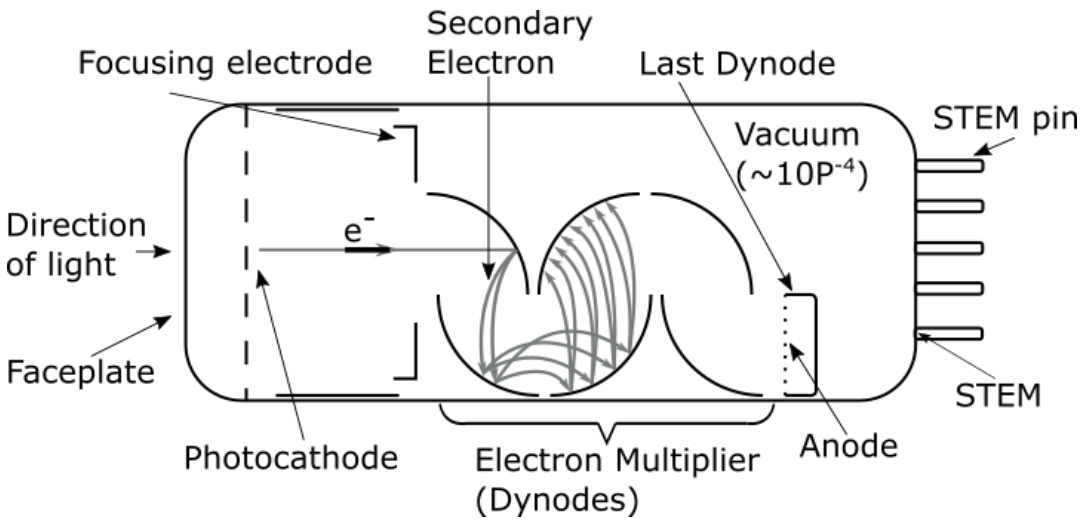

Figure 1-1 Schematic of a photomultiplier tube [9]

Light detection process in a PMT starts with light passing through the input window. External photoelectronic effect causes the light to excite electrons in the photocathode and they are emitted into the vacuum. Spectral range of a PMT is determined by the photocathode, namely the combination of metals used and the process of fabrication. Photocathodes are mostly made of semiconductors which contain alkali metals with low work functions. Emitted electrons are then focused on the focusing electrode and sent to the first dynode, where they knock more electrons out. This process is repeated on every subsequent dynode, creating a current multiplication up to 10^8. Efficiency of the photon to electron conversion in the device is also greatly influenced by the electrode configuration and shape. Finally, the anode collects the electrons emitted by the last dynode.

Active area of a PMT is considerably large (diameters bigger than 1 cm) and they cover a large spectral range (from 115 nm to 1,7 µm). They require very high operating voltages (up to 1 kV and higher). They are also quite fragile and expensive due to reliance on the vacuum technology. Another drawback is the sensitivity to EM fields. Maximum detection efficiency of PMTs operating at 500 nm with GaAsP photocathodes is around 40%, highest count rates reported are as high as 10 MHz with dark count rate only 100 Hz [10]. In [10], PMTs at wavelengths used for telecommunications are also available (InP/InGaAs photocathode cooled to ~ 200 K). However, the performance is very poor compared to PMTs operating at 0,5 µm (η= 2% at 1,55 µm and dark count rate = 200 kHz).

It should be mentioned that some PMT models have noise gain low enough to roughly recognise number of incoming photons by inspection of the output pulse [11]. Another mode of operation has been presented in [12], where bandgap of the photocathode material is higher than the energy of the incoming photons, so more than one photon is needed to generate an electron.

1.2.2 Superconducting nanowire single-photon detector

Superconducting nanowire single-photon detectors are capable of sensing light with visible to infrared wavelengths with good timing resolution, low dark counts and short recovery times. First demonstrated in 2001 by Gol'tsman *et al* [13], this device is based on niobium nitride nanowire. Superconducting energy gap is about hundred to thousand times lower than in normal semiconductors, resulting in an avalanche electron charge hundred to thousand times higher for the same absorbed photon energy. This is also the reason why detection in infrared wavelength range is possible.

The operating principle of SNSPDs can be described as follows: the niobium nitride nanowire is kept at the temperature lower than its critical temperature for superconductivity and biased at a current just below the specific current at which it becomes resistive. When a photon is absorbed, so called hotspot is created. This process can be seen in Figure 1-2:

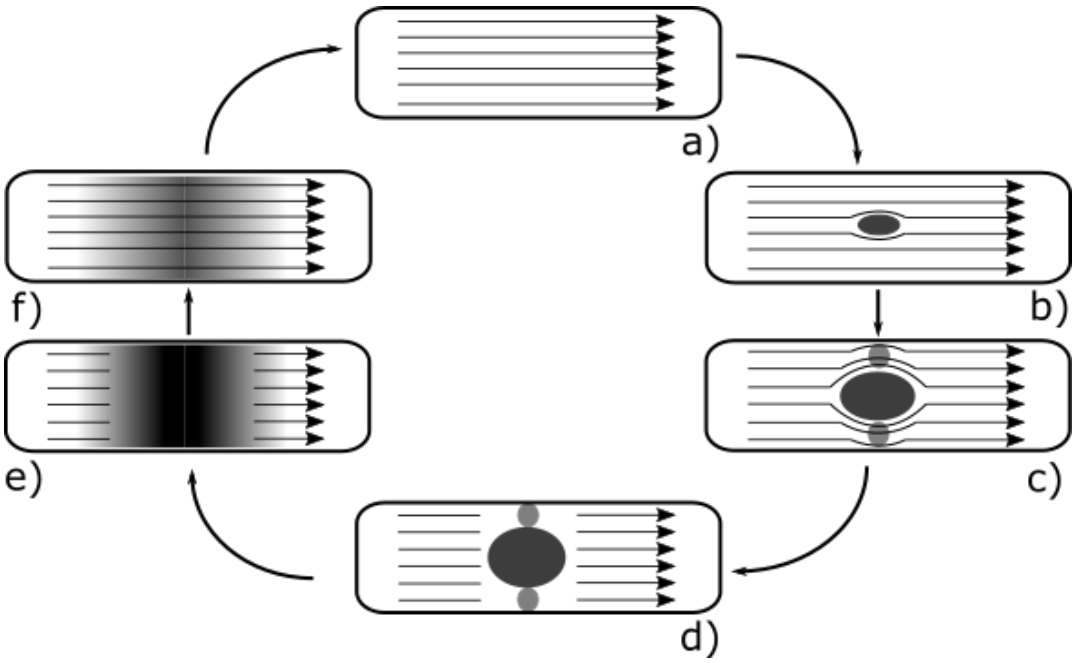

Figure 1-2 Hotspot creation process in SNSPD [14]: a) SNSPD is biased below the specific current for superconductivity loss and kept below the critical temperature. b) After photon absorption local resistive hotspot is created. c) hot electrons diffuse to the sides of the nanowire and the hotspot grows. This forces the current density on the edges to increase, because the current flowing through the nanowire is forced to the sides. d) If the current density at the edges exceeds critical current, barrier is formed across the whole device. e) Resistive barrier spreads across the nanowire through the Joule heating f) External electronic circuit is needed to reduce the bias current and the barrier is fading. a) The device is fully superconductive again.

Detection efficiency and dark count rate depend greatly on the biasing current. With biasing current approaching the critical current, dark count rate increases dramatically. Recently, optical waveguides were introduced to improve the coupling efficiency. At 1.55μ wavelength, η= 20%, timing jitter only 65 ps and dark count rate below 1 kHz have been reported [2].

1.2.3 Frequency up-conversion

The main principle of frequency up- conversion is to somehow reduce the frequency of incoming photon (usually telecommunications- wavelength), so it can be efficiently detected with available detectors. This approach has been demonstrated in [15]: periodically poled lithium niobate nonlinear crystal was used. Photons with λ= 1 548 nm have been converted in the crystal by a pumping signal of λ= 1 064 nm to photons with λ= 631nm with maximal input power P_{MAX}= 17 W. This arrangement is shown schematically in Figure 1-3. The conversion efficiency reached 93% with an uncertainty estimated to ± 3%, caused by the non-ideal calibration accuracy. Conversion efficiency increases with input power, theoretically 100% could be reached with sufficient power.

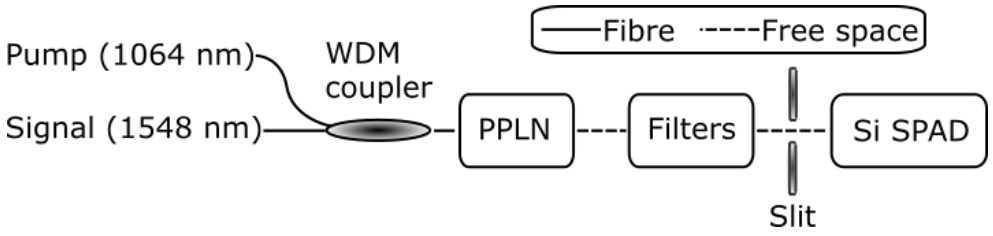

Figure 1-3 Schematic picture of a frequency up-conversion detector [2]

There are several disadvantages that come with frequency up-conversion- the nonlinear crystal has to be stabilized, which is a difficult task, and the coupling waveguides have high losses. They also exhibit large dark count rates due to the presence of nonlinear processes that cause fluorescence at the targeted wavelength.

Detection efficiencies of these detectors with Si SPADs (will be discussed later) used as detectors reaches 59% for photons with wavelength of 1,55 μm, 400 ps timing jitter and 20 kHz dark count rate [1].

1.2.4 Quantum-dot phototransistor

This device consists of an array of quantum dots between the conduction channel and a gate electrode in a field effect transistor. Quantum dots are embedded in a layer which absorbs light. When a photon is absorbed in this layer, it generates an electron. These photoelectrons move to the quantum dots where they are captured and produce a charge that acts against the gate potential, altering the conductance of the FET channel. Efficiency up to 68% with a counting rate of 400 kHz for photons with 805 nm have been reported [16].

Another approach utilising quantum dots for single photon detection relies on alternation of the tunnelling probability in a tunnel diode structure after a photon absorption in QD. [17] demonstrates that this principle can be used to detect photons with telecommunications wavelengths with efficiency of 12%, timing jitter 150ns and low dark count rates.

1.2.5 Avalanche photodiodes

Avalanche photodiode is a photodiode that consists of p-i-n layers biased such that the multiplication of carriers via impact ionization occurs. It is usually illuminated from the p+ side to obtain the best noise performance [18]. The thickness of the p+ layer is designed to ensure that most of the photogenerated carriers are produced within one diffusion length of the depletion region. Generated holes are collected at the p+ contact, while generated electrons diffuse to the depletion region. The high electric field in the depletion region provides acceleration for the electrons to energies at which they can cause impact ionization. However, this high electric field can produce tunnel breakdown, which vastly increases the dark current of the device [19].

Conventional avalanche photodiodes are biased close to the breakdown voltage, but still below it. In these devices, avalanche effect is used to produce pulses that are linearly amplified from the initial signal. An absorbed photon generates an electron-hole pair, where the hole is than accelerated by the electric field in the opposite direction of the primary electron and can generate another electron-hole pair. This effect greatly increases the fluctuation of multiplication value. As a result, the gain in APDs is lower than 1000 while keeping the statistical fluctuations at a reasonable level, as opposed to PMTs where the gain can be 10^6 and higher.

1.2.6 Single photon avalanche diodes

Single photon avalanche diodes were available for experimental usage from 1990s. However, the basic principle (avalanche phenomenon) was known much earlier, from 1960s [20]. Here, large voltage pulses were observed in a homogeneously designed p-n junction reversed biased higher than breakdown voltage after an absorption of a single photon. These devices performed very poorly as single photon detectors due to the quality of silicon technology at that time. Since then, immense progression has been made in this field, and today the avalanche photodiodes belong to the best single photon detectors commercially available.

Operation of a SPAD (device that can register single photons) is different from the one of a conventional avalanche photodiode (Figure 1-4).

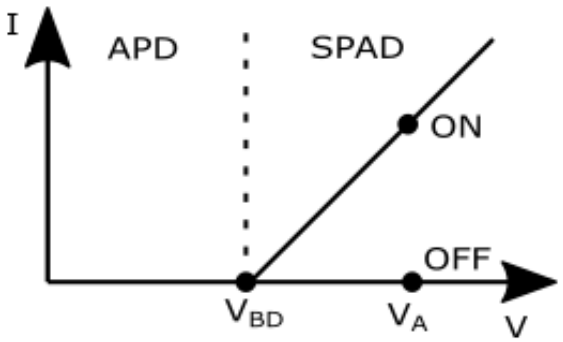

Figure 1-4 APD vs SPAD region of operation

The avalanche effect is exploited to acquire a device that is similar to a bi-stable circuit. In the initial state the SPAD is kept above the breakdown voltage and there is no current flowing through the device. The electric field in the depletion layer is very high, but there are no free charge carriers. When a photon is absorbed, photoelectron is generated and if it is injected into this region, it produces secondary electron-hole pairs, which in turn produce more electron-hole pairs and a self-sustained avalanche is ignited. In this state, the avalanche diode is switched on and the current (in the range of mA) flows through the device until the effect is quenched by external electronics- the voltage needs to be lowered below the breakdown voltage. From the time of an avalanche ignition to the restoration of the voltage above breakdown level after it has been quenched, the SPAD is insensitive to any other incoming photons.

Two different structures for a SPAD device fabricated in silicon technology are shown in Figure 1-5. Figure 1-5 a) depicts epitaxial planar SPAD developed by Lacaita *et al.* [21]. The p-n junction between

epistrate and substrate reduces the neutral region, limiting the timing jitter. Active area of the detector is defined by the upper p^+ region. Around this p^+ region, guard ring is formed by a lightly doped p implant to prevent edge breakdown. Lower highly doped p^+ layer reduces the resistance of the path to avalanche current. Diameter of the active area is between 10 and 50 µm. Typical breakdown voltage V_{BD} of this device is ~ 20V, detection efficiency is highest at around 0,5 µm (40 %) and declines to <0,1% at 1,064 µm. Detection efficiency can be improved with thicker depletion region; however, this also increases the breakdown voltage. Advantages of this structure are low dark count rates, low afterpulsing probability and high timing resolution. These devices have low power dissipation due to the low breakdown voltage and hence do not need to be cooled. The technology used to fabricate the planar epitaxial SPADs is compatible with the processing technology of integrated circuits. They can be manufactured on common Si wafers in high volumes at low cost.

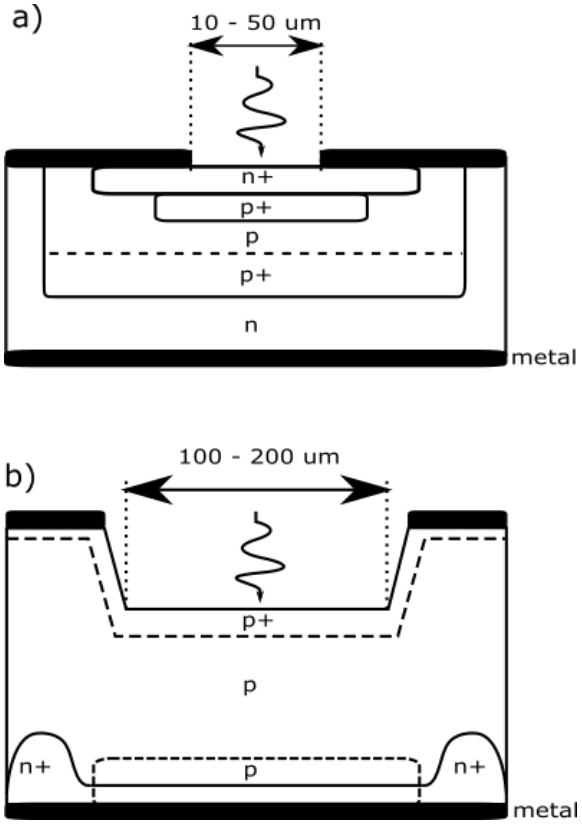

Figure 1-5 Cross-section of SPAD device structures fabricated from silicon

Figure 1-5 b) depicts a device produced by PerkinElmer Optoelectronics [22]. It is a reach-through SPAD structure built in highly resistive, ultrapure silicon wafers with special processing technology. Active area of these devices is much wider than the active area of planar SPADS- 200µm diameter and more. It is determined by the p^+ layer in the middlemost region and deep diffusion. The back of the wafer is then etched to ~ 30µm thickness. Here, the guard ring to prevent edge breakdown is formed by the diffusion of the n^+ layer. Resistive path to the avalanche current is quite low. Light enters the device

from the back side. Maximal electric field is at the p-n junction and decreases gradually, what causes the avalanche region to be fairly large. This makes the breakdown voltage to be much higher than in the case of planar SPADs. It ranges from 200 to 500 V and is variable from sample to sample. The depletion region is thick, resulting in high detection efficiency- more than 60% in the visible range (0,55 – 0,85 μm) and 3% at 1,064 μm. These devices offer low dark count rates, afterpulsing probability below 1% and acceptable timing jitter. Power dissipation of the reach-through SPADs is considerably high due to high breakdown voltages and effective cooling of the device is required. The need for special processing technology makes the costs high and the yield low. The driving circuitry cannot be fabricated in the same process, making the monolithic integration with the detector not possible. Comparison showing the main advantages and disadvantages of the two discussed structures can be seen in Table 1-1.

Thin Si- SPADs	Thick Si- SPADs
• Good photon detection efficiency	• Excellent photon detection efficiency
• Good photon timing resolution (tens of picoseconds)	• Photon timing resolution at hundreds of picoseconds
• Low dark count rate	• Low dark count rate
• Lower breakdown voltages -> low power consumption (no need for cooling)	• High breakdown voltage -> High power consumption (cooling necessary)
• Fabrication in planar technology, can be integrated with circuitry	• Fabrication in technology uncompatible with integrated circuitry
• Common Si substrate	• Special, ultrapure Si substrate
• Low production cost	• High production cost

Table 1-1 Comparison of Thick and Thin Si- SPAD detectors

As was previously mentioned, detecting light with wavelength longer than 1110 nm requires different materials than silicon, as the bandgap of silicon is only 1.11 eV. Mostly used are III-V semiconductors. Some germanium diodes have also been reported to work as SPADs. They are not specifically fabricated to work for single photon detection- they are produced as APDs and some of them with favourable characteristics can also be biased at voltage higher than the breakdown voltage [23]. Ge-SPADs have to be cooled to very low temperatures due to native dark count rate being very high. Afterpulsing rates are also high, caused by the high trap concentration, while the trap lifetimes at these temperatures are long (Figure 1-7). The selection of the excess breakdown voltage V_E is crucial because

an optimal trade-off between detection efficiency and dark count rate has to be chosen. Detection efficiency is highest at 1.3 µm.

For photon detection at 1550 nm, III-V semiconductors offer an optimal performance. An example is InGaAs with a bandgap of 0.73 eV. Separate-absorption-and-multiplication devices have been developed [24], where photons are absorbed in InGaAs region with low bandgap, but the multiplication takes place in InP layer (1.35 eV bandgap energy) with more suitable properties for avalanche effect. Devices with high breakdown voltage have to be selected, as it has to be higher than the so-called reach-through voltage (it is the voltage at which the depletion region is large enough to also include InGaAs layer). Reach-through voltage does not change significantly with temperature, whereas breakdown voltage does [24], so sufficient margin is needed. When the breakdown voltage drops below reach-through voltage, the device can no longer detect infra-red photons, because the photons absorbed in the InGaAs layer cannot be detected. Downside is that the traps are much more concentrated than in the Ge leading to significantly higher afterpulsing probability. As a result, gated detector operation is required. The hetero-barrier between the InGaAs and the InP limits the timing resolution due to random time delays. Figure 1-6 shows a separate-absorption-and-graded-multiplication (SAGM) structure. In SAGM devices, InGaAsP gradual layer has been added between the InGaAs and InP to make the differences between the bandgaps smaller and the barrier transition smoother.

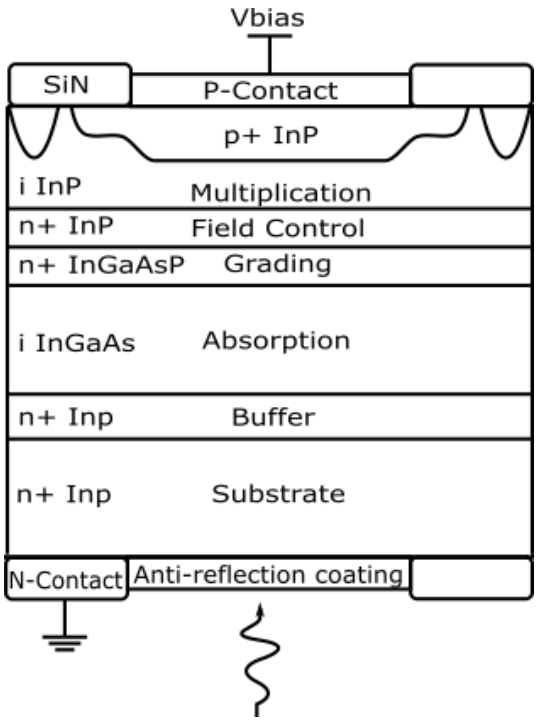

Figure 1-6 Schematic of an InGaAs/ InP SPAD structure with a graduated InGaAsP layer is added [25]

It is necessary that the p-n junction is of the highest quality, because any local defects in the material cause concentration of the electric field. The breakdown voltage in this area is lowered and the SPAD may produce an output pulse as soon as it is biased. It is clear that for an output pulse to be generated, charge carrier needs to be absorbed in the active zone of the SPAD and generate an electron-hole pair. This initial electron-hole pair also needs to successfully trigger an avalanche. The probability of avalanche triggering increases as the excess voltage V_E above Geiger threshold V_{BR} increases. With low V_E, this probability raises linearly and saturates at high excess voltages.

Dark count rate of a SPAD also increases with increasing V_E. This is caused by the elevated ignition probability and the higher electric field that augments the generation of charge carriers. With higher electric fields, tunnel effects may take place. Even a very small tunnel current in the range of fA represents generation of thousands of carriers per second that are able to trigger an avalanche. This effect sets the limit to reducing the dark count rate by lowering the temperature as it is unaffected when the device is cooled. SPAD noise is also enlarged by the impurities and defects in the crystal, as they are responsible for creation of generation-recombination centres in the middle of a silicon bandgap, as well as formation of energy levels near the bands (deep levels). These energy levels can act as carrier traps, in which carriers can be captured after an avalanche and then released, generating an afterpulse. As the trap level population is not saturated [25], it increases linearly with the avalanche current. This pulse current (charge) should be therefore kept as small as possible. This is another task for quenching circuit. This can be done by increasing the dead time of the circuit, rendering the SPAD unable to produce pulses for a longer period of time, which in turn reduces the counting frequency. Cooling the device has also negative impact on lifetime of the traps, as it increases exponentially.

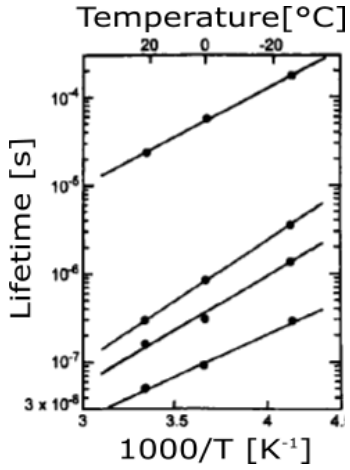

Figure 1-7 Trap lifetime versus temperature

As shown in the Figure 1-7, lifetime of the traps is increased by an order of magnitude when the temperature is reduced by ~ 40 K. As previously mentioned, this has to be compensated by the quenching circuit, increasing the dead time. SPADs that are designed to operate in the infrared

wavelength range have to be fabricated from semiconductor materials that have a smaller bandgap and hence have to be cooled to reduce the dark count rate. This severely decreases the maximum obtainable counting frequency.

Due to diverse physical effects the time delay from the photon absorption to output pulse generation (timing jitter) is not constant, but it is subjected to fluctuations. The cause of these fluctuations is depicted in Figure 1-8. The photons that are absorbed in the depletion region of the SPAD generate an electron in the region with high electric field and thus produce an avalanche effect almost instantly. However, some of the photons may by absorbed in the neutral region close to the depletion layer of the SPAD. Electrons generated by those photons need to diffuse to the depletion layer to be able to cause an avalanche [3]. This reduces the timing resolution. This is problematic for the light sources that are not monochromatic.

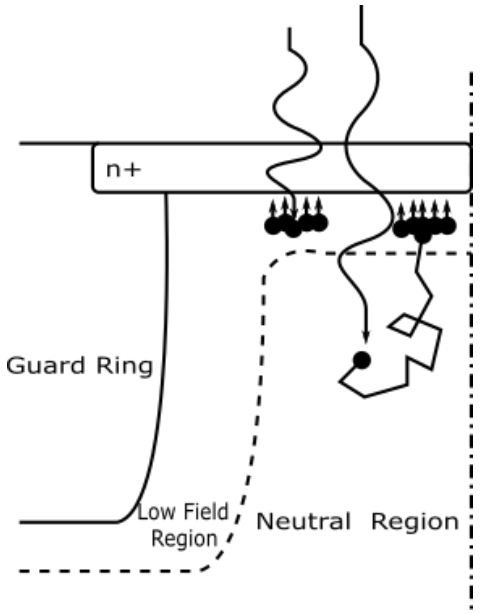

Figure 1-8 Schematic of the avalanche effect caused by an electron generated in the neutral region of the SPAD and an electron generated in the SPAD depletion layer nearby [3]

1.2.7 Comparison of single-photon detectors

In Table 1-2, most important single-photon detectors are compared base on the characteristics mentioned in 1.1. Additionally, to better compare the performance of these detectors, figure of merit should be introduced. Figure of merit that is most frequently quoted for photodetectors is the noise equivalent power (NEP) [26]:

$$\frac{hv}{\eta}\sqrt{2D} \quad (2)$$

where h is the Planck's constant, v is the photon frequency and D is the dark count rate. For a single-photon detector, measuring optical power does not make sense and timing jitter is also not involved. Therefore, new figure of merit has been provided that better suits the single-photon detectors [2]:

$$H = \frac{\eta}{(D\Delta t)} \quad (3)$$

The higher the H value, the better the detector in a specific wavelength range.

Detector type	Operating temperature [K]	Detection efficiency	Jitter time	Dark count rate [Hz]	Figure of merit	Maximal counting rate [Hz]	Work
PMT (visible-near-infrared	300	40% @ 500nm	300 ps	100	1.33 x 10^7	10 M	[27]
PMT (infrared)	300	2% @ 1.55 µm	300 ps	200 k	3.33 x 10^2	10 M	[28]
Si SPAD (thick)	250	65% @ 650 nm	400 ps	25	6.5 x 10^7	10 M	[29]
Si SPAD (thin)	250	49% @ 550 nm	35 ps	25	5.6 x 10^8	10 M	[30]
InGaAs SPAD (gated)	200	10 % @ 1.55 µm	370 ps	91	2.97 x 10^5	10 k	[31]
InGaAs SPAD (self-differencing)	240	10% @1.55 µm	55 ps	16 k	1.14 x 10^5	100 M	[32]
Frequency up-conversion	300	9% @ 1.55 µm	400 ps	13 k	1.7 x 10^4	10 M	[33]
Frequency up-conversion	300	2% @ 1.55 µm	40 ps	20 k	2.5 x 10^4	10 M	[33]

Table 1-2 Comparison of available single photon detectors [1]

1.3 Single-photon detector applications

Improvement of single-photon detectors has introduced many possible applications in the fields of quantum optics, medicine, environment, defence and aerospace. In this chapter, some examples will be provided to illustrate the potential of single- photon detectors.

1.3.1 Single-molecule fluorescence spectroscopy

With this powerful technique, individual behaviour of nanoscale molecules can be observed. It is therefore possible to study dynamic state changes directly, rather than averaging the behaviour of a molecular group. Single-photon detectors used for this purpose need to maximize the signal-to-noise ratio as well as very high quantum efficiency. The time information is of very high importance, which means that timing jitter has to be kept as small as possible.

Basic principle of operation has been described in [34]. Light emitting laser is used to excite molecule which is in resonance with the wavelength of the laser. As a result, photon is absorbed by the molecule and this absorption is detected. To achieve resonance of a single molecule, the laser is focused on a very small area and a very small concentration of the molecules of interest has to be used.

Molecules that absorb light from the laser emit secondary photons. These emitted photons represent the signal that should be detected. This signal is naturally much smaller than the signal emitted by the laser, which would make the detection very difficult. Fortunately, the photons emitted by the single molecule are usually shifted to longer wavelengths (which is caused by the energy loss between adsorption and emission). Emission process that is mostly common is shown in Figure 1-9. Optical transition $S_0 \rightarrow S_1$ with radiation energy is $h\upsilon$, where υ is the optical frequency. The transition from S_0 directly to S_1 does not need to take place, as the molecule excited to the higher sidebands by the photon relaxes quickly by emission of vibrational modes to the lowest excited state S_1. From this state, fluorescent photons can be emitted (depicted in the Figure 1-9 as dashed lines). After fluorescent emission, the molecule again quickly relaxes to the ground state through vibrations and phonon emissions.

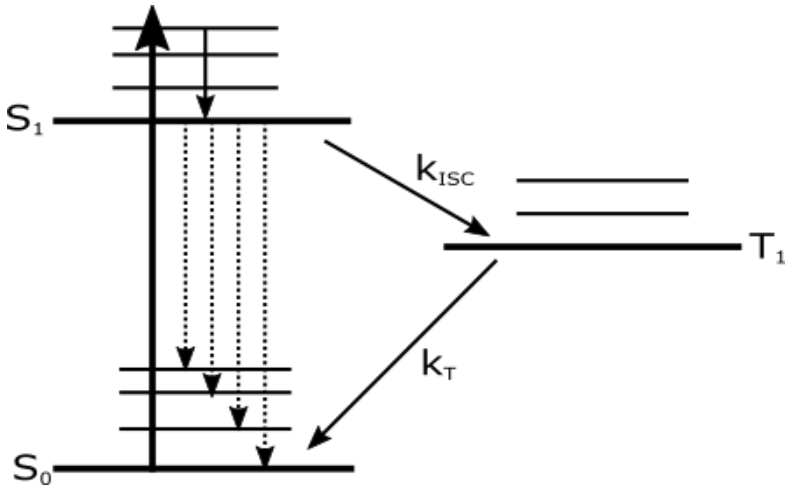

Figure 1-9 Band scheme for single-molecule emission

The probability P with which an incident photon will be absorbed by the molecule can be expressed as [34]:

$$P = \frac{\sigma_P}{A_{BEAM}}, \tag{4}$$

where σ_P is the area of the molecule which is able to capture photons from the laser beam and A_{BEAM} is the area of the laser beam cross section. σ_P is connected to the transition dipole moment and depends on the wavelength of the incoming light, spontaneous fluorescent rate and the width of the absorption frequency spectrum.

T_1 in the Figure 1-9 represents the lowest triplet state or an intermediate state- in this state, the molecule is no longer able to produce light, as both the absorption and emission cease for a time interval given by $1/k_T$. K_T is the rate with which the molecule decays from state T_1 to S_0 and k_{ISC} is the rate of the intersystem crossing (this is how the mechanism of molecule getting to T_1 is called). The performance of the device is mainly limited by the so-called background noise, which is caused by photons incident on the detector from all the other sources but the molecule itself. Another limit is caused by the dark count rate of the detector.

As was already mentioned, detectors for this kind of employment need to be able to detect single photon arrivals with very small dark noise and with very high quantum efficiency. Two classes of the photodetectors are able to fulfil these tasks: single element detectors and detector arrays.

Among single element detectors, photomultiplier tubes have been used at the start [35]. Dark noise level of these devices is quite small, but they have to be cooled. However, quantum efficiency of PMTs

is below 40 % for visible light (Table 1-2), which limits their use in quantum spectroscopy. However, detection area of PMTs can be very large (diameters bigger than 10 mm). PMTs have been recently replaced by SPADs, mainly in integrated packages with quenching circuits cooling and amplifiers. They offer far better performance regarding the dark counts and quantum efficiencies (Chapter 1). Their only disadvantage compared to PMTs, namely the smaller active area, is not so important in single-molecule spectroscopy and microscopy, because the size of the spot at microscope image can be made smaller than the active area of the detector chip [36].

An example of 32 x 32 array has been presented in [37]. 1024 independent SPAD detectors have been produced in CMOS technology. Variable-load quenching circuit has been integrated together with the detector for each of the 1024 pixels. Dead time of this device is only 50 ns, while dark count rate was reported below 4 kHz at V_E 5 V. However, with such a short dead time, afterpulsing probability reached 20 %. Optical setup used can be seen in Figure 1-10. Two lasers were used for the experiments, diode laser emitting at 0.976 µm (frequency doubled to 0.488 µm) and pulsed laser diode with a repetition rate of 50 MHz. The laser beam was multiplied 10x by the lens L_1 and L_2 forming a telescope. With the help of mirrors M_1, M_2 and periscope assembly (PA), the beam was guided to enter the illumination port at the back of the microscope. It was than focused again by the Lens L_3 and passed through diffractive optical element (DOE) and hence the 100 µm array consisting of 32 x 32 spots has been created. This diffractive optical element is a glass hologram created to diffract a single laser beam into 1024 parts under different angles. The SPAD camera was connected to the microscope by a side port. Images acquired from the camera were transferred to PC.

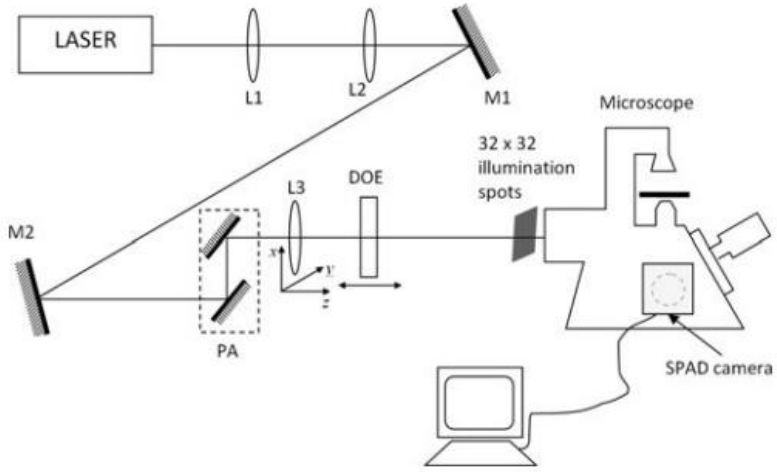

Figure 1-10 Schematic of the optical setup for multifocal microscopy

1.3.2 Quantum random-number generator

In classical physics, one can predict the outcome of a measurement almost definitely. On the contrary, in quantum physics no such thing is possible and only certain probabilities for the all possible outcomes of the measurement can be predicted. This fact can be exploited in quantum cryptography. It is based on a key sequence generation between two parties, transmitter and receiver. This key has to be secret, used only once and perfectly random. The key can be created by computer, however, computers are deterministic and use algorithms to produce random numbers. They apply mathematical formulas to develop random bits from a source. This source is usually unknown to a potential eavesdropper, but if the source is known, the random numbers can be predicted. As a result, the generation is not truly random. The only truly random number generators are based on random physical processes and are implemented hardware-wise.

Quantum random bit generation is based on measurement of a system in superposition of basis quantum states. This superposition is called a qubit (quantum bit). These qubits can be realized quite easily- for example with single photons and a beam splitter. The beam splitter has a 50% chance of either reflecting or transmitting the photon and the photonic quantum bit arises from its path. Another way how to produce qubits is measuring the time difference between the arrival of two photons from an uncorrelated source to the detector or counting the number of photons that arrive at the detector in a defined time interval.

An example of optical quantum random number generator (QRNG) has been introduced by [38]. Photon detection is realized by SPAD, and a 32 x 32 array of these detectors is used. The chip was fabricated in standard 0.35 µm CMOS technology. The system is very fast, achieving a maximum bit rate of 200 Mb per second. The SPAD detectors exploits both external (incoming photons) and internal (thermal-based generation) SPAD ignitions for random number production.

The architecture of the QRNG module can be seen in Figure 1-11. Each SPAD cell has its own quench circuit and front-end electronics. A linear feedback shift register (LSFR) with 8 bits serves as a counter for the quantum ignitions. They are saved in time slots that are well defined by the start and stop pulses. Another electronics that are on-chip individually address each of the 1024 SPAD cells and the collected data is than send to an external FPGA chip.

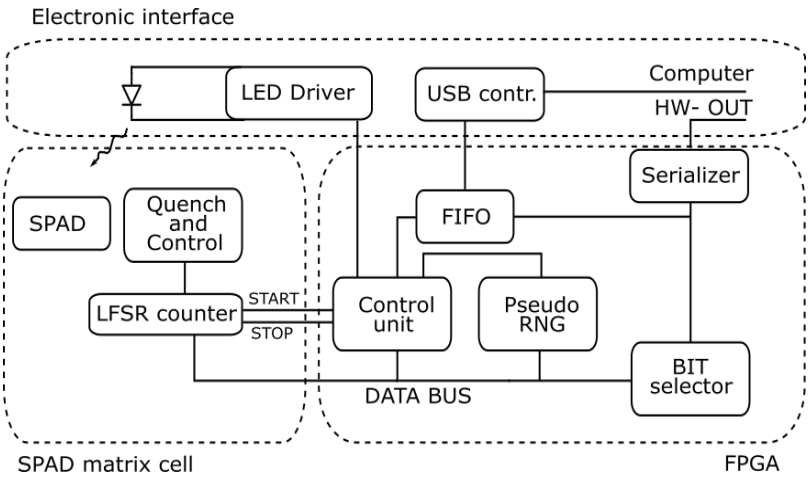

Figure 1-11 Schematic of the QRNG module architecture

FPGA reads the generated random bit number stream and it is transmitted via USB. All of the control signals are also provided by the FPGA, from time-slot setting for the LSFR integration to the reading of the counter. Bit selector is present to provide the option of removing some of the bits from the stream to generate equal number of ones and zeros. As was previously mentioned, after this processing random number generation with a rate of 200 Mb/s is guaranteed. Pseudo random number generator (PRNG) is also present to test the security of the QRNG and potentially enhance it. This PRNG is initialized at the start-up of the electronics through the random number stream provided by QRNG and runs indefinitely afterwards. If the security enhancing by the PRNG is turned on, logical XOR operation between the QRNG and PRNG ensures the randomness of the data stream even by QRNG chip failure. The resulting data stream is then sent to FIFO register and can be read by USB link or redirected to a serial hardware output (HW-OUT). The whole chip is illuminated by a simple light emitting diode. LED DRIVER monitors the number of SPAD ignitions and controls the LED bias current to keep the desired data rate. This way, various physical conditions that may affect the random number generation rate like chip drifts and tolerances, temperature shifts, SPAD sensitivity and LED efficiency are supressed.

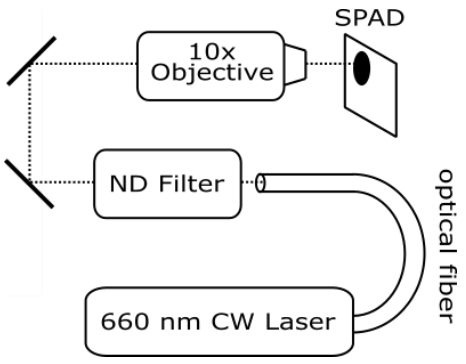

Figure 1-12 Setup for QRNG chip optimization

The dead time of the SPAD circuit is 60ns, but no information about the quenching circuit deployed was provided. Dark count rate is 4 kHz, however, in this kind of application higher dark count rate is actually better and desired to a certain point, as it increases the random number generation rate. Second parameter that usually decreases the performance of the circuit, namely afterpulsing, is also desired in this case for the reasons previously described. There is also a limit for these two processes, after which they are no longer useful. When the afterpulsing and dark count rates are too high, the Poisson process of random bit generation is not effective in generating random bits any longer, as the probability of generation of one event is much higher, namely a one will be almost certainly produced.

To overcome these issues and to set the standard deviation of the counter value to the optimum, laser beam emitting at 0.66 μm, coupled to a fiber and electrically attenuated is focused on a single SPAD element in the chip. This setup can be seen in Figure 1-12. Firstly, average number of incident photons as a function of laser attenuation was acquired. Then the value of the counter was measured as a function of increasing photon rate and this measurement was repeated around 60 000 times to compute its standard deviation and mean. The mean value of the counter saturates at high rates of the photons and the long dead time. As a result, dead time of the circuit must be kept as small as possible (around 50 ns in this case).

2. Quenching circuits

As was already mentioned in Chapter 1, once an avalanche in the SPAD device is started, the current flowing through the photodiode cannot be internally stopped and the device is thus unable to detect subsequent photons. Therefore, the device has to be brought back to its original state by stopping the current and then restoring the nominal bias voltage. This is the purpose of the quenching circuit. Quenching is the breaking of the avalanche process of multiplication. The time that is needed to interrupt the process is called quenching time. Properties of the quenching circuit play a major role in the performance of the detector. In this chapter, different approaches to quenching will be examined, operation modes explained, advantages and disadvantages discussed and example circuits provided.

2.1 Passive quenching circuits

One way to cease an avalanche is to reduce the bias voltage of the photodetector below its breakdown voltage. Simplest way to achieve this is to connect a large resistor R_S in the series with the photodiode (Figure 2-1).

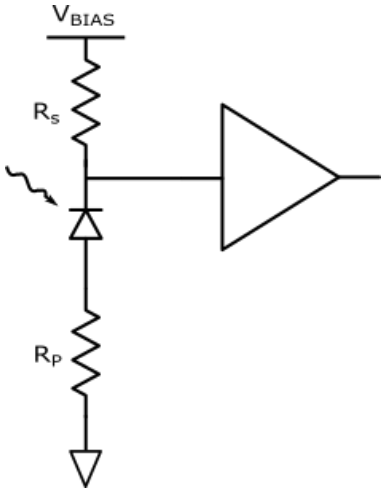

Figure 2-1 Simple schematic of a passive quenching circuit

In the inactive state, the SPAD is biased to a voltage higher than the breakdown voltage and a negligible current is flowing through the device. After a photon absorption, an avalanche is triggered the current rises to its maximal value given by [25]:

$$I_{MAX} = \frac{V_E}{R_p}. \tag{5}$$

Where R_P is the diode parasitic series resistance. This current will discharge the diode parasitic capacitance C_P and the voltage V_E first decreases and after quenching slowly recovers to its initial value with a time constant τ_R [25]:

$$\tau_R = C_P R_S \,. \tag{6}$$

The final value of the current, I_F, can be approximated as [25]:

$$I_F \approx \frac{V_E}{R_S}. \tag{7}$$

The value of this current has to be lower than the so called *latch* current of the SPAD. I_{LATCH} of a SPAD is current low enough that one can say with high probability that there will be no charge carriers in the space charge region to sustain the avalanche after a random time delay. It is not precisely defined, but usually a value of 100 µA is estimated. This gives the lowest possible value of R_S:

$$R_S \geq \frac{V_E}{I_{LATCH}}. \tag{8}$$

The time period t_Q, that is needed to quench the avalanche passively by the resistor can be estimated as the instant when the diode current drops below the I_{LATCH} and calculated as [39]:

$$t_Q = C_P \frac{R_S R_P}{R_S + R_P} \ln\left(\frac{I_{MAX} - I_F}{I_{LATCH} - I_F}\right). \tag{9}$$

Discrete SPADs have ussualy larger values of the capacitance C_P, even 10 pF [40]. With this capacitance, I_{LATCH} = 100 µA and V_E = 10 V, minimum value of τ is ≈ 1 µs. This is one of the reasons why recently quenching circuits have been integrated directly with the detector, lowering the parasitic capacitance to <1 pF for small SPADs. Diode current and the voltage at the cathode with R_P = 5 kΩ, R_S = 100 kΩ, V_E = 5 V and C_P = 1pF are shown in Figure 2-2.

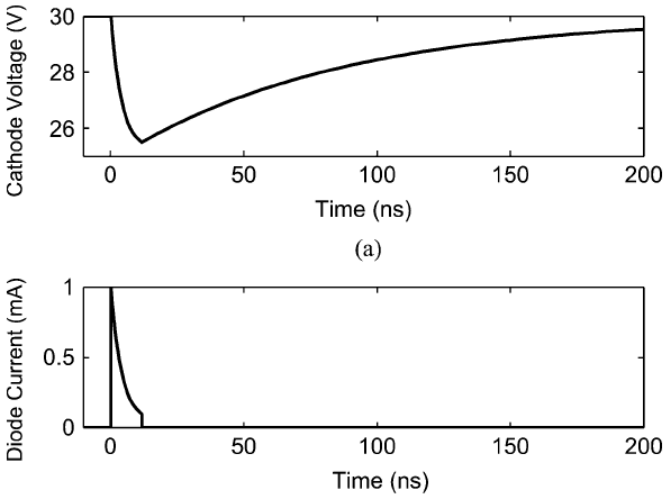

Figure 2-2 Current and the voltage at the cathode of a SPAD [39]

It can be seen on the figure that the maximal current I_{MAX} = 1 mA decreases exponentially from its peak value towards I_F = 50 μA. After the quench, the current is zero and the voltage recovers with a time constant τ to its nominal value.

It is worth mentioning that discrete SPADs are not symmetrical; parasitic capacitance at the anode and cathode may differ. This leads to different quenching times based on the connection of the current limiting resistor to the anode or the cathode. Power dissipation during detection is proportional to the avalanche charge and the breakdown voltage. It is therefore important to limit the avalanche charge, which is proportional to the parasitic capacitance and the resistor. Another factor influenced by the avalanche charge is the afterpulsing probability, as some of the charge carriers may be trapped in the trap centres (Chapter 1.2.6). This is an additional advantage of the integration of the SPAD. This is one of the possibilities to reduce the afterpulsing in passive quenching circuits, as it is not able to prolong the dead time.

Adding a small signal-pickup resistor R_L enables to obtain the output pulse from the device in two ways (Figure 2-3). In Figure 2-3 a), pickup resistor R_L is connected to the ground lead of the current-limiting resistor R_S. Output pulse in this configuration is a scaled version of the voltage waveform at the SPAD (Figure 2-2). This setup is called voltage-mode output. Peak value V_{P_OM} of the voltage across the resistor R_L is given by:

$$V_{P\_OM} = (V_E - I_{LATCH}R_P)\frac{R_L}{R_L + R_S} \approx V_E \frac{R_L}{R_S} \approx I_F R_L \,. \tag{10}$$

The main drawback of this approach is the low-pass filter with the time constant t_Q, delaying the current pulse. This may be compensated when the threshold in the signal processing circuit is increased. This is however not always possible, because the V_{P_OM} value is tied with the I_F current and therefore quite small, unless big R_L is chosen. This implies that a comparator with very small offset voltage has to be used.

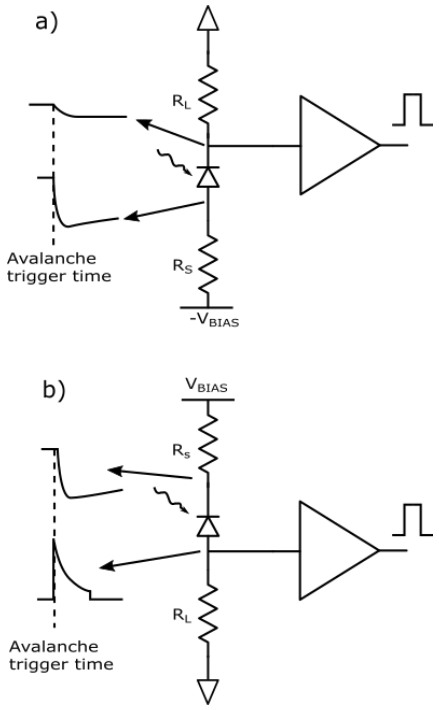

Figure 2-3 Passive quenching circuit configuration a) in voltage-mode output; b) in current-mode output

In Figure 2-3 b), R_L is connected to the ground lead of the SPAD. This produces an output pulse that is a scaled version of the diode current, therefore called current-mode output. To correctly calculate the output voltage pulse peak, diode capacitance C_P has to be split into two parts- stray capacitance C_S of the SPAD (which is the capacitance from the SPAD terminal connected to the current-limiting resistor R_S to ground) and C_D, junction capacitance. Current-mode output equivalent circuit is shown in the Figure 2-4. If the stray capacitance is too small compared to the junction capacitance, only a very small current will discharge through R_L; almost all of the avalanche current will flow in the internal loop of the device and through R_P. The peak voltage V_{P_CM} can be expressed as:

$$V_{P\_CM} \approx V_E \frac{R_L}{R_P\left(1+\frac{C_D}{C_S}\right)} \approx I_F R_L \frac{R_S}{\left(1+\frac{C_D}{C_S}\right)} \approx V_{P_{VM}} \frac{R_S}{\left(1+\frac{C_D}{C_S}\right)}. \quad (11)$$

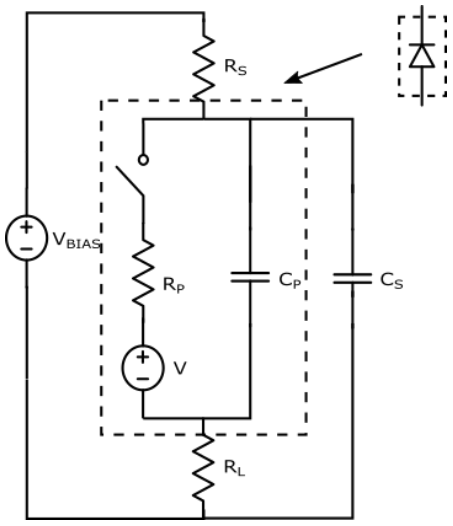

Figure 2-4 Current output equivalent circuit

It can be seen from (11) that the peak value V_{P_CM} is higher than V_{P_VM}, as it is generated by the current V_E/R_P as opposed to V_E/R_S. This means that smaller R_L resistances can be used.

Estimation of the maximal counting frequency can be done using Poisson statistics [41]. For less than 1% probability of counting losses due to a photon incoming while still a previous quench cycle hasn't been completed, there has to be a less than 1% probability P_A that a photon arrives in the dead time of the circuit τ_D:

$$P_A = 1 - e^{-n_T \tau_D} . \tag{12}$$

Where n_T is the repetition rate of the pulses that consists of rate of the detected photons and dark counts. (12) can be further approximated to $P_A = n_T \tau_D$ when the average number of events $n_T \tau_D$ is small. After inserting 1% as the probability, the result is:

$$n_T < \frac{1}{100 \tau_D} . \tag{13}$$

According to [41], τ_D can be roughly estimated as ½ of the recovery time constant τ_R (6). Finally, inserting R_S = 100 kΩ and C_P = 10 pF, maximal counting rate 20 kHz is obtained. However, assuming a detector integrated with the circuit ([42]) with a dead time of 32 ns (R_S = 270 k and C_P = 120 fF), 625 kHz counting rate is possible.

2.2 Passive quenching circuit with active reset

To make the charging of the SPAD after the avalanche quench faster, an active circuit can be used. Quenching still occurs passively with a current limiting resistor in series with a diode, but the parasitic capacitance is not charged through the large resistor, but by other means. An example is shown in Figure 2-5. Here a transistor is connected parallel to the large resistor R_S and turned on for a short time to charge the capacitance and restore the SPAD to the operating voltage. Additionally, holding time can be set. Making the holding time longer reduces the afterpulsing, because the carriers have more time to leave the depletion region.

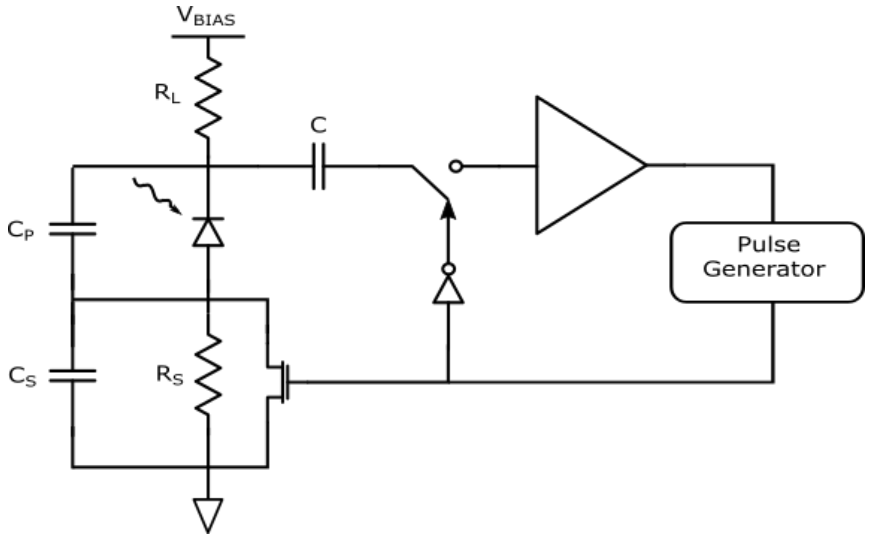

Figure 2-5 Schematic of a passive quenching circuit with active reset [43]

This circuits operation can be described as follows. The transistor that is connected parallel to the quenching resistor is normally in off-state , and the switch behind the decoupling capacitor C is closed. By triggering an avalanche, diode capacitance C_D is quickly discharged and C_S charged. After the SPAD current drops below the I_{LATCH}, the avalanche is quenched and the voltage on the SPAD equals approximately to $V_B + I_{LATCH} * R_L$. This way, negative voltage pulse at the cathode is generated and coupled through the decoupling capacitor to the amplifier. The amplified voltage pulse triggers a pulse generator and after a specific delay a pulse is generated which turns on the mosfet switch. Through this switch, C_D is charged and C_S discharged. While the generated output pulse from the generator holds the mosfet switch closed, the switch in front of the amplifier is being hold open through an inverter.

[43] reports quenching time of 2 ns, dark count rate of 14 kHz with V_E = 2 V and temperature 230 K. Under these conditions, detection efficiency of 23% has been achieved.

2.3 Active quenching circuits

To get over the main drawbacks of the passive quenching circuits (dead time not precisely defined and the voltage recovery too slow), different approach was chosen: active quenching. First reported in 1982 [44] basic operation of these circuits requires the sensing of the avalanche and reacting back on the SPAD by reducing the bias voltage and bringing it swiftly back up. The avalanche is sensed through a low impedance and the quenching is carried out by the active components. In this chapter, some of the different design concepts will be presented.

The schematic of a basic active quenching circuit using pulse generator is shown in Figure 2-6. During a quench period in active quenching circuits, bias voltage of the SPAD is lowered below breakdown voltage. That means that the quenching time stays always the same as opposed to passive quenching, where the quenching time changes with the variations in avalanche multiplication process. One drawback of the active quenching circuits might be, that the quenching time itself can be actually longer than in the passive quenching circuits. The reason is that before quenching signal can be released, the circuit has to detect the pulse produced by the SPAD, process it and then intervene.

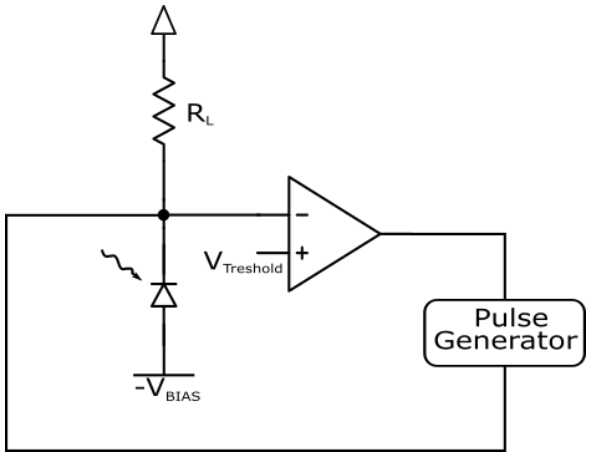

Figure 2-6 Schematic of a basic active quenching circuit

This time is subject to different factors, such as length of the connections between the SPAD and the circuit, its sensitivity, maximal avalanche current, delays on the electronic components in the signal processing way and so on. In the time between the instant of the avalanche triggering and production of the quenching signal, the current in the SPAD keeps flowing at its maximal value. With this time, both the afterpulsing chance and the power dissipation increase. Total charge Q_T of this current is given by:

$$Q_T = I_{MAX}\tau_Q = \frac{V_E}{R_L}\tau_Q \tag{14}$$

Where I_{MAX} is the maximal value of the avalanche current and τ_Q the quenching time. If the quenching time is bigger than that of a time constant given by $C_P R_L$, the total SPAD charge will be bigger than that of the passive quenching circuit.

Figure 2-7 shows the SPAD current and the cathode voltage waveforms. It can be seen on the figure that even if the quenching time is shorter than that of the passive quenching circuit (13.5 ns in this case), the total charge can be larger (13.5 pC in this case).

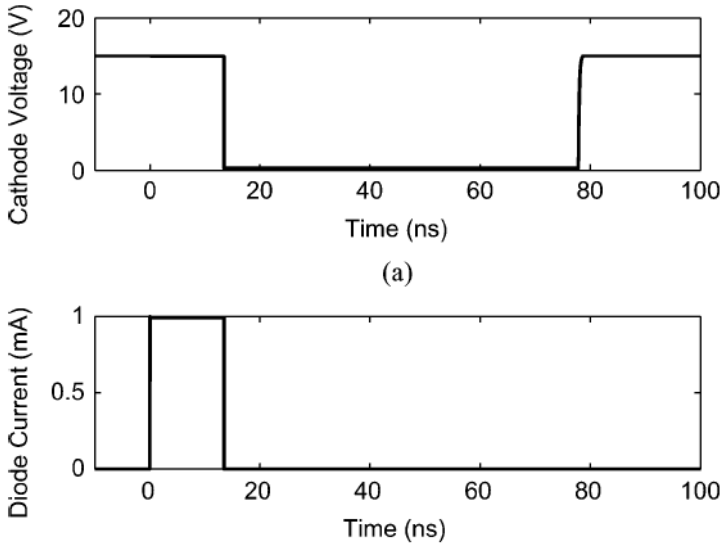

Figure 2-7 Voltage at the cathode and SPAD current waveforms [39]

As was already mentioned, the main advantage of active quenching circuits is the shorter voltage reset time, starting at few nanoseconds, enabling much faster counting rates than passive quenching (this time depends on the V_E and C_P). For example, using (13) and a reset time of 10 ns, maximal counting rate with 1 % probability that an avalanche will be triggered during reset time is 1 MHz. Further problem represents an uncertainty of photon arrival time with the variations in dead time caused by these avalanches triggered during dead time.

An example of active quenching circuit made from discrete components can be seen in Figure 2-8 [45].

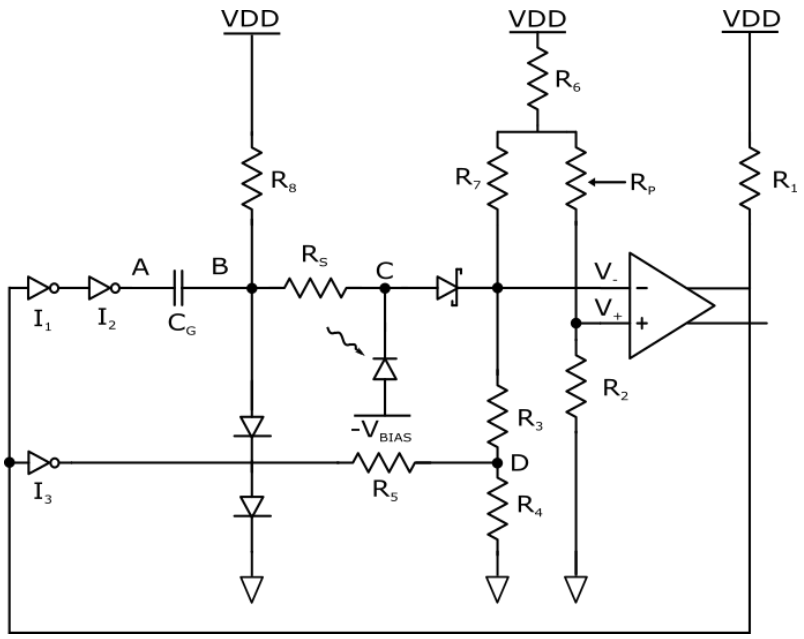

Figure 2-8 An example of discrete active quenching circuit [45]

This circuit has three tasks: it amplifies the small SPAD avalanche signal, quenches the avalanche and shapes the output pulse. Initially, the SPAD does not conduct current and the output of the AD8611 comparator is at 0 V. A small current through the R_S is present, keeping V_- above V_+ and the output at 0 V. This difference can be set by the potentiometer R_P. The potentiometer is present to be able to set the reference voltage so low as possible but still avoid oscillations. In the absence of the current through BAT83 Schottky diode, the V_- would go below V_+ and the output would be switched to 3,6 V (logic 1). When the avalanche is triggered, some of the current flowing through BAT83 will be drawn by SPAD, lowering the voltage at C and V_-. V_- goes below V_+ and after a propagation delay, output is switched to logic state 1. This causes the output of inverter I_1 to change and consequently I_2, making a voltage step from +7 V to 0 V. capacitor C_G transfers this negative voltage step (-7 V) to the point B and resistor R_S back to the point C, quenching the avalanche. Biasing voltage of the SPAD goes below breakdown voltage and the Schottky diode BAT83 switches off, rendering the detector unable to detect any more photons. The dead time of the circuit is set by the propagation delays of the inverter I_3 (about 16 ns). After this time period, output of the I_3 will make a 500 mV step, increasing the voltage at point D and subsequently V_-, setting the comparator output to 0 V. I_1 output goes low, I_2 output high restores the operating bias voltage on the SPAD. SPAD capacity is charged through resistor R_S, which has to be chosen sufficiently small to enable fast voltage recovery.

This circuit has been also experimentally proven in [45]. Photodiode C30902S, which was cooled was used. The reason for the cooling was temperature dependence of the breakdown voltage. It was about 186 V at -30 °C. Afterpulsing was measured as a function excess voltage V_E, as the afterpulsing dramatically increases when this voltage is set too high. The results are shown in Figure 2-9, showing

afterpulsing probability around 7% at 5 V, dominated by the SPAD afterpulses to this point. With increasing V_E ineffective quenching dominates the afterpulsing. The data were measured with 7 V quenching voltage and counting frequency of 10 kHz.

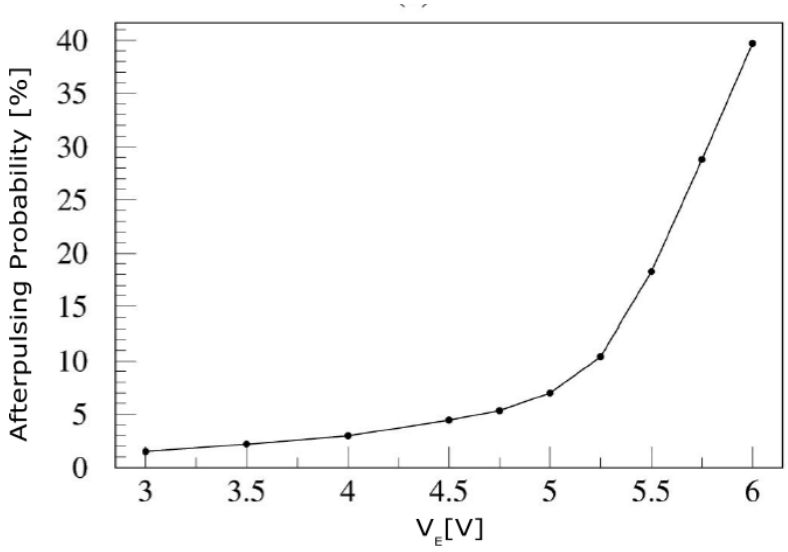

Figure 2-9 Afterpulsing probability vs V_E [45]

The dead time of the circuit was also measured. The measurement was done using an oscilloscope and measuring many avalanche events, adding them together and determining the minimum distance between the events. The minimum dead time obtained by this method is 39 ns. Maximum counting frequency, strongly affected by the dead time of the circuit, can be seen in Figure 2-10. It is plotted as a function of V_E for three different temperatures. It can be seen that the maximum counting rate rises with V_E , is almost independent of temperature and the maximum lies at ~ 14 MHz.

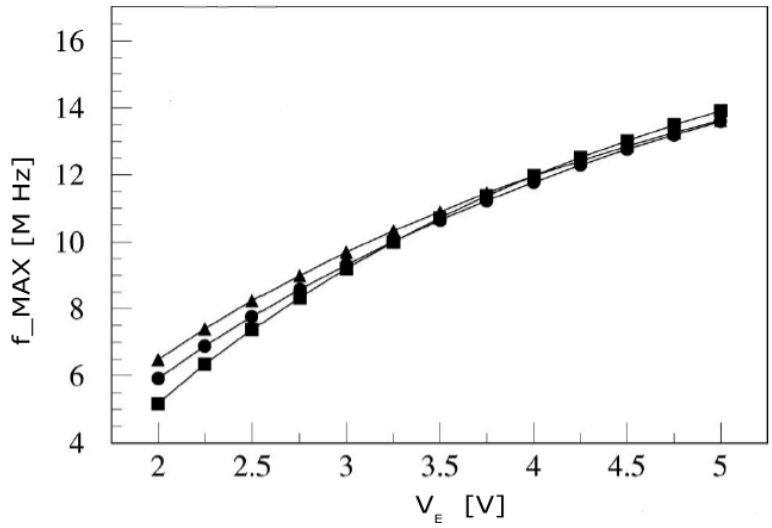

Figure 2-10 Highest counting rate vs V_E [45]

An example of a fully integrated active quenching circuit has been presented in [46]. Figure 2-11 shows a basic schematic of this circuit, consisting of 4 blocks. A stage where the avalanche on the anode of the SPAD is sensed, the low-side logic block and the high-side logic block, where the control signals are generated and two transistors M_{QUENCH} and M_{RESET}, where the reset and quenching phases are regulated. Main advantage of this structure is the possibility of setting different bias voltages for the SPAD during quench and reset phase. The maximal drain source voltages of M_{QUENCH} and M_{RESET} limit the quenching voltage, what means that high- voltage transistors must be used. This architecture has another advantage, which is the possibility of exploiting low-voltage transistors for the logic, which are faster than the high-voltage ones, because they are separated from the quenching signal by the high voltage transistors.

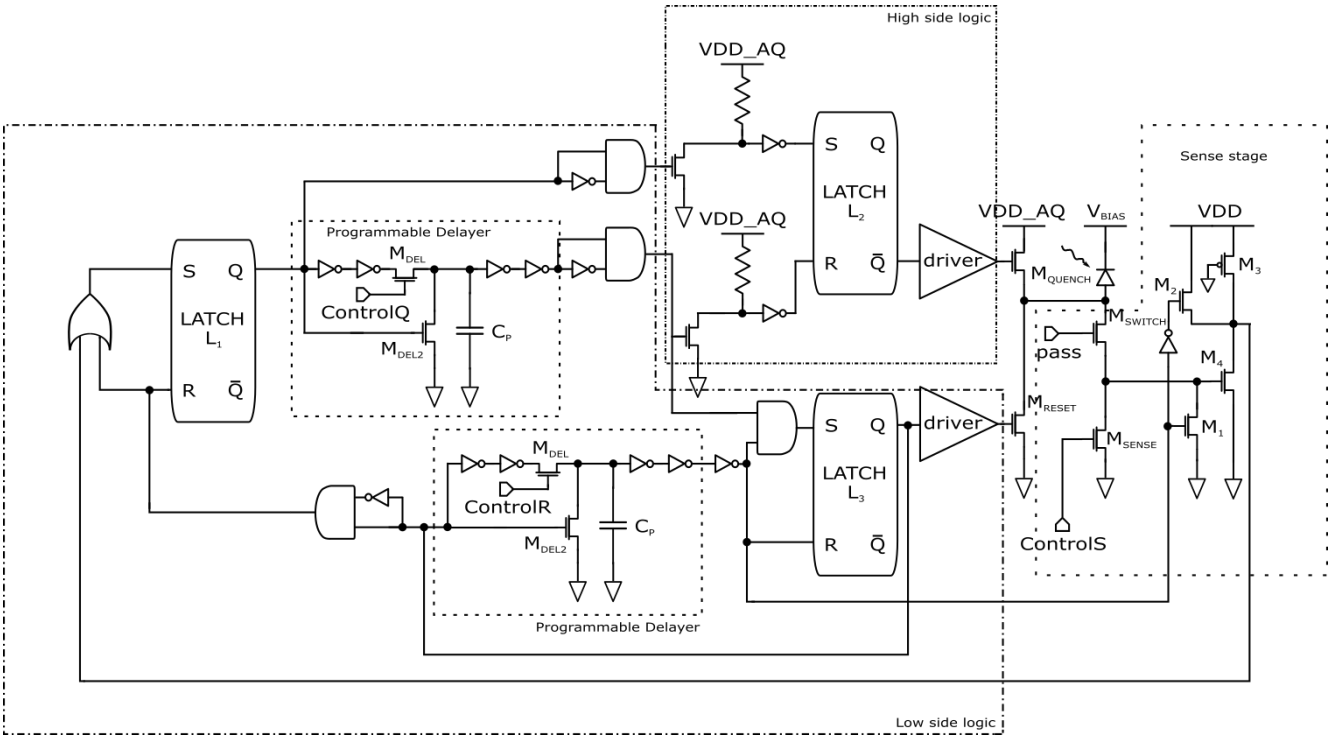

Figure 2-11 Simplified schematic of a fully integrated active quenching circuit

Sense stage, which determines instant of the avalanche ignition, includes 5 low-voltage transistors M_1-M_4 and M_{SENSE}, connected to the SPAD by a high-voltage transistor M_{SWITCH}, preventing the high SPAD voltage to damage them. For example, when 1.8 V transistors are used as the low-voltage devices and the gate voltage of M_{SENSE} is also limited to 1.8 V, its source voltage cannot exceed 1.8 V and all of the low-voltage circuitry connected to this node is safe. When M_{SWITCH} is closed, the avalanche current induces a voltage drop on the equivalent output resistance of the M_{SENSE}. This resistance can be controlled by the variation of gate voltage of M_{SENSE} and can be externally adjusted by the “ControlS” pin. This equivalent switch resistance also determines the response speed of the circuit after photon

detection. The inverter M_4, M_3 produces the output signal and for a fast response, W/L ratio of the M_4 should be as large as possible. M_1 and M_2 are used to lock the inverter during reset phase.

The low-side and the high-side logic blocks are responsible for generating all the internal control signals. Low-voltage transistors are used, while using as few logic gates as possible to obtain high operating frequency. Initially, output (Q) of the latches L_1, L_2, and L_3 is set to logical 0. Falling edge of the output signal coming from sense stage sets the output of L_1 to logical 1, setting "pass" signal to logical 0 and turning off the M_{SENSE}. Additionally, output of the L_2 is also set to logical 1, which generates signal V_Q, turning on the transistor M_{QUENCH} and initiating quenching sequence. To allow fast transition of the quenching voltage across the transistor to the SPAD, W/L ratio of the M_{QUENCH} is high. Downside of making the transistor big is the increase of the gate capacitance. To be able to swiftly drive this capacitance, driver between the output of the latch and the switching mosfet is introduced. The output of latch L_1 is additionally fed to a programmable delay. Output of this programmable delay resets latch L_2, which drives the gate of the transistor M_{RESET} high and completes the quenching phase, restoring the operating bias voltage on the SPAD.

Hold-off duration is set by the delay of the programmable delayer. The delay depends on the capacitance C_P and on the drain-source resistance of the mosfet switch M_{DEL}. The gate voltage of the transistor can be externally set through the pin "ControlQ", enabling to control the resistance and delay.

To evaluate the circuit, it has been connected to a custom-made SPAD with low stray capacitance. V_E of 5 V has been used, chosen because of a good trade-off between the photon counting efficiency and the dark count rate. [46] reports dead time of only 12.2 ns, enabling maximum counting frequency of 82 MHz.

To summarize, active quenching circuits provide well-defined, often adjustable hold-off times and faster restoration of the SPAD bias voltage than the passive quenching circuits. The disadvantages of these circuits are dependency of the avalanche charge on the delay from the instant of avalanche triggering to quenching of the circuit and the circuits are larger, leading to larger area occupation (this issues a problem only in integrated circuits).

2.4 Mixed active-passive quenching circuits

To exploit the advantages both of the active and passive quenching circuits, without the disadvantages, mixed active-passive quenching circuits have been developed. In these circuits, the SPAD is connected

both to the active circuitry and a large current-limiting resistor. Basic schematic of such a circuit is shown in Figure 2-12.

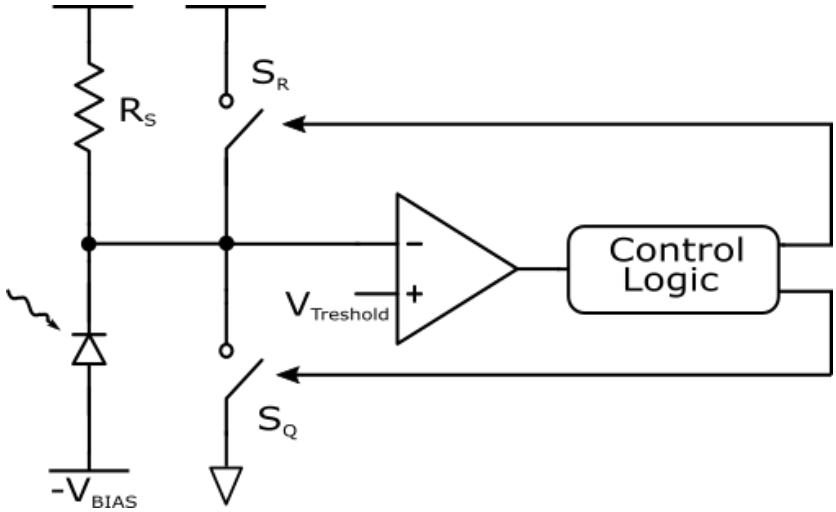

Figure 2-12 Basic schematic of a mixed active-passive circuit

Following a trigger of the avalanche, the avalanche current starts to flow through the large resistor R_S, initially quenching the avalanche passively. However, when the avalanche is sensed by the active circuitry, active quenching is initiated. The circuit operates like a common active quenching circuit after that. This enables to choose the hold-off time freely. Typical SPAD current and cathode voltage waveforms are shown in Figure 2-13.

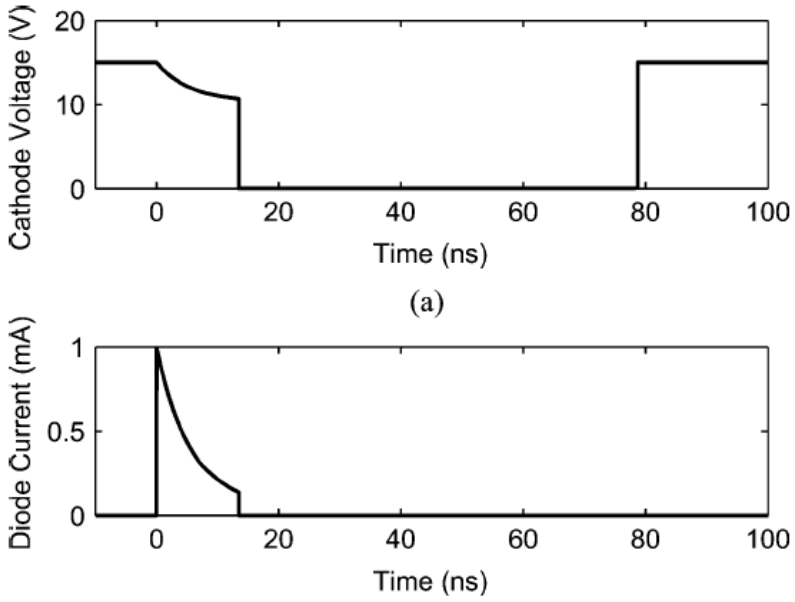

Figure 2-13 SPAD current and cathode voltage waveforms in mixed passive-active quenching circuits [39]

As with all the circuits shown here, integration of the circuit together with the detector reduces the parasitic capacitance significantly, leading to faster voltage reset, smaller delay of the intervention signal and a much smaller amount of avalanche charge.

The total avalanche charge is at worst as big as in the passive quenching circuits, because when the active circuitry takes too long to react, the avalanche is quenched passively anyway by the large resistor. On the other hand, when the response of the active circuitry is fast, the avalanche charge could be much smaller. The total charge Q_T can be calculated as [39]:

$$Q_T = I_F \tau_{QD} + (I_{MAX} - I_F)\tau_R (1 - e^{\frac{-\tau_{QD}}{\tau_R}}) \quad (15)$$

When Figure 2-7 and Figure 2-13 are compared, it can be seen, that the quenching time is the same (13.5 ns), but the total avalanche charge Q_T is smaller in the case of mixed active-passive approach (5.1 pC).

An example of mixed active-passive circuit that uses an active load instead of the large current limiting resistor can be seen in Figure 2-14 [47]. Usually, resistors with values of a few tens of kΩ are necessary to initiate the passive quenching sequence. When a signal driving the switches that drive the active circuitry (mosfets are commonly used) couples to one terminal of the SPAD, an overshoot in the voltage is caused and decays with a time constant. With such a high value of the load resistor, together with the parasitic capacitances of the switches and the SPAD, this constant is quite long. Therefore, an active load is introduced to prevent this issue.

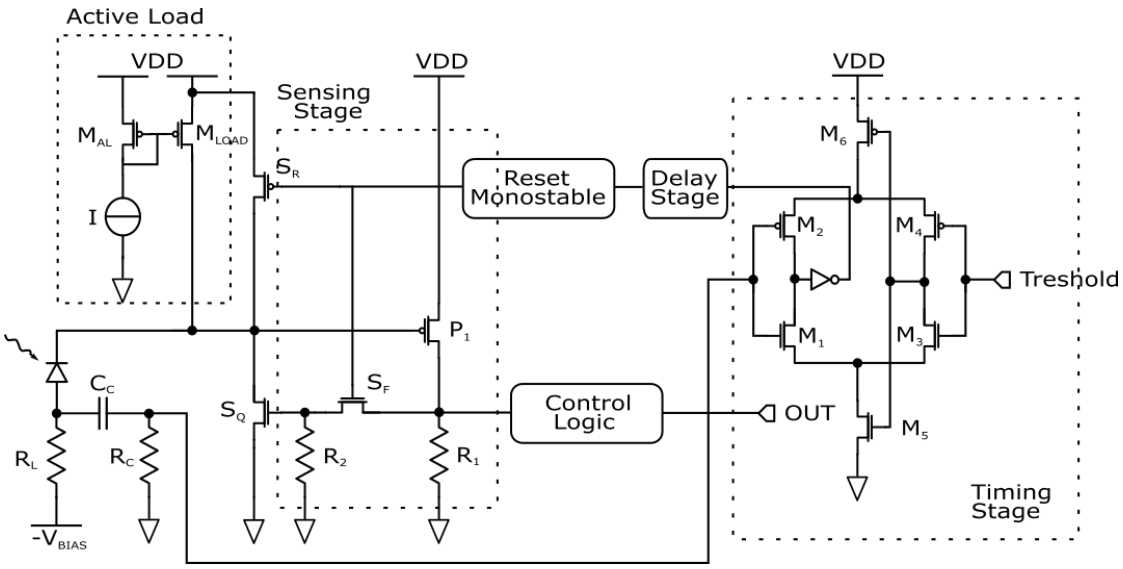

Figure 2-14 An example of mixed active-passive quenching circuit with active load

The circuit works as follows. The SPAD is initially biased at the voltage V_{DD}-V_A higher than the breakdown voltage, through the active load. When an avalanche is triggered, parasitic capacitance at the SPAD cathode is discharged and the passive quenching phase starts. The voltage drop on the active load causes the gate voltage of the transistor P_1 to also decrease, letting current through resistor R_1. This pulls the gate of the transistor S_Q high, opening the switch. SPAD cathode is hence pulled to ground and active quenching takes place. Control logic produces a measurable pulse, which passes through a stage with programmable delay. This delay sets the hold -off time of the circuit and can be adjusted by the hold-off time pin. The pulse passes the reset monostable block which turns both the transistor S_F and S_Q off and the transistor S_R on. After the hold-off delay, transistor S_R is switched off, S_F on and the quenching cycle is completed.

The main purpose of the timing stage is to swiftly pick-up the avalanche current to provide an accurate time of avalanche ignition. The voltage signal from R_L is coupled through the coupling capacitor C_C to the coupling resistor R_C and picked up the comparator. This comparator formed by two inverting differential pairs M_1, M_2 and M_3, M_4 and the current sources M_5, M_6. The voltage at the anode is pulled up to VDD in very short time during reset phase. This produces a pulse that could trigger the comparator again, leaving the circuit oscillating. Control logic produces a pulse that disables the comparator during the reset phase to avoid this problem.

A current mirror, representing the active load was employed. When the SPAD is biased at the V_{DD}, no current can flow through the transistor M_{LOAD} and the device is kept in the ohmic region. After an avalanche ignition when the cathode voltage is lowered, current starts flowing through M_{LOAD}. It exits the ohmic region and enters saturation. The output resistance of the mosfet increases dramatically and starts quenching the avalanche passively. Due to the overshoot mentioned earlier, drain voltage goes higher than the source voltage and the device enters a state similar to the ohmic region. However, in this region the resistance of the device is quite small and the recovery from the overshoot is fast.

The results were evaluated in [47]. SLIK photodiodes were used with a bias voltage of 455 V. These diodes have breakdown voltage of 439 V, so V_E was about 16 V. The voltage recovery with use of a resistor and an active load as to bias the device can be seen in Figure 2-15. It can be seen that the recovery time is much faster with the active load than with a passive resistor. The time constant in the first case is below 100ns, whereas in the second case more than 1 μs. Counting frequencies higher than 1 MHz are possible, without any impact on the timing resolution.

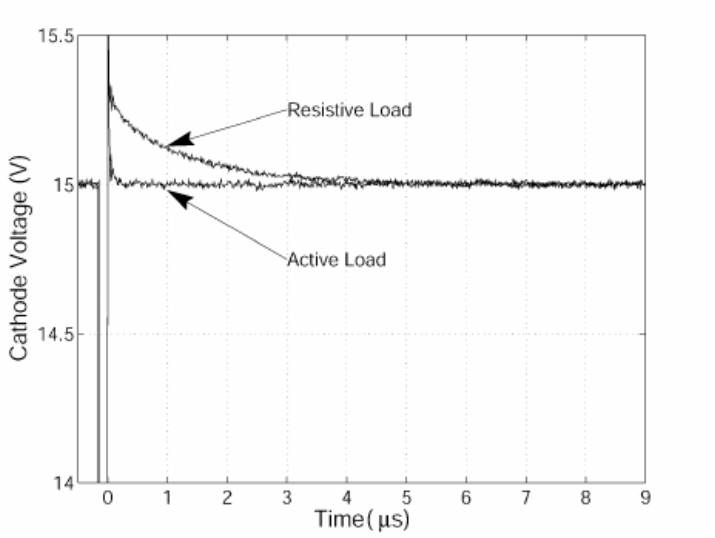

Figure 2-15 The recovery of the cathode voltage with a resistor compared to recovery of the voltage when active load is used [47]

Main drawback of the mixed active-passive quenching circuits is their high area occupation, making the integration of detector arrays quite challenging. However, smaller detector arrays are still doable and have been reported [48]. As was already mentioned, main advantages of these circuits are well defined dead time and also less avalanche charge compared to active quenching circuits. These circuits also offer an easy implementation of gated operation (will be discussed later).

2.5 Special quenching circuits

Some of the quenching circuits found in the literature cannot be assessed to any of the categories mentioned so far. In this chapter, diverse circuit approaches to quenching will be presented. All of these circuits were designed to be integrated with the SPADs.

Circuit capable of high counting rates and with low area occupation has been presented in [49]. The circuit is designed to fit in detector arrays. Simplified schematic of the circuit can be seen in Figure 2-16. The idea is to replace the large current limiting resistor or the active circuitry by simple digital switches and to take advantage of the reverse-biased SPAD parasitic capacitance. This capacitance depends on the diameter of the detector, and can range from 10 to 160 pF for a device with 10 and 40 µm diameter respectively. The Anode of the SPAD is biased to negative breakdown voltage. At the start of the cycle, write switched is closed and the diode is pre-charged to a desired V_E. The write switch

is then opened, but the cathode of the device remains at the V_E, as the charge is stored in the parasitic capacitance of the SPAD. This charge is maintained in the parasitic capacitance unless a photon is detected- in which case avalanche current discharges it. In the read cycle, this value is read- a 0 is acquired when a photon was detected and 1 when not. During this cycle the capacitance is discharged through the read switch. After the end of this sequence, write switch is closed, read switch opened and another detection cycle begins.

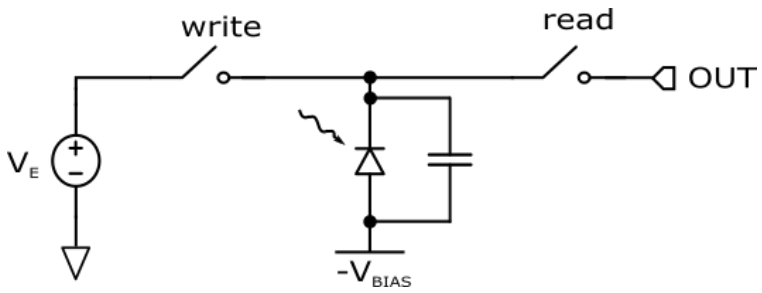

Figure 2-16 Simplified schematic of DigitalAPD circuit

This one stage can be arranged into arrays similar to dynamic RAMs. However, due to individual devices discharging a little over time and the charge leaking to the interconnects parasitic capacitances or gate capacitances of the switches, taking absolute values as the reference voltage of the comparators could be misleading. Therefore, the authors have chosen a charge sharing model over the static voltage one, assuming that once the SPAD is connected to the comparator, charge will either flow from the device to the reading node or vice versa. When the voltage at the beginning of the cycle is known, it is easy to compare this value to the value at the start of the cycle and determine if the photon was detected or not. The parasitic capacitance of the circuit have to be kept as small as possible, because when this capacitance would be larger than the SPAD capacitance, charge stored in this parasitic capacitance on the readout side of the circuit would flow into the SPAD node, faking a 0, when in fact a photon has been detected. Therefore, the switches and buffers have to be kept as small as possible. Sampling rate 5 MHz and quenching time of about 50 ns have been achieved in a 4x4 array.

A different approach was presented by [50]. This design is based on CMOS thyristor delay. This circuit is shown in Figure 2-17. The anode of the SPAD is biased to its negative breakdown voltage while the value of VDD is the V_E. Initially, point A and the B are high-impedance nodes and there is no power consumption. When an avalanche is ignited, the feedback loop formed by M_1 and M_4 clamps the cathode of the SPAD to 0 V. After a time set by the inverter propagation delays the circuit is reset by the M_3 and disabled through M_2. Transistors M_5 and M_6 form capacitances.

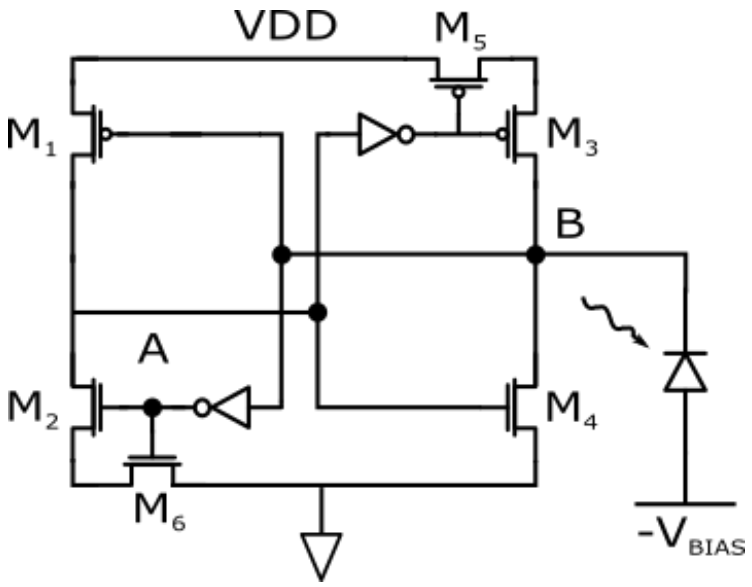

Figure 2-17 Simplified schematic of a thyristor-based quenching circuit

No quenching resistor is needed in the circuit, as the width of the M_3 gate is about 8 times larger than that of the M_4, making the subthreshold leakage of the PMOS dominant. This circuit was developed in 0.35 µm CMOS technology, consuming an area of about 130 µm^2. Dead time of 2-30 ns was achieved with timing jitter of 300 ps.

A quenching circuit based on different paradigm was proposed in [51] and can be seen in Figure 2-18. It is based on so called current-mode approach. This circuit first senses avalanche through current-mode output and then breaks the current path afterwards, switching the avalanche current off. As was already mentioned in Chapter 2.1, current-mode output is faster than voltage-mode output.

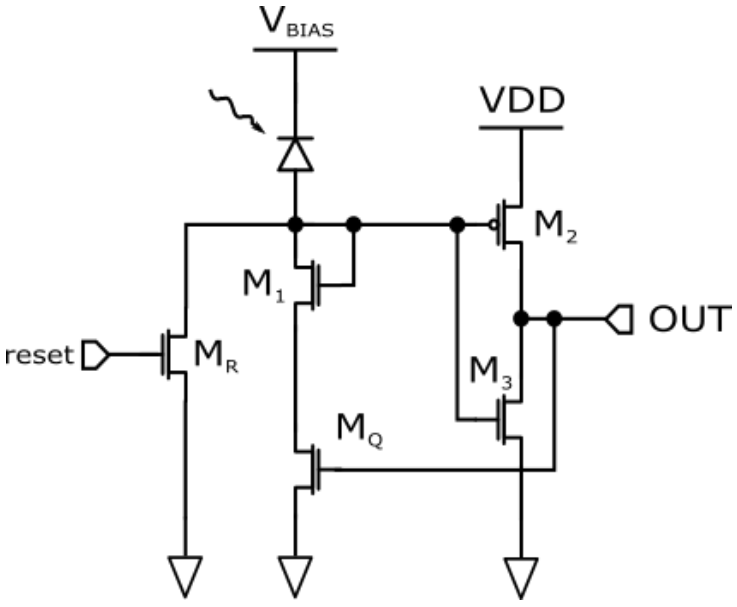

Figure 2-18 Schematic of an active quenching and recharging circuit

This circuit works as follows. In quiescent state, the SPAD is biased at voltage $V_E + V_B$, because the transistor M_R is opened and the node A is sitting at ground. Node out is set high by the inverter formed by transistors M_2, M_3. After an avalanche ignition, current starts flowing through the transistor M_1 connected as a diode and transistor M_Q. This current is also forced to flow through transistors M_2 and M_3, as the diode connected M_1 and M_3 form a current mirror. A voltage drop across M_2 reduces the voltage at node out, which lowers the gate-source voltage of transistor M_Q, increasing its channel resistance. As a result, voltage at node A increases. Positive feedback formed by M_Q, M_3 and M_1 speeds this process up. When the voltage at node out is reduced below threshold voltage of M_Q, current can no longer flow and the avalanche stops abruptly, finishing the quenching phase. The transistor M_R is then switched on to allow fast recharging of the SPAD through low impedance path.

W/L ratio of M_Q, M_1 and M_2 should be kept as small as possible to reduce capacitances of these devices and allow high-speed operation. However, to increase switching speed of M_3, W/L ratio of this transistor should be larger. This same principle applies to transistor M_R.

The circuit has been developed in 2 µm BiCMOS technology. However, it has been validated only with simulations. Hold off time was set to 14 ns, while the SPAD was kept at V_E of 5 V. Quenching time obtained at this voltage was lower than 3 ns, reset time 1 ns, making theoretical photon counting rate 250 MHz with 4 ns dead time.

Similar but slightly different approach was chosen by [52]. Variable resistance is also deployed, but the avalanche is sensed by a voltage comparator. The value of this resistance is adjusted accordingly to the operation phase of the SPAD. The resistance must be increased at ignition to allow passive quenching and reduced afterwards to speed up the SPAD charging. This can be achieved by a MOS transistor. However, this transistor does not work as a simple switch, being turned on or off. Implementation of this concept is shown in Figure 2-19.

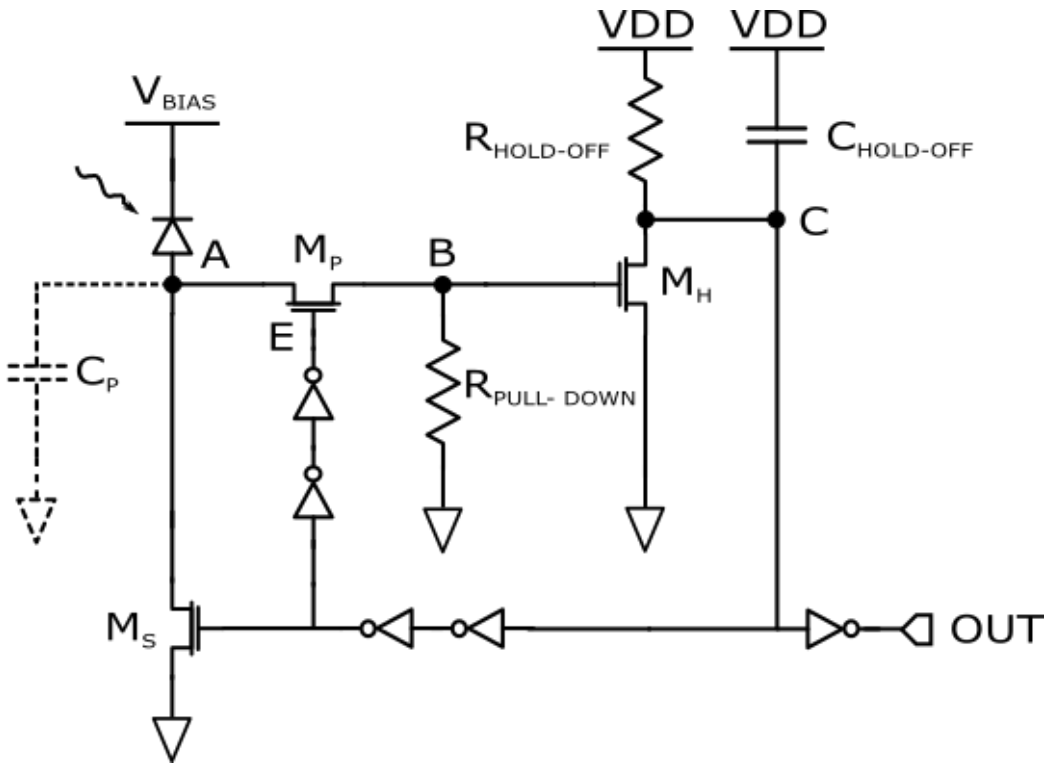

Figure 2-19 Schematic of a variable load active quenching circuit

To minimize the area occupation, MOS transistors are used as passive components. The comparator is replaced transistors M_H and M_P. The sense node A is decoupled from the node B by the transistor M_P, reducing the gate-drain and gate-source capacitance loading of the transistor M_H. This transistor works as a single transistor amplifier. Initially, transistor M_S is opened and the node A is at ground and the SPAD is biased at the voltage V_E above the breakdown voltage. When node A is at ground, node B is grounded too through the transistor M_P. Node C as well as node D are at VDD. When an avalanche is triggered, voltage drop across M_s increases, increasing the voltage at node A and consequently at node B. When the voltage at node B exceeds the threshold voltage of M_H, current starting to flow through this transistor produces a voltage drop at R_H, lowering the voltage at node C and D. Eventually, this voltage drops below threshold voltage of M_S, switching off the transistor and quenching the avalanche. Voltage at node E also drops to 0, switching off the transistor M_P and disconnecting the transistor M_H from the SPAD. This causes it to switch off and the voltage at node C rises back to VDD, with the time constant given by $C_H * R_H$. This allows to adjust the hold-off time of the circuit, given by the delay from the instant when M_P switches off to the instant when M_S switches back on. The inverters are present to secure reliable operation. Namely, when the voltage at node D rises high too quickly after quenching, M_H could sense the SPAD anode again, producing a false detection. This is achieved by Inverters I_3 and I_4, keeping the M_P switched off long enough. Inverters I_3 and I_4 also make it possible to detect photons also during reset phase, as node E will go high after a delay set by these devices.

The circuit was validated using custom SPAD with a breakdown voltage V_B = 24 V. With V_E = 5 V, counting frequency 20 MHz was achieved and the total current drawn by the circuit did not exceed 50 µA. Dark count rate was reported at 4900 Hz with a detection efficiency of 42 %. Light source with a wavelength 0,43 µm was used. Afterpulsing probability was kept below 1% with the deadtime of 600ns.

2.6 Circuits with gated operation

All the circuits mentioned so far were ready to detect photon at any time because they were operated continuously. SPAD was kept at excess bias voltage at all times. However, some applications do not need to be always active. Circuits for these applications only need to be able to sense photons at well-defined time intervals as the transmitter is not always transmitting. This style of operation is called gated operation. Basic schematic of this circuit can be seen in Figure 2-20. The SPAD is biased above breakdown voltage only for a portion of the operating cycle and then the biasing voltage is switched off. Depending on the time period for which the detector is active, there may be no need for a quenching circuit- when the time is short, the avalanche will be quenched when the detection period ends. This kind of approach has a major drawback- only one photon per active period can be detected. It is therefore advisable to keep the on-period as small as possible (often below 1 ns). For longer active periods, quenching circuits must be deployed.

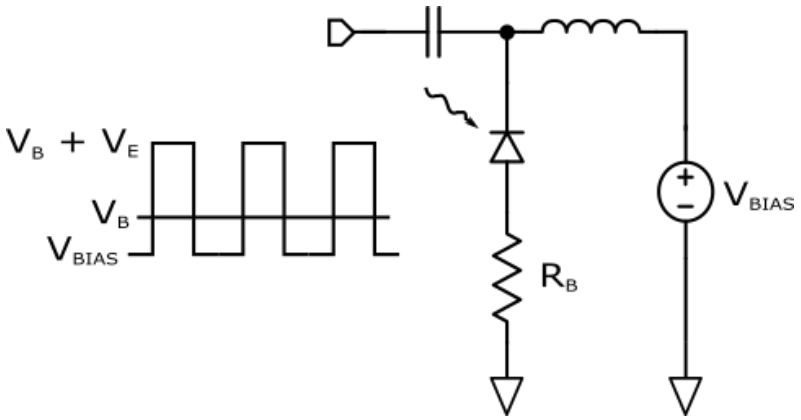

Figure 2-20 Basic schematic of a quenching circuit with gated operation

For a SPAD under gated operation with passive quenching circuit, signal has to be AC coupled, as the DC coupled current limiting resistor together with the SPAD parasitic capacitance form a low pass filter that slows down the circuit response to switching from active to inactive phase. When AC coupling is used, high pass filter is formed instead, leaving the response to fast switching uninfluenced. However,

the coupling capacitance cannot be too small, as the voltage pulse from the detector would be decreased by the capacitive voltage divider formed by the diode parasitic capacitor and the decoupling capacitor. This imposes difficulties when the circuit should be integrated, as the area increase is significant.

An implementation of passive quenching circuit with gated operation was presented in [53]. This circuit can be seen in Figure 2-21. The time needed to recharge the decoupling capacitor limits the counting rate in passive quenching circuits with gated operation. To overcome the problem, this circuit introduces AC coupling together with diodes.

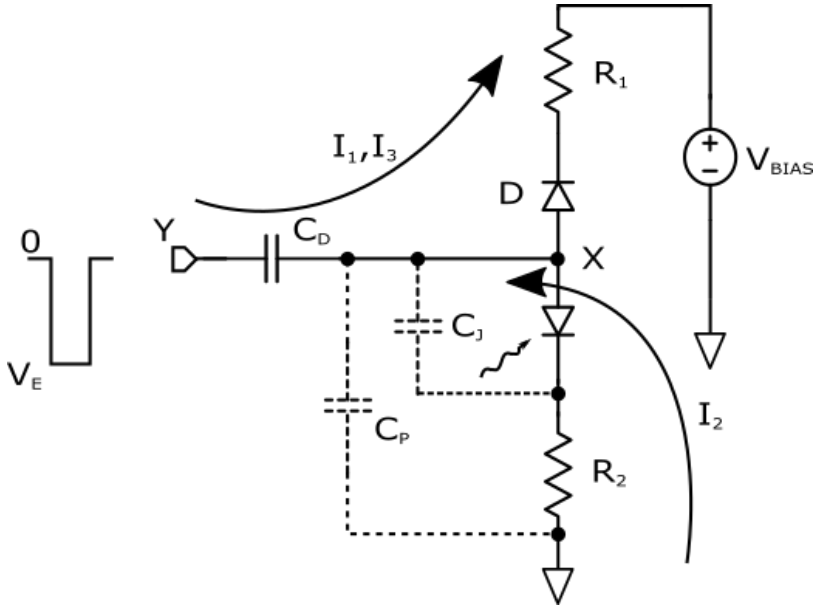

Figure 2-21 Schematic of a passive quenching circuit with gated operation presented in [53]

This circuit works as follows. Voltage source V_1 provides negative voltage bias somewhat lower that the breakdown voltage of the SPAD. Negative voltage pulse with the amplitude V_E provides the excess voltage needed to bring the detector to active state is AC coupled from the SPAD through capacitor C_D. When the voltage at node Y is 0, node X is charged to ~ V_1 by the current I_1 flowing through R_1, D_1 and C_D. When the voltage at the node Y changes to V_E, voltage at node X is also pulled down through C_D. After a short time delay caused by the charging of C_P and C_J, voltage at node X settles at V_X [53]:

$$V_X = V_1 + V_E \frac{C_D}{C_D + C_J + C_P} \tag{16}$$

If no avalanche has been triggered, the voltage at node X will return to V_1 at the end of the active phase. However, when an avalanche has been triggered during this phase, current I_2 will start through the SPAD, the resistor R_2 C_D and until the voltage at node X is approximately equal to V_E. This quenches

the detector. The quenching is done using a capacitor, instead of a resistor, thus the total charge of the avalanche current is limited to the capacitance of C_D. Resistor R_2 is then used to generate a voltage drop that can be sensed by the following circuitry. When an avalanche has occurred, current I_3 replaces charge lost from the parasitic capacitances and the coupling capacitor. The time interval needed to restore the voltage at the node X to ~ V_1 is given by R_1, C_D, C_J and C_P. This time constant sets the highest possible frequency with which the active and inactive cycles can be repeated and can be adjusted by C_D and R_1. With R_1 = 500 Ω, C_D = 27 pF and $C_J + C_P$ = 10 pF this time constant is equal to 18,5 ns.

This circuit has been validated with a photodiode from PerkinELmer, C30902S. V_1 was set to 231.8 V, voltage slightly less than the breakdown voltage of the detector. With a voltage pulse V_E equal to 8 V, quenching times of ~ 20 ns have been obtained.

In [54], single photons with a wavelength of 1,55 µm have been detected using gating operation. The authors utilized InGaAs/InP SPAD and a sinusoidal wave to operate as the gated signal. Together with a band elimination filter, AC noiseless avalanche pulses can be obtained. Authors report detection efficiency at 1,55 µm 10 - 30% and the counting rate of the setup 800 MHz.

Active and mixed active-passing quenching circuits are also used, because they can be easily adapted to work under gated operation. One way of achieving this is to switch the quenching transistor on and off by the gating-operation signal (for example an OR gate can be used with one of the inputs connected to the gating-operation signal, the second one to the signal that would be produced by the active quenching circuit to quench the avalanche and the output to the switch that quenches the avalanche). The only limitation in these circuit with regards to duration of the gated pulse and repetition rate would be the shortest time interval required to increase or decrease voltages to the desired values.

In this chapter, different approaches to quenching circuits have been summarized, examples for each provided together with respective experimental results.

3. Comparison of the quenching circuits

In previous chapters, an overview of the available detectors and quenching circuits has been provided. In this chapter, performance of some of the quenching circuits together with appropriate detector will be evaluated. Focus will be put on the discrete circuits and commercially available detectors. This of course imposes some limitation on the functionality for the reasons described in chapter 1.3. Two detectors will be picked together with two circuits. The circuits have been realized on a single PCB.

3.1 Detector selection

The overview of the available single photon detectors has been provided in chapter 1. Single-photon Avalanche diode has been selected as the optimal detector. They are easily implementable with the quenching circuit and also commercially available. Following a research of the market it has been found that two types of the diodes are mostly used, namely C30902 from Excelitas Technologies and SAP 300 from Laser components.

The C30902 SPAD is fabricated with a reach-through, double-diffused structure (Figure 3-1 a). As was already mentioned in Chapter 1.2.6, this kind of structure has much wider active area compared to planar diodes. Diode used in the experiment has an active photosensitive surface area with a diameter of 500 µm. The detector chip has been hermetically sealed and covered with a glass window in a T0-18 package (Figure 3-1 b), which has been slightly modified. There are two types of diodes in the C30902 family, namely C30902EH and C30902SH. C30902EH is the standard diode type and the C30902SH diodes have been specially selected for having extremely small dark-current and low noise. Their typical usage will be in applications with very small optical power (1pW and less). They can be operated both in linear mode (when V_{BIAS} is lower than the V_{BR}) with gain of 250 or more, or as a single photon counter in Geiger mode. In this case, detected photon ignites an avalanche of about 10^8 carriers [55].

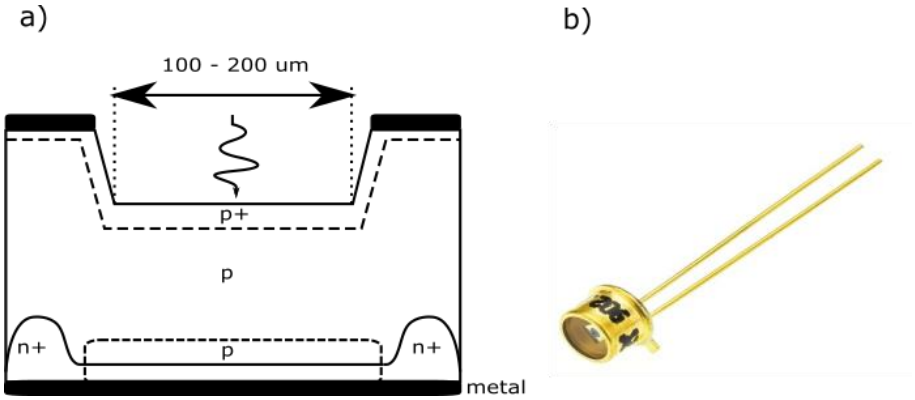

Figure 3-1 a) Schematic of a C30902 reach-through structure, b) picture of the diode [55]

The key parameters of C30902EH diode can be found in the datasheet [55]. These diodes feature high detection efficiency at wavelengths between 400 nm and 1µm with a peak value of 77 % at 830 nm. Typical time response of these diodes is 0.5 ns and they can be operated in a temperature range from -40 °C to +70 °C. Typical breakdown voltages of these diodes are above 220 V. Dark current at 0 °C is 15 nA, dark count rate at 5% photon detection probability (830 nm) being 800 counts per second. All of the C30902EH parameters are shown tabularly in Table 3-1.

Parameter	**Min**	**Typ**	**Max**	**Units**
Photosensitive area		0.2		mm^2
Field of view		90		Degrees
V_{BR}		225		
Temperature coefficient of reverse bias voltage for constant gain	0.5	0.7	0.9	V/°C
Gain		150		
Responsivity @ 830 nm	70	77		A/W
Quantum efficiency @ 830 nm		77		%
Dark cuirrent @ 0 °C		15		nA
Capacitance		1.6	2	pF

Table 3-1 C30902EH key specifications

The second chosen diode is the SAP 300 from Laser Components. The structure and the package of the diode are very similar to that of C30902EH and shown in the Figure 3-2 [56]. It is a reach-through structure which is illuminated from the back side. However, there is a difference between the thicknesses of the conversion regions, situated between the two p^+ layers. It is quite thin in the case of SAP 300, measuring about 25 µm. This is compensated by the metal coverage of the junction side. This metal layer serves as a mirror, effectively doubling the conversion area. This improves the

quantum efficiency in the red spectrum. To further improve the photon absorption, antireflection (A/R) coating is applied on the area through which the photons enter the device. Having a short conversion region introduces the advantage of smaller timing jitter, as the carriers have higher velocity. SAP 300 can naturally be used in linear mode with gains up to 250, or in Geiger mode. The diode can be supplied in a modified TO-46 package (without cooling), named SAP 300Sx, or with TEC cooling (SAP 300Tx).

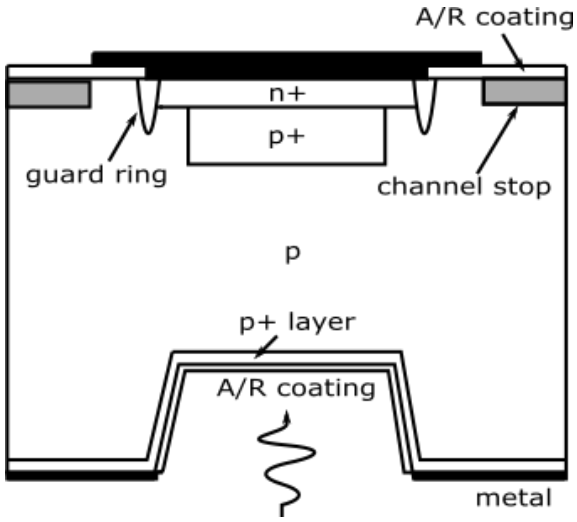

Figure 3-2 Schematic of a SAP 300 structure [57]

SAP 300 has V_B that is almost twice as small as the one of C30902EH, only about 125 V. The SAP 300 operates in wavelengths from 400 to 1100 nm, with a peak sensitivity at 700 nm and quantum efficiency close to 86 %. Diameter of this SPAD's active area is about 500 µm, same as C30902EH. Responsivity at 830 nm is 110 A/W. Quantum efficiency at this wavelength is 65 %. Dark current of the uncooled version should be around 200 pA. Dark count rate at 5% photon detection probability at 830 nm wavelength and 22 °C should be lower than 15 000 cps. All of the key specifications of SAP 300Sx are shown in Table 3-2.

Parameter	Min	Typ	Max	Units
Photosensitive area		0.2		mm^2
Field of view		100		Degrees
V_{BR}		125		
Temperature coefficient of reverse bias voltage for constant gain		0.35		V/°C
Gain		250		
Responsivity @ 830 nm		110		A/W
Quantum efficiency @ 830 nm		65		%
Dark current @ 0 °C		200		pA
Noise current, i_n^2		90		$fA/Hz^{1/2}$
Capacitance		3.3		pF
After-pulse Ratio at 5% Photon Detection Probability (830 nm)		2	15	%
Dark count rate at 5% photon detection probability (830 nm, 22°C)		10000	15000	cps

Table 3-2 SAP 300Sx key specifications

3.2 Circuit simulations

To examine the circuit functionality and to ensure proper performance of the circuit, they will be first tested in a simulator environment. LTspice has been chosen as the software platform to perform these checks, as it is free to use for non commercial purposes (freeware). It has a graphical interface, but text-file netlists can also be used for simulations. Waveform viewer is also included. LTspice includes most models of LinearTechnology operational amplifiers, MOSFETs, passive components and switching regulators. Models from other companies can also be imported. All basic analysis like DC, AC, transient and noise can be performed.

As was already mentioned, 3 different circuits will be tested, each with both SAP 300Sx and C30902EH photodiodes. In this section, spice SPAD model will be introduced that can be modified to fit both diodes and basic functionality of the circuits will be checked.

3.2.1 SPAD spice model

In order to predict the performance and simulate the behaviour of quenching circuits as accurately as possible, detailed model of the photodiode detector must be deployed. The simplest model of a SPAD is a capacitor in parallel with a current source. This model was introduced in [58] and can be seen in Figure 3-3. Parasitic capacitances are also included in this model and represented by junction capacitance C_{AC}, parasitic capacitance from cathode to substrate C_{CS} and anode to substrate C_{AS}. Diode resistance R_D is the sum of resistances of neutral regions and space charge resistance. It depends strongly on the device structure and is around 500 Ω for SPADs with thick (10-30 µm) depleted regions and wide active areas, which is the case for both our SPADs, or up to few thousands ohm for photodiodes with relatively small active areas and thin depleted regions (0.5 – 1 µm) [41].

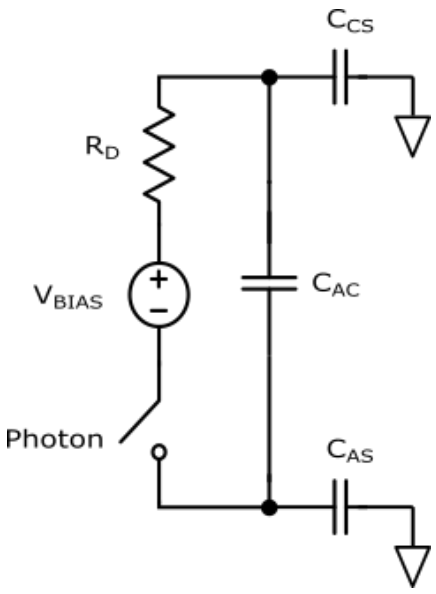

Figure 3-3 Schematic of basic SPAD spice model

Avalanche ignition is simulated by closing the n-MOS switch (Photon). Before the diode voltage changes the diode current reaches its peak value. The current then discharges the capacitors, decreasing the current and the voltage on the diode exponentially. Time dependent current through the diode, $I_D(t)$, can be written as (Chapter 1.3):

$$I_D(t) = \frac{V_D(t) - V_B}{R_D} = \frac{V_E(t)}{R_D} \tag{17}$$

Where $V_D(t)$ is the time dependent voltage across the diode. As the V_D decreases, I_D intensity also declines and the number of charge carriers that crosses the depletion region is small. With the

avalanche process being a statistical process, none of the small amount of carriers that cross the depletion region may impact an atom, stopping the avalanche multiplication. This probability of carrier impacting a crystal atom approaches zero when $I_D \approx 100$ µA (this has been experimentally proven in [41]). It can be therefore assumed in the model, that if the diode current I_D drops below 100 µA, the avalanche will stop by itself. When this happens, the n-MOS switch in the Figure 3-3 opens and the parasitic capacitances C_{AC}, C_{AS} and C_{CS} slowly recharge. Based on the resistances on the cathode and anode side of the SPAD, one of these capacitances can be neglected (the one with the small resistance on its side, see chapter 2.1) and the recharge time constant is than given by the sum of C_{AC} and the non-neglected capacitance, divided by R_D.

However, this model is not sufficient to simulate the detector behaviour during triggering, active-quenching, self-quenching and recovery. The new enhanced model of the SPAD was introduced in [59]. In the previous model, the incident photon was simulated though an external stimulus on a Photon switch. The length of this stimulus determined the quenching time and other properties, not the actual quenching circuit. Passive quenching could have been roughly estimated, but estimation of the active quenching behaviour was almost impossible. Also the effect of different excess voltages leading to different quenching times was neglected. As discussed in the section above, the diode should quench when the I_D drops below 100 µA, which was also impossible to realize in the old model. The new SPAD model from [59] is depicted in Figure 3-4.

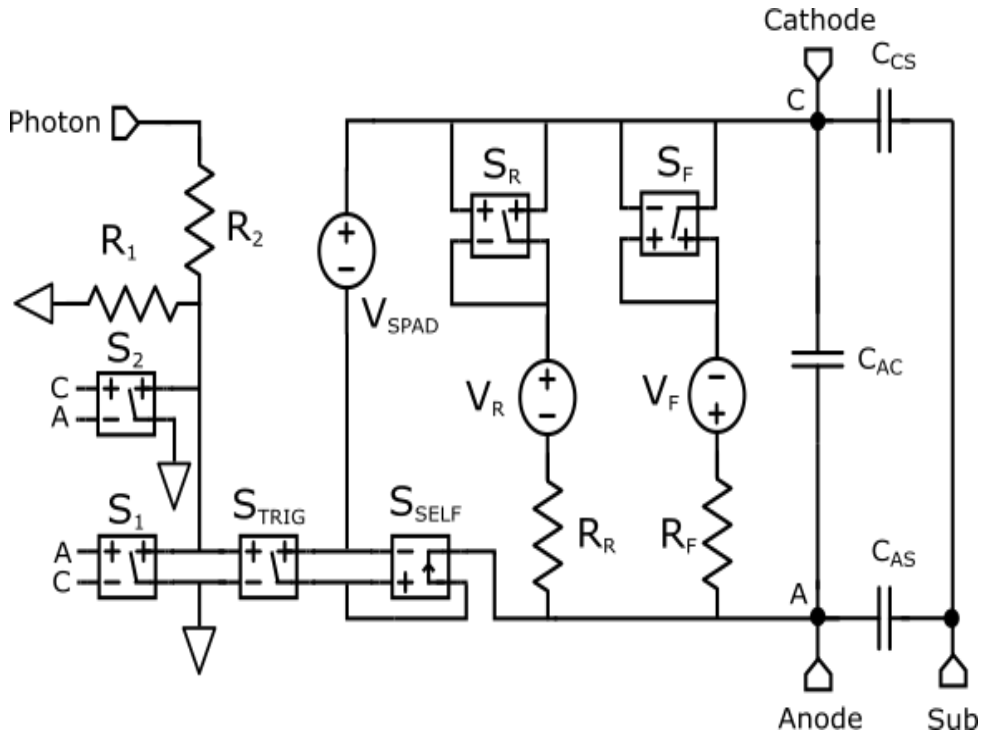

Figure 3-4 Schematic of an enhanced SPAD model

C_{AC}, C_{AS} and C_{CS} represent the same capacitances as in the previous model. Depending on the chosen SPAD, the substrate pin (Sub) can be left floating or connected to proper node. The I-V curve of the diode can be modelled realistically through a piece-wise linear approximation. In LTspice, voltage dependent voltage source V_{SPAD} has been used. To specify the transfer function, look-up table is used, which is a list of pair of numbers. The second value indicates the output voltage when the control voltage is equal to the first value. The values between the numbers in the look-up table are extrapolated. After the measurement of the diode I-V characteristic, the curve can be approximated very accurately. However, when the circuit is being designed for an unknown diode, these values have to be estimated with the help of the datasheet.

The operation of the model circuit can be described as follows. S_F switch should simulate the forward bias operation and is described by the means of DC voltage source V_F in series with R_F, thus representing a linear I-V curve. The switch S_F has the threshold set to 0 V. When the anode voltage rises above cathode voltage, but its still lower then the voltage set in the voltage source V_F, the switch is opened and no current flows through the resistor R_F. The switch closes when the voltage difference rises above V_F and the current starts flowing. Second breakdown is modelled similarly by the means of voltage source V_R, resistor R_R and switch S_R. When the second breakdown voltage V_R is exceeded, the device goes into permanent breakdown and the input pin Photon in disabled by the S_2 switch with threshold set to V_R.

With the diode being biased above its breakdown voltage, in Geiger mode, switches S_F and S_R are opened. The incident photon is simulated again by the means of a short pulse on Photon pin. The user can apply either current or voltage pulse (because of resistors R_1 and R_2). This pulse closes the S_{TRIG} switch. The current rises quickly to its peak value. This opens the current controlled switch S_{SELF} (with a threshold value set to 100 μA). This ensures that the avalanche will be self sustained even when the S_{TRIG} switch opens, provided that the current does not drop below 100 μA. Switch S_1 (with threshold set to $-V_B$) ensures that the avalanche can only be triggered by the Photon pulse when the device is biased above its reverse breakdown voltage.

To develop the enhanced model to its full potential, the R_D, C_{AS}, C_{CS} and C_{AC} parameters have to be estimated as close to reality as possible. A good starting point would be the datasheet of the diode, but since every manufacture piece may have slightly different parasitic capacitances and resistances extracting these parameters for used diode from the measurements would improve the accuracy a lot. Additionally, some parameters like R_D may not be found in the datasheet. For example, R_D value has to be taken into account to properly set the comparator value for the ignition readout, since it forms a voltage divider with the external resistor. Parasitic capacitances, on the other hand, determine quenching and reset times in all kinds of quenching circuits. Measuring the diode resistance is not very

difficult, as it can be done by the means of an I-V curve tracer. Extraction of junction and stray capacitances may prove a bit more difficult. Since the capacitance values may be very small, even below 1 pF, very precise capacitance meter is needed. The method of extraction proposed in [59] is to measure the capacitance between two terminals and then move clockwise to other two (between anode, cathode and substrate) to obtain 3 capacitance values as follows [59]:

$$C_{SPAD1} = C_{AC} + \frac{C_{AS}C_{CS}}{C_{AS} + C_{CS}} \quad (18)$$

$$C_{SPAD2} = C_{AS} + \frac{C_{AC}C_{CS}}{C_{AC} + C_{CS}} \quad (19)$$

$$C_{SPAD3} = C_{CS} + \frac{C_{AS}C_{AC}}{C_{AS} + C_{AC}} \quad (20)$$

C_{AC}, C_{AS} and C_{CS} are obtained by solving this system of equations.

3.2.2 LTspice simulations

After acquiring an accurate model of the SPAD, quenching circuit simulations can be started. As was already stated, two types of quenching circuits will be simulated and compared- passive quenching circuit and active quenching circuit. In this chapter all of the circuits will be examined to ensure proper functionality, before proceeding to PCB design.

3.2.2.1 Passive quenching circuit

The core of a passive quenching circuit is a large resistor in series with the diode (chapter 2.1). The implementation in LTspice is shown in Figure 3-5. The diode model is biased at voltage V_R. After voltage source V_photon1 produces a voltage pulse which closes the S_TRIG switch. When the current limiting resistor R4 is chosen sufficiently large, the avalanche will cease by itself, as the current flowing through the S_SELF will be lower than its threshold set to 100 µA. This current pulse is picked up by a small resistor R5 and switches the comparator U2. Following a comparator, custom-made pulse shaper has been developed by a D-type flip flop. The output pulse length can be adjusted by increasing or decreasing the A2 delay.

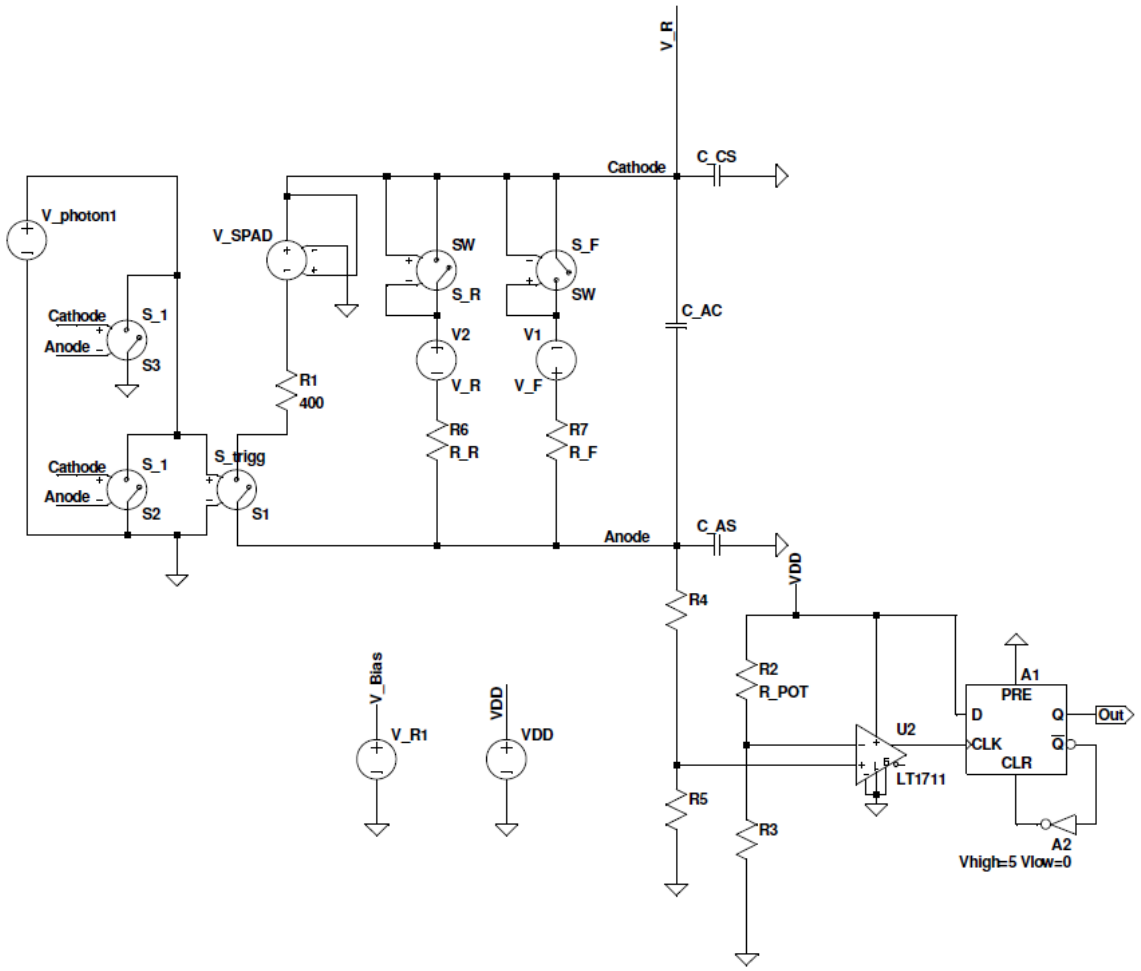

Figure 3-5 Schematic of a passive quenching circuit in LTspice with current limiting resistor at the anode

All values of the passive components and voltage sources are listed in Table 3-3. V_B of the diode was set to 225 according to datasheet and the diode resistance was estimated to 400 Ω. With V_E = 8 V, maximal current flowing through the diode is limited to 36.3 µA, well below 100 µA and thus the avalanche should quench immediately. Incoming photon was simulated by setting the V_photon1 voltage source to 1.25 V after 2 µs delay. Length of the output pulse was set to 20 n with A2 inverter. Voltage at the anode and output current through resistor R4 can be seen in Figure 3-6. After the avalanche, voltage recovers with a time constant given by resistors R4, R5 and parasitic capacitance:

$$\tau = (R4 + R5) * (C_{AC} + C_{AS}) = 440.9\,ns \tag{21}$$

This is also confirmed by the simulation, as seen on the Figure 3-6.

Component	Value	Component	Value
V_R1	233 V	R4	220 kΩ
VDD	5 V	R5	440 Ω
V_Photon1	1.25 V (after 2µs delay)	R3	100 Ω
C_AC	1.6 pF	R_POT	50 kΩ
C_AS	0.4 pF	C_CS	0.4 pF

Table 3-3 : Passive component and voltage source values for simulation of passive quenching circuit

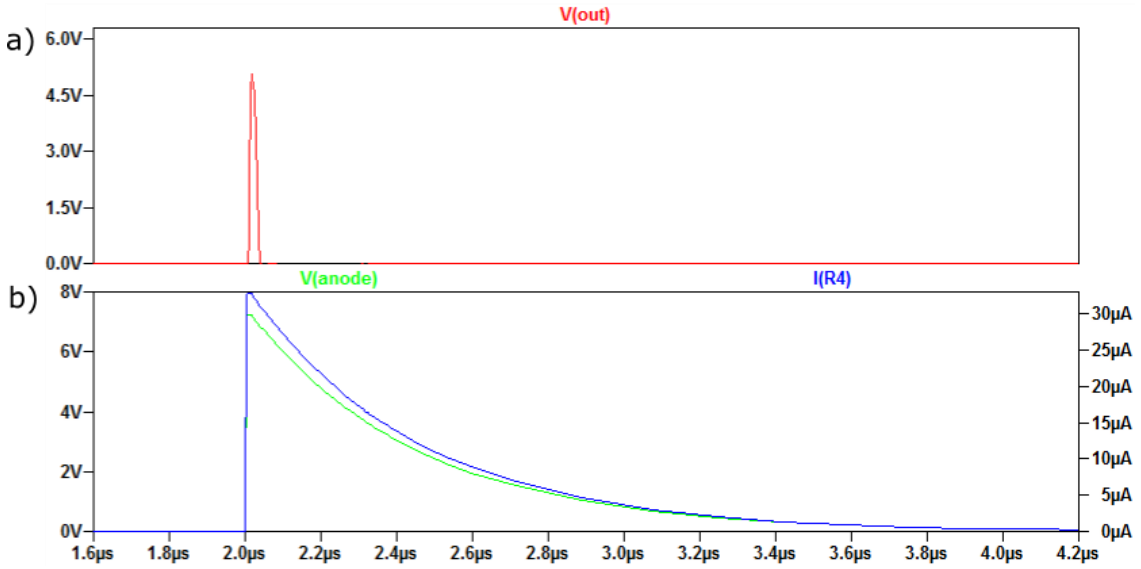

Figure 3-6 Passive quenching circuit with resistor at the anode simulation results: a) Voltage at the output b) Voltage at the anode and current through R4

To examine the influence of the parasitic capacitance on the passive quenching circuit, small modification of the presented circuit will be made. The large quenching resistor will be connected to the cathode of the diode, as opposed to the anode. Only difference between these two circuit configurations is the different parasitic capacitance of the diode, and hence different time constant. The whole circuit can be seen in Figure 3-7. Voltage and current curves are shown in Figure 3-8. Time constant stays the same – parasitic capacitances are not listed in the datasheet and have been both estimated to the same value. Passive components and voltage source values are listed in Table 3-3.

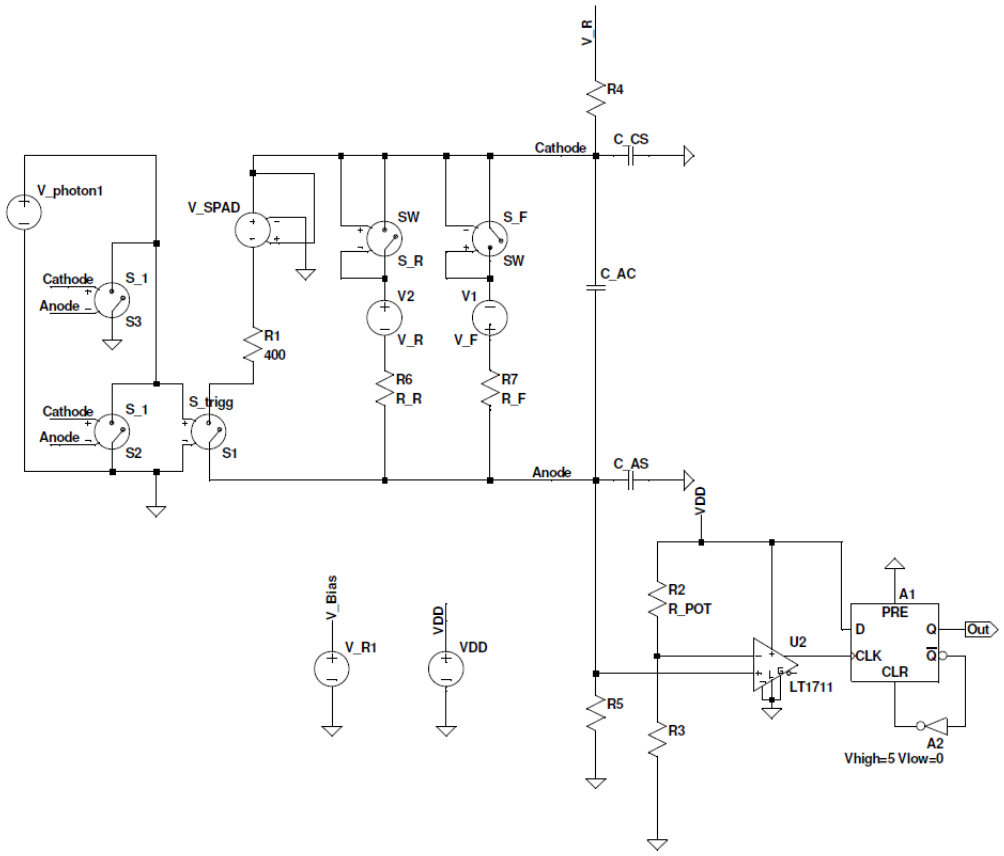

Figure 3-7 Schematic of the passive quenching circuit with quenching resistor at the cathode

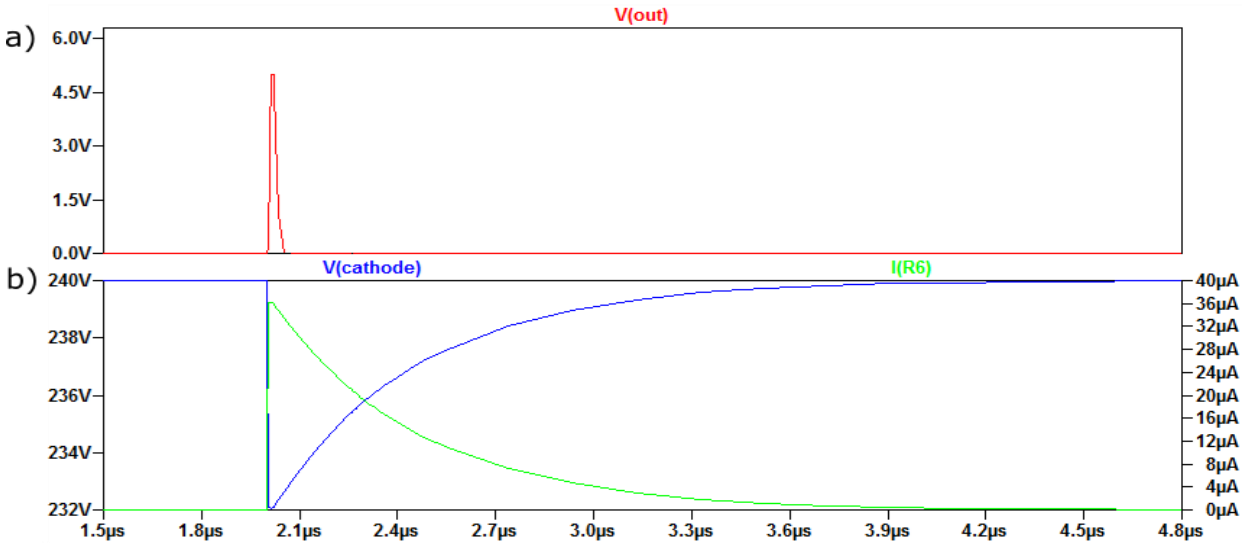

Figure 3-8 Passive quenching circuit with resistor at the cathode simulation results: a) Voltage at the output b) Voltage at the cathode and current through R4

3.2.2.2 Active quenching circuit

Last quenching circuit to be examined is the active quenching circuit. As a reference, circuit presented in [60]. It is an improved version of the circuit discussed in chapter 2.3 ,Figure 2-8. Schematic of this improved circuit is shown in Figure 3-9. The main difference between these two circuits is that the capacitive coupling of the quenching signal has been replaced with galvanic one. After a photon arrival is simulated and s_trigg switch closed, voltage at the positive input of the comparator rises above negative input (this voltage can be set by the potentiometer) and the comparator switches. Via the inverting output of the comparator, the N-MOS switch is closed, and the quenching voltage step is transferred via the R2 resistor to the anode of the SPAD, quenching it. After a delay time introduced by the A2 inverter, negative output of the comparator goes above the positive one and the N-MOS switch is closed again. Passive parameter and voltage source values are listed in Table 3-4. Simulation results, namely voltage at the output and anode and current through resistor R1 can be seen in Figure 3-10.

Parameter	Value	Parameter	Value	Parameter	Value
V_R1	233 V	C_CS	0.4 pF	R5	100 Ω
VDD	5 V	C_AS	0.4 pF	R_POT	75 kΩ
V_Quench	30 V	R2	1 kΩ	C1	1 nF
C_AC	1.6 pF	R3	300 Ω	L1	1.8 nH

Table 3-4 Passive parameter and voltage source values for the active quenching circuit simulation

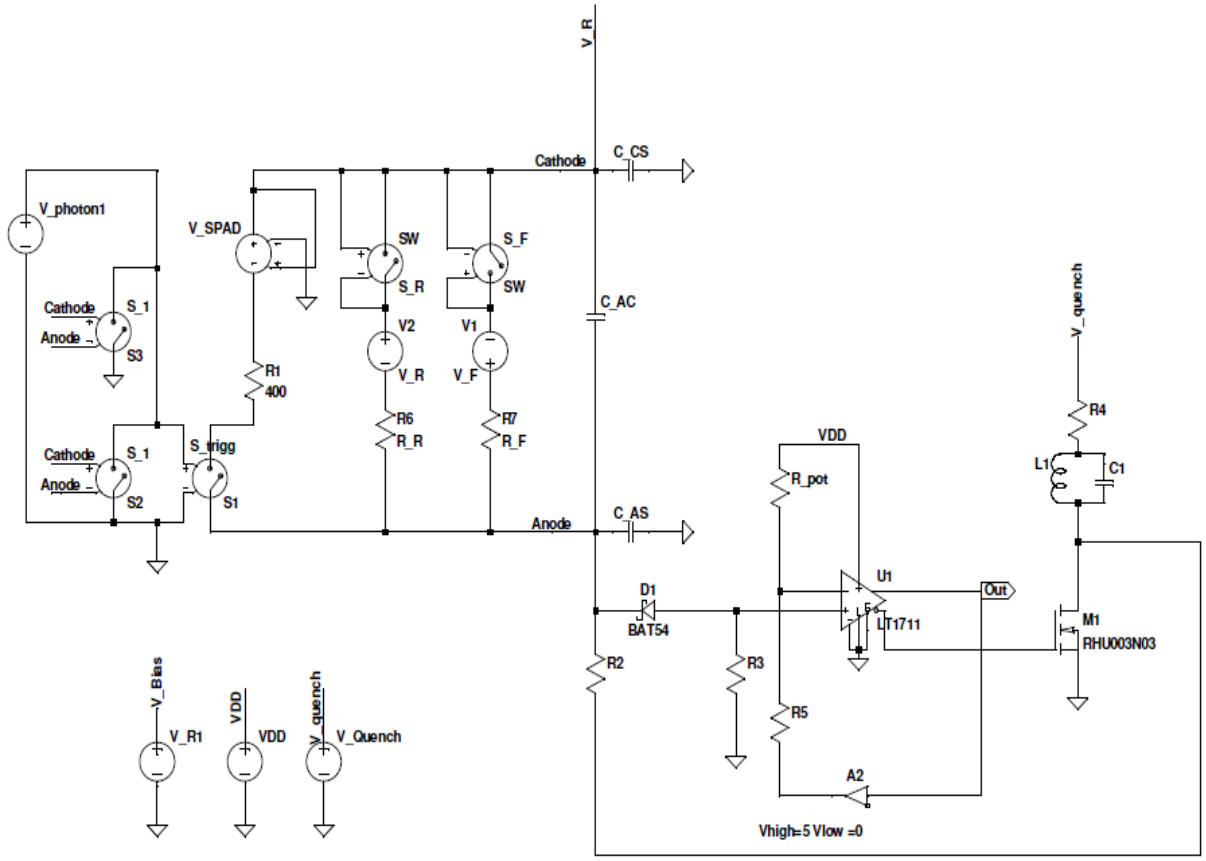

Figure 3-9 Schematic of an active quenching circuit

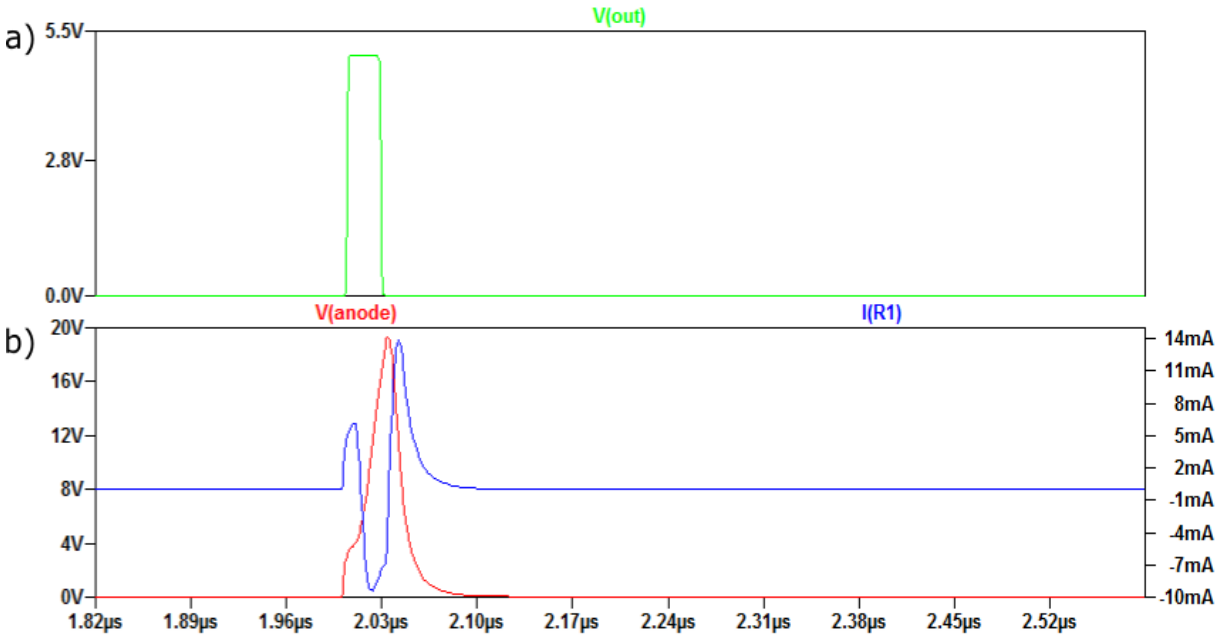

Figure 3-10 Active quenching circuit simulation results: a) Voltage at the Output b) Voltage at the anode and current through R1

3.3 PCB Design

All 3 circuits have been manufactured on a single PCB. The reason for this is to keep the production costs low. However, to be able to use and measure only one circuit at a time, some modifications to the circuits were necessary. Both the schematic of the circuit and layout were drawn in the PCB software development tool EAGLE. Complete schematic with all four circuits can be seen in Figure 3-11.

Passive quenching circuits are on the right side of the SPAD, active quenching circuit on the left. The circuit to be measured is selected with resistors R1, R2, R6 and R21. With resistors R1 and R2, passive quenching with quenching resistors on cathode and anode may be chosen, while the value of the second resistor is 0 Ω. Resistors R6 and R21 are not soldered. To select the passive quenching circuit with active reset, resistor R1 is 0 Ω, R2 220 kΩ and R6 0 Ω. To select active quenching circuit, R1 and R21 are 0 Ω and the other two are not soldered. To provide a possibility to adjust the threshold of the comparator according to the actual SPAD current, as this was just estimated, 2 potentiometers BOURNS 3296P have been used with max. resistance of 100 kΩ. Two ultrafast, rail-to-rail comparators, LT1711 were chosen to provide fast response, mainly for the active circuits.

For the D-type flip-flop, single positive edge triggered flip-flop with clear and preset was chosen (SN74LVC2G74-EP). Clear pin input is actually inverted, hence no inverter in the delay loop was needed. As a delay, IC from MAXIM, DS 1100 was selected. This is a delay line with 5 output pins, which means that the delay may be altered and adjusted to the best circuit performance. It should also be able to drive 50 Ω load (output) with no problems. IC with a total delay of 25 ns was used for the active quenching circuits (delays of 5, 10, 15, 20 and 25 ns) and 500ns (100, 200, 300, 400, 500 ns delays) for the passive quenching with active reset. To each output pin of the delay, 0 Ω resistor may be soldered to select the appropriate output, while others will be left floating.

To power pins of all ICs, 100 nF capacitors were connected to smoothen the supply voltage. The readout electronics can be connected to the PCB with SMA connectors. The outputs from the SPAD anode, comparator, and the flip-flop may be inspected with an oscilloscope. Supply voltage is connected to the PCB via banana connectors. For the N-MOS switches, input capacitance has to be considered, as too high input capacitance could load the outputs and the leading and falling edges of the output pulse would not be very sharp. For this reason, N-MOS RHU003N03FRA from ROHM with extremely small input gate capacitance, only 20 pF at V_{GS} 0 V was chosen. The values of all passive components are listed in

Parameter	Value	Parameter	Value	Parameter	Value
R1	0 / 220 kΩ	R12	0 Ω / -	C1	100 nF
R2	0 / 220 kΩ	R13	0 Ω / -	C2	100 nF
R3	440 Ω	R14	0 Ω / -	C3	100 nF
R4	100 Ω	R15	0 Ω / -	C4	1 nF
R6	0 Ω / -	R16	0 Ω / -	C5	2.2 µF
R7	1k Ω	R17	100 Ω	C6	100 nF
R8	300 Ω	R18	0 Ω / -	C7	100 nF
R9	100 Ω	R19	0 Ω / -	C8	100 nF
R10	0 Ω / -	R20	0 Ω / -	C9	100 nF
R11	0 Ω / -	R21	0 Ω / -	C10	100 nF

.

The PCB will be produced by manufacturer Seeed Studio. Design rules can be downloaded at the Seeed Studio website and imported to EAGLE, to make sure that the board will be produced correctly. Layout of the PCB with individual layers can be found in Appendix A. To utilize power and ground planes, 4-layer board was selected. This also allows the conduction wires to be thinner, as the distance between the ground plane and the wire is smaller. The ideal wire thickness has been calculated with software TXLINE. This software takes the skin effect into account. The thickness of the FR-4 between the first layer, used for routing and second layer used as ground plane is 0.2 mm, copper thickness 35 µm, and the relative permittivity of the FR-4 material is around 4. Maximal frequency was estimated to 50 MHz. After these parameters have been input into the software, wire width of 15 mil (0.371 mm) was obtained.

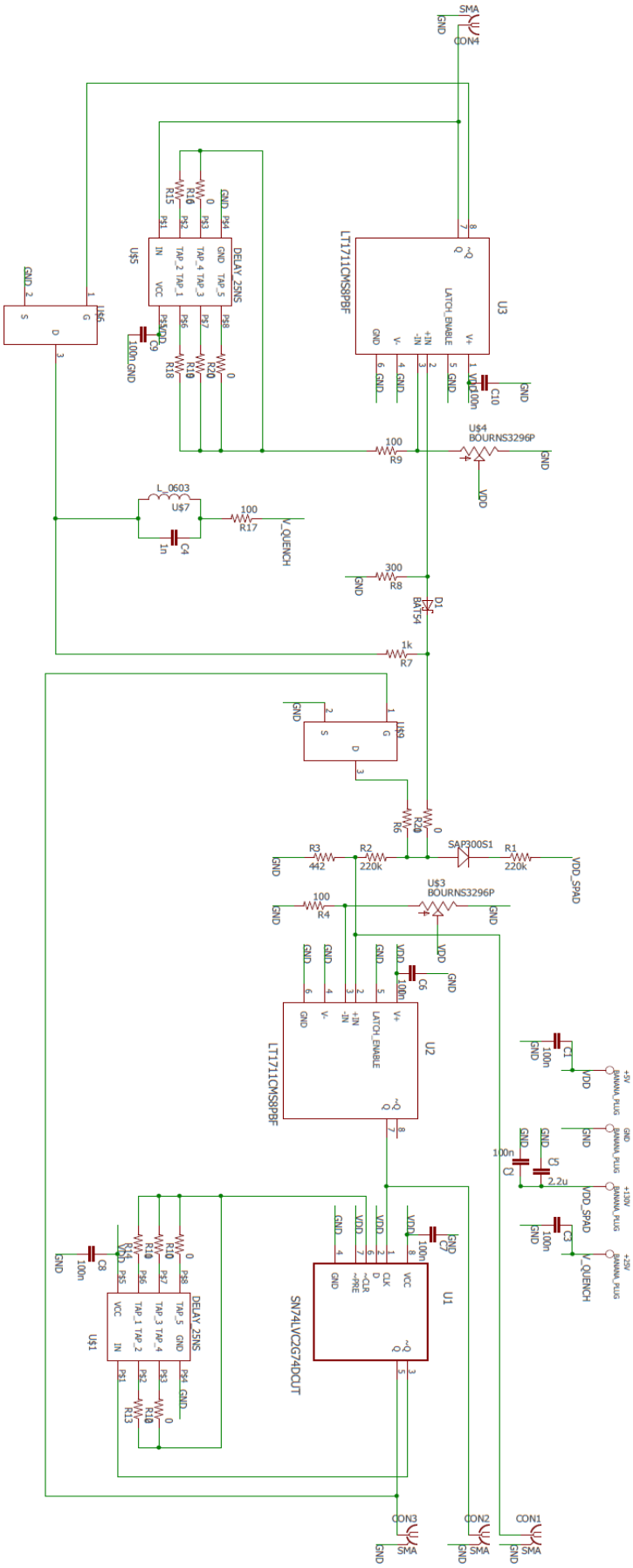

Figure 3-11 Schematic of the PCB with all circuits from EAGLE

Parameter	Value	Parameter	Value	Parameter	Value
R1	0 / 220 kΩ	R12	0 Ω / -	C1	100 nF
R2	0 / 220 kΩ	R13	0 Ω / -	C2	100 nF
R3	440 Ω	R14	0 Ω / -	C3	100 nF
R4	100 Ω	R15	0 Ω / -	C4	1 nF
R6	0 Ω / -	R16	0 Ω / -	C5	2.2 µF
R7	1k Ω	R17	100 Ω	C6	100 nF
R8	300 Ω	R18	0 Ω / -	C7	100 nF
R9	100 Ω	R19	0 Ω / -	C8	100 nF
R10	0 Ω / -	R20	0 Ω / -	C9	100 nF
R11	0 Ω / -	R21	0 Ω / -	C10	100 nF

Table 3-5 Table of PCB passive component values

3.4 Measurement setup

To compare the circuits and the SPADs, some of the parameters crucial for the detector performance have been measured: dark count rate, afterpulsing probability and the dead time. The picture of measurement setup can be seen on Figure 3-12.

Figure 3-12 Picture of the measurement setup

For the afterpusilng probability and dark count rate measurements, the PCB was put inside an opaque box and covered with an additional one to ensure total darkness and prevent any photons to reach the active area of the SPAD. The PCB was connected to an embedded device myRIO from National Instruments. It includes, among other features, analog inputs and outputs, digital I/O lines, Xilinx FPGA and a dual-core ARM Cortex-A9 processor. It can be programmed with LabVIEW software from NI. MyRIO was connected to a computer via USB cable. Two voltage sources, electrometer Keysight B2987A and power supply Hameg HM7042-3 were also connected to the PCB to provide the necessary supply voltages. The electrometer can output up to 1000 V DC voltage and was used to bias the SPAD above breakdown voltage and was also responsible for measuring the SPAD current. The power supply supplies then 5 V voltage for the ICs and also the quenching voltage of 25 V for the active quenching circuit.

As was already mentioned, LabVIEW software was used to program the Xilinx FPGA on myRIO. The device carries out the measurement and saves the measured data on the computer hard drive as txt file. Txt file is than processed in Matlab software to finally obtain the afterpulsing probability and dark count rate.

3.5 Measurement results

3.5.1 Passive quenching circuit with quenching resistor at the SPAD cathode

For the measurement of passive quenching circuit with resistor at the SPADD cathode, resistors R2 and R6 (see schematic on Figure 3-11) were not soldered, and R3 value was 430 Ω. R1 resp. R2 value was 560 kΩ. Initially intended value of 220 kΩ was not enough to quench SPA300S2 beacause of much higher avalanche current of this device. 100 kΩ Potentiometer was used to adjust the threshold value of the comparator.

Voltage curves at the anode of the SPAD, measured at CON1 (Figure 3-11) with 1 MΩ input Lecroy Waverunner 204Xi oscilloscope can be seen in Figure 3-13. Voltage curves for both SPADs are present. Both devices were biased 5 V above the V_{BR}: V_{BIAS} for SAP300S2 was 162 V and V_{BIAS} for C30902SH was 236 V. Voltage peak value is ~ 126.5 mV for SAP 300S2 and ~ 79.9 mV for C30902SH. SAP300S2 produces a narrower and higher peak, which implies higher avalanche current. Rise time (10 – 90 %) can also be read off the Figure 3-13: 11.6 ns for C30902SH and 4.7 ns for SAP300S2, which is about 2.47 times faster.

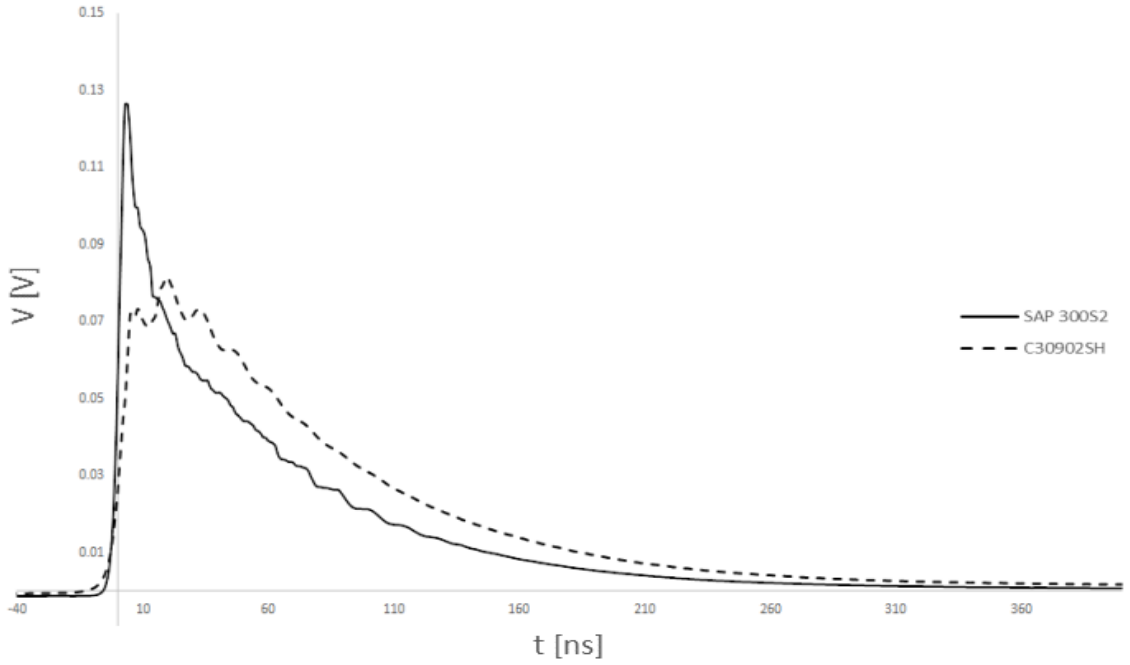

Figure 3-13 Voltage curve at the anode of the SPADs for passive quenching circuit with resistor on the cathode

Dark count rate was measured as follows: the bias voltage of the SPAD was stepped from voltage lower than the breakdown voltage, V_{MIN}, to voltage V_{MIN} + 15 V in 1V steps. For every voltage step, 100 measurement cycles were done to obtain a representative value for the dark count rate. The SPAD was connected to a metal heatsink, but the temperature was not otherwise controlled. Dark count rate for both diodes can be seen in Figure 3-14. C30902SH has dark count rate at 5 V about 8 kHz higher.

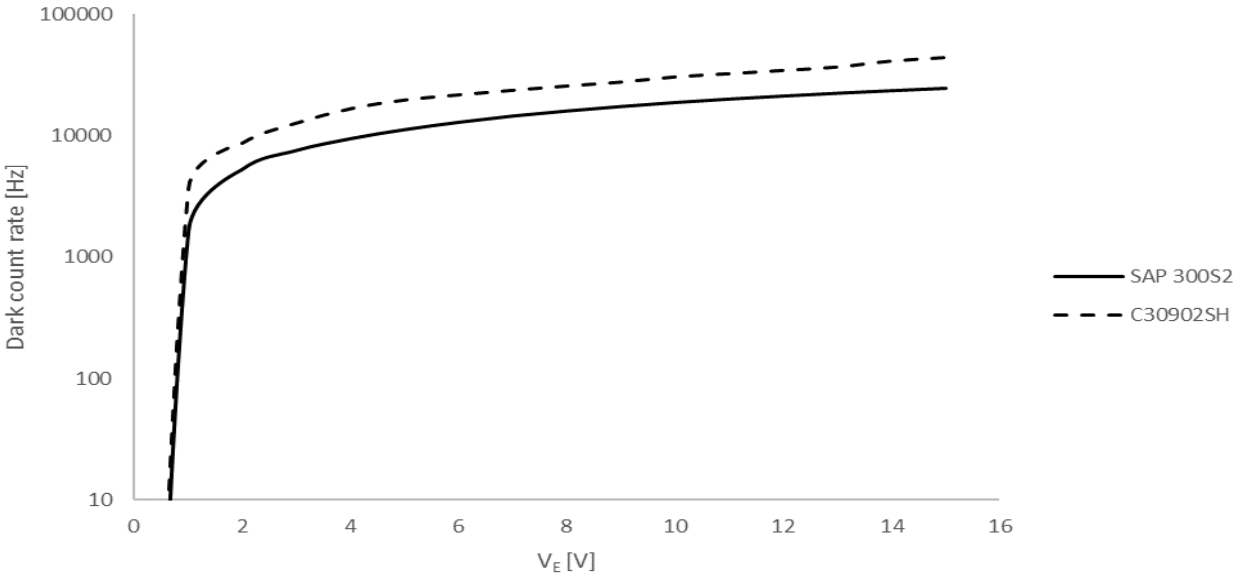

Figure 3-14 Dark count rate vs V_E for the passive quenching circuit with quenching resistor on the cathode

To measure the afterpulsing, inter-arrival time histogram method was measured [61]. In this method, time distance between the rising edges of the avalanche pulses are examined. This method can be explained using Figure 3-15. Afterpulses cease after a specific time, called τ in the figure. A fitting curve, that extends the number of pulses after this time to the time 0 distinguishes between regular dark counts and afterpulses. It should be noted that the number of pulses is in logarithmic scale.

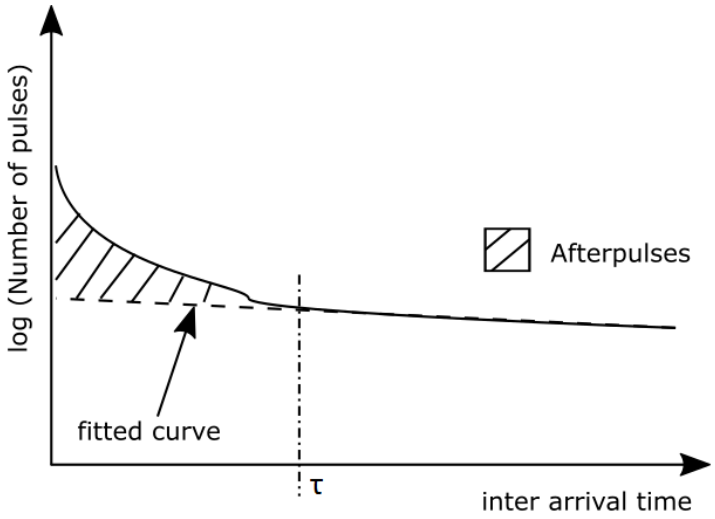

Figure 3-15 An example of inter arrival time histogram method for the afterpulsing acquisition

Afterpulsing probability was acquired in the following way: the bias voltage was swept again from V_{MIN} to voltage V_{MIN} + 15 V with a step of 1 V. Number of pulses for each voltage step was measured in 100 cycles, and the time distance of the pulses was recorded. Afterwards a graph similar to Figure 3-15 was examined and the value τ extracted for every voltage step and an integral of the extracted curve from 0 to τ was taken. Afterpulsing probability was finally obtained when the area under the fitted curve was substracted from this integral.

Such a graph can be seen in Figure 3-16 for C30902SH and two V_E voltage values, 5 and 10 V. The curve differs from the one in Figure 3-16. The reason is that the dead time in passive quenching circuit is not clearly defined and is subject to statistical variations. As a result, pulses start to occur at some minimal inter arrival time, then saturates and finally starts to decrease again. Afterpulsing in Si diodes occurs only up to a few hundreds of nanoseconds by room temperature, the minimum dead time (given mainly by the large current limiting resistor, as explained in Chapter 1.3) of this circuit is much higher, thus the afterpulsing probability is practically 0 %.

When the results from Figure 3-16 (C30902SH) and Figure 3-17 (SAP 300S2) are compared, results are almost identical. Minimal dead time of the circuit with both diodes is in the range 670 ns – 900 ns.

Indicating only a small difference between the device capacitances. Graphs for every V_E looks similar to those in Figure 3-16 and Figure 3-17 for both diodes. Afterpulsing probability for the whole V_E range examined is also 0 % for both diodes.

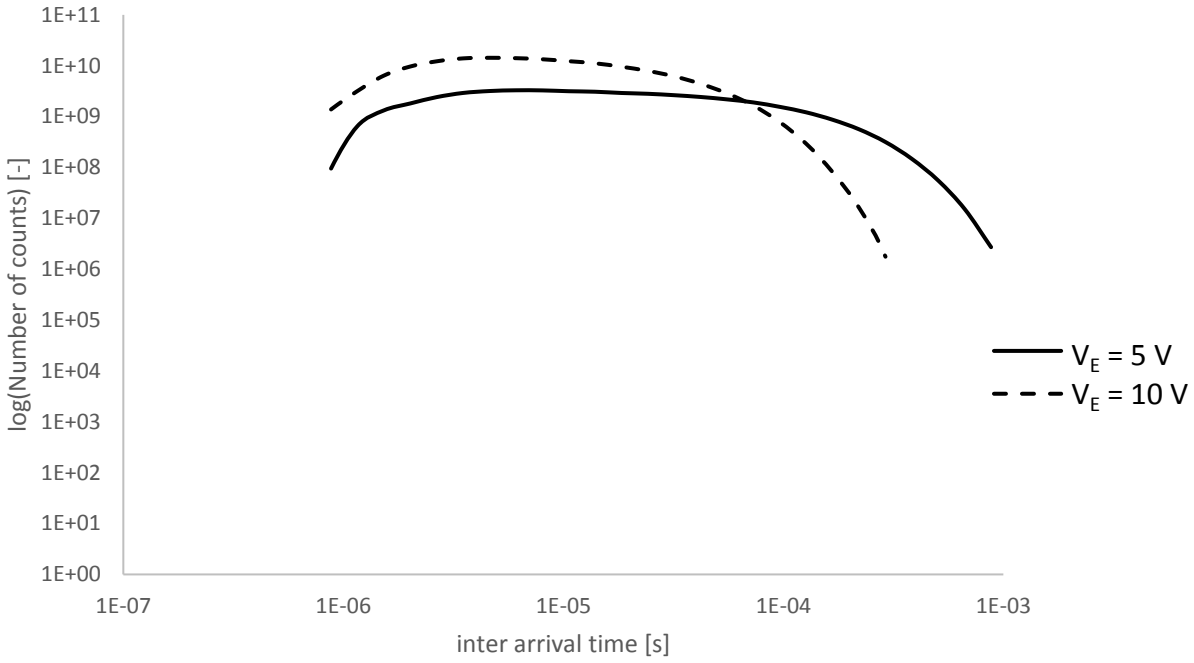

Figure 3-16 Number of counts vs inter arrival time (C30902SH)

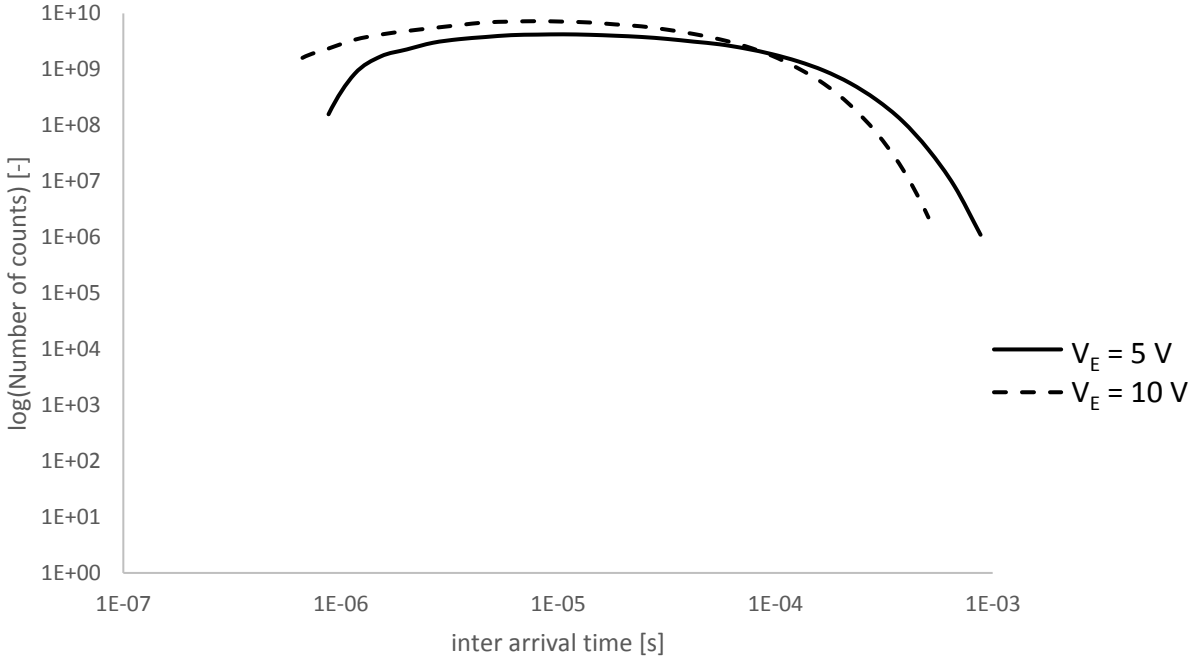

Figure 3-17 Number of counts vs inter arrival time (SAP 300S2)

3.5.2 Passive quenching circuit with quenching resistor at the SPAD anode

Measurements were done the same way as in the previous chapter, with the difference that the value of resistor R2 was 560 kΩ and R1 0 Ω. This kind of setup is not very beneficial for pure passive quenching circuit, as the large resistor limits the avalanche current of the SPAD as well and the voltage peak at the comparator is much smaller. However, this kind of circuit is well suited for passive quenching circuits with active reset, presented in Chapter 2.2. With the addition of some control logic, the current limiting resistor can be bypassed with a switch.

Voltage curves at the input of the comparator U2 (Figure 3-11) for V_E = 5 V can be seen in Figure 3-18. At this overvoltage, only 2.27 mV peak is produced at the pick-up resistor for C30902SH. Voltage peaks produced at the V_E = 1 V and lower cannot be detected at all. This is a significant drawback of the circuit. Peak values for both diodes are almost identical, as well as the rise times (10 - 90%) which is equal to 120 ns.

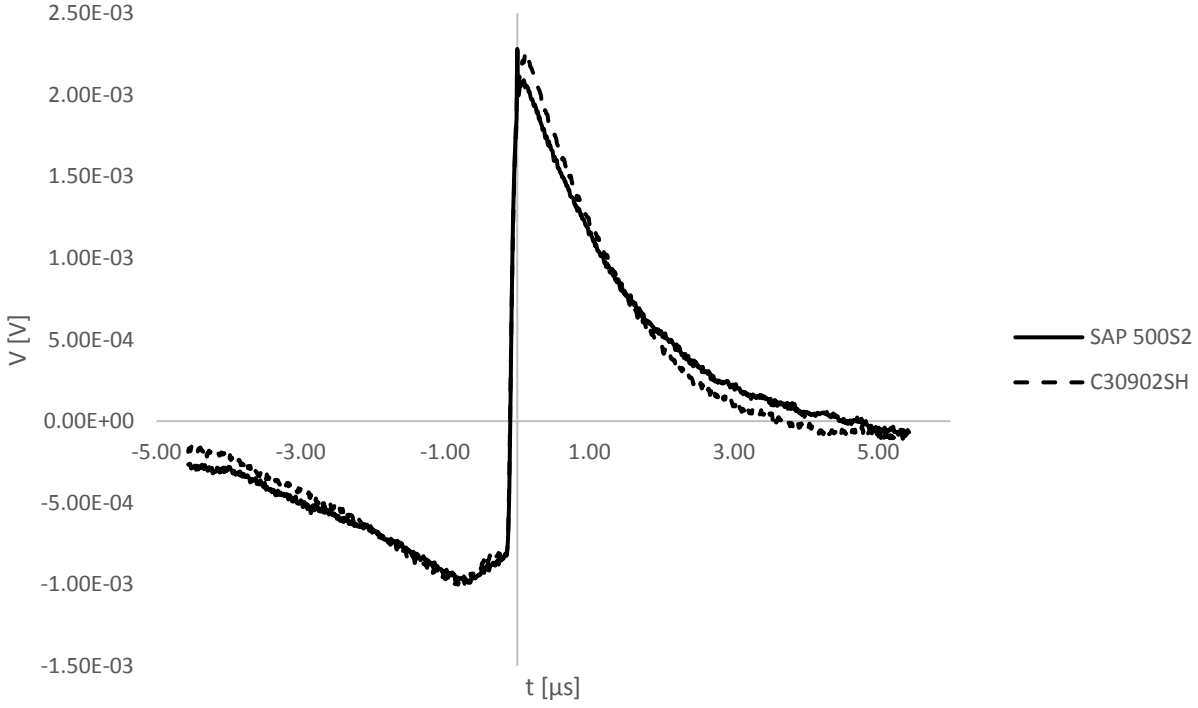

Figure 3-18 Voltage at the input of the comparator

Dark count rate is depicted on Figure 3-19. Dark count rate starts at V_E = 2, because, as mentioned before, pulses at smaller V_E cannot be detected by the comparator. Dark count rate is similar to that in Figure 3-14 as expected, because the changes made to the circuit should not affect the number of dark counts.

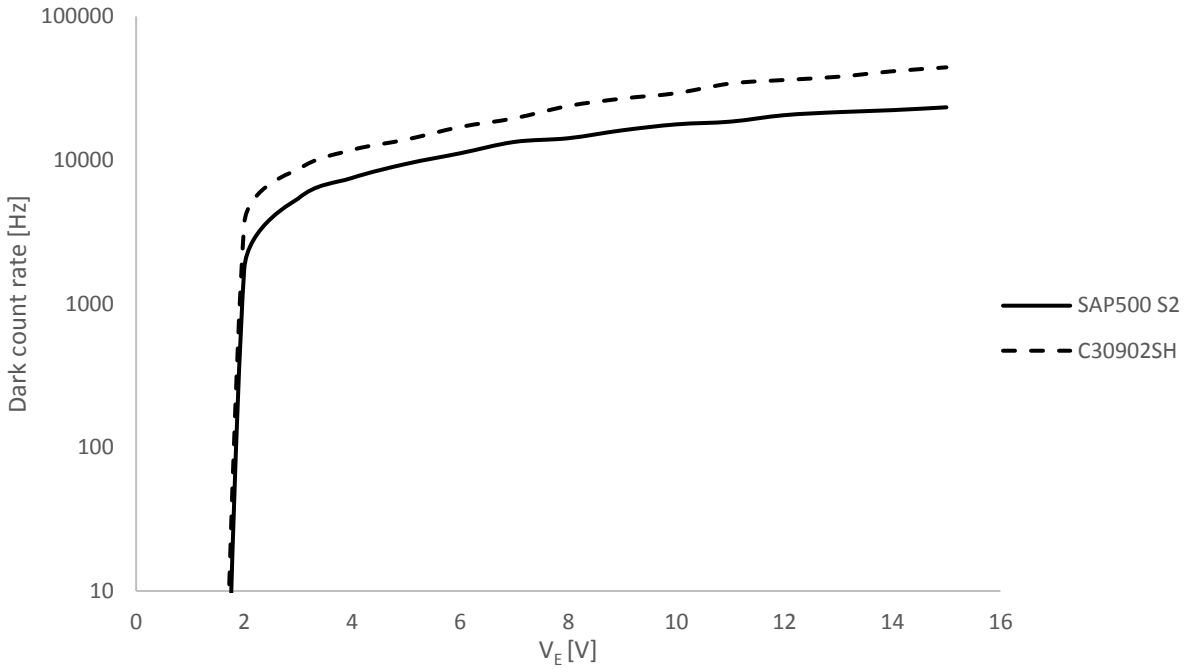

Figure 3-19 Dark count rate vs V_E for passive quenching circuit with resistor at the anode

Inter arrival time histograms for both diodes are shown in Figure 3-20 and Figure 3-21. As expected, graphs look very similar to those in Figure 3-16 and Figure 3-17. Minimum dead time of the circuit did not change (670 – 900 ns). Afterpulsing probability stayed at 0 %.

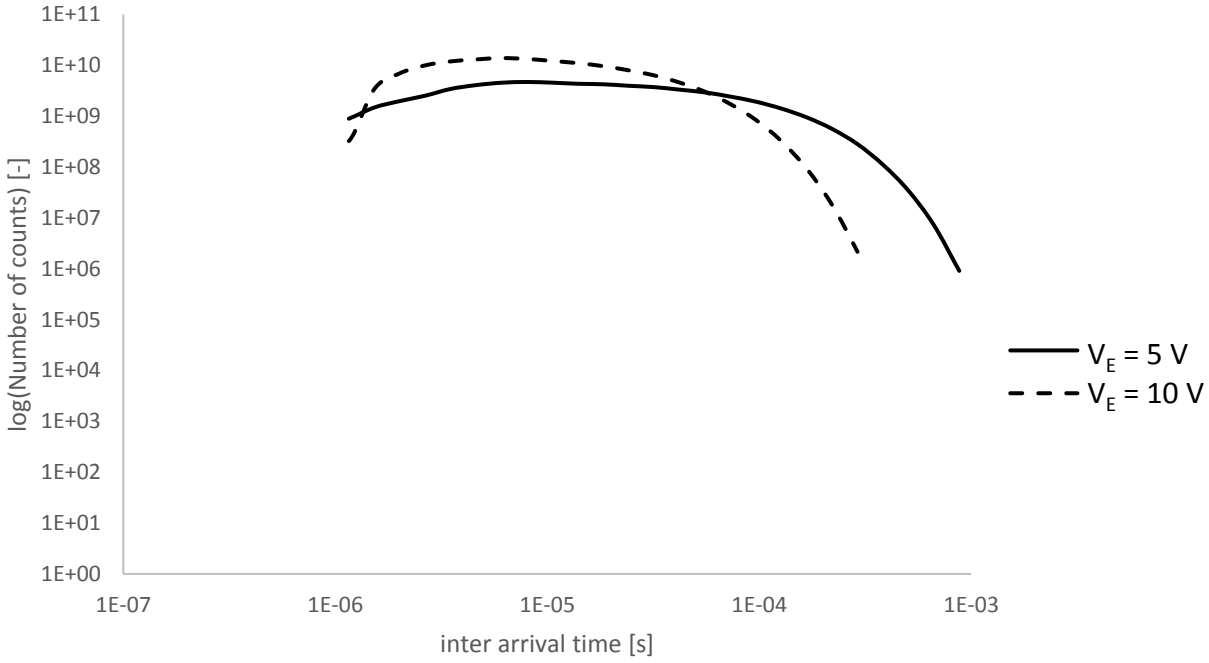

Figure 3-20 Number of counts vs inter arrival time (C30902SH)

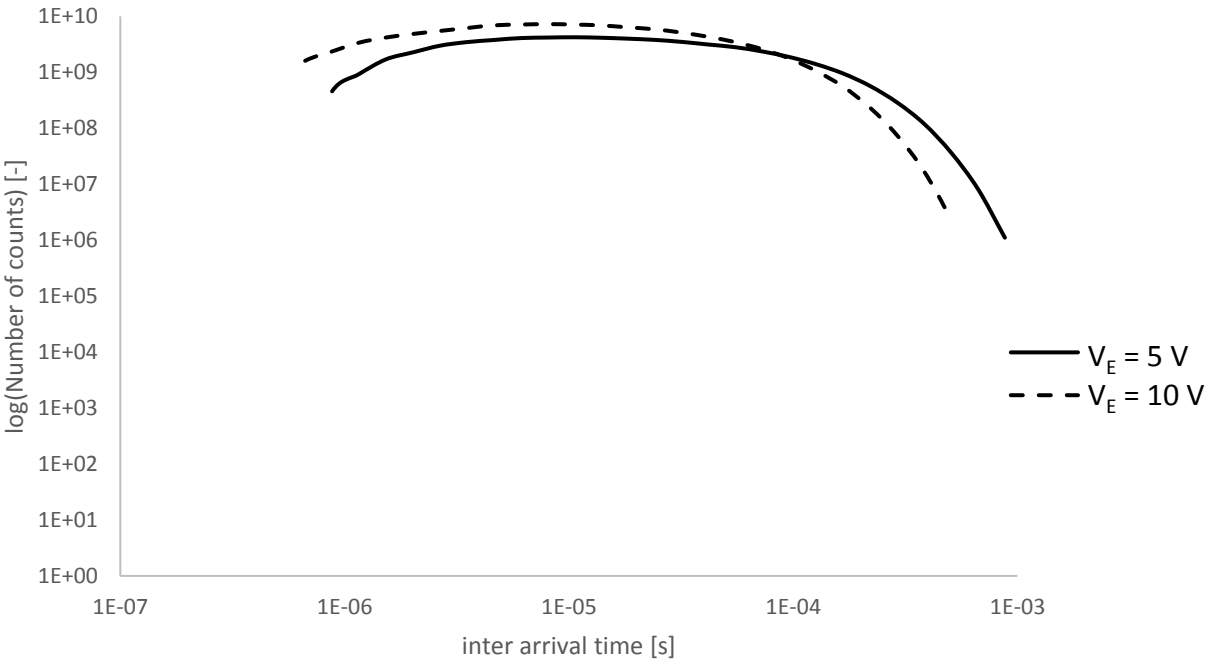

Figure 3-21 Number of counts vs inter arrival time (SAP 300S2)

3.5.3 Active quenching circuit

For the active quenching circuit measurements, upper half of the PCB from the Figure 3-11; R2 was no soldered as well as R6 and R1 and R2 were 0 Ω. Quenching time, which could be chosen with 0 Ω resistor soldered to one of R15, R16, R18, R19 or R20 places. Quench time of 10 ns proved to be long enough to successfully quench the avalanche and hence R16 was soldered.

Dark count rate measured for both diodes can be seen in Figure 3-22. It can be seen that for the active quenching circuit it is a little higher than that of a passive quenching circuit: For C30902 SH, dark count rate is 19,744 kHz with passive quenching circuit and 21 kHz for active quenching circuit with 5 V V_E, which is about 6 % higher. This can be explained with afterpulsing on one hand and with the fact that the pulses that happened during the long dead time of the passive quenching circuit have been counted in active quenching circuit on the other. Situation is similar with SAP 300S2: 11,442 kHz for passive and 11,951 kHz for active quenching circuit (4.25 %).

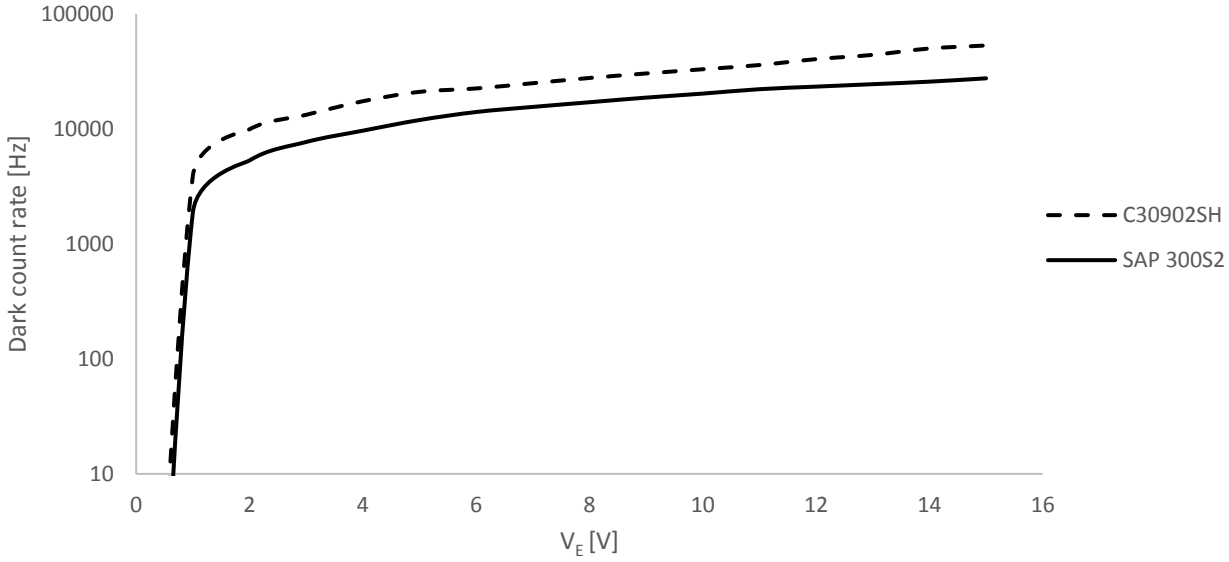

Figure 3-22 Dark count rate vs V_E for the active quenching circuit

Inter arrival time histograms for the active quenching circuit and both diodes are shown in Figure 3-23 and Figure 3-24. The Exponential part of the curve can be clearly distinguished in these histograms. Curves with V_E = 10 and 15 V have been chosen, because there is still very little afterpulsing at 5 V and it cannot be so clearly distinguished. Final graph that compares afterpulsing probability of both diodes can be seen in Figure 3-25. SAP 300S2 has lower afterpulsing probability throughout the whole V_E range. Both didoes perform very well up to V_E = 10 V (afterpulsing below 1%). At V_E = 15 V, afterpulsing probability for C30902SH is 8.41% and for SAP 300S2 6.14%.

From the Figure 3-23 and Figure 3-24 can be read that the deasd time of the active quenching circuit is between 73 and 94 ns. To acquire an accurate value, the circuit was connected to an oscilloscope and the dead time of 87 ns was measured.

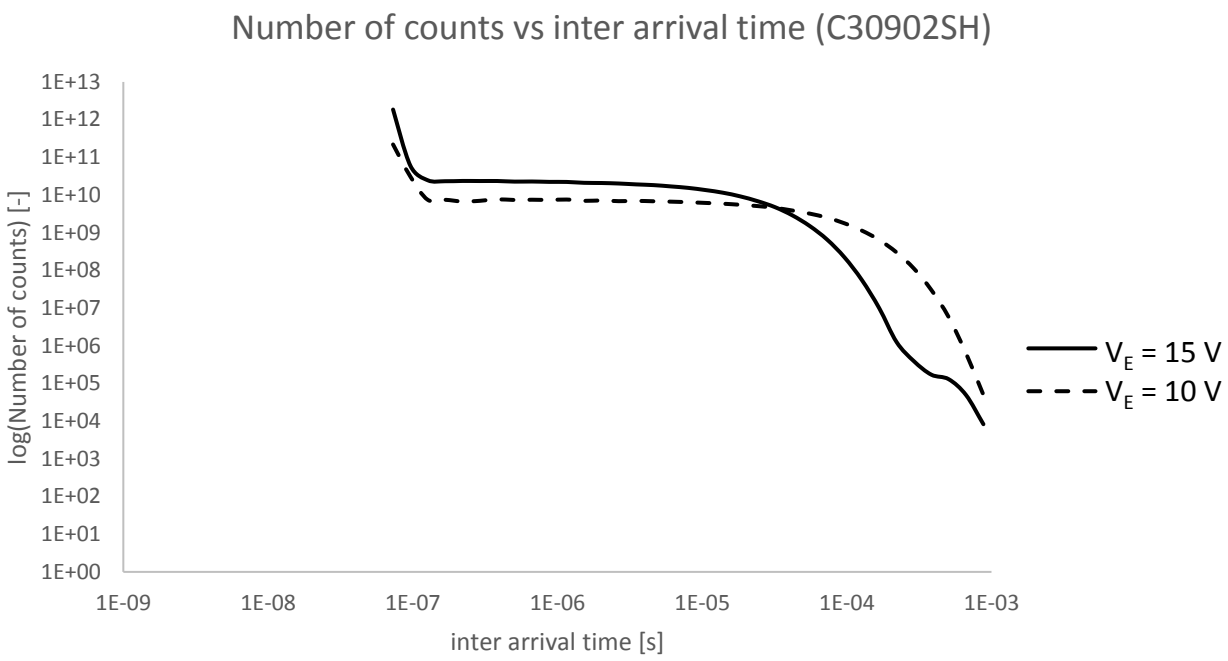

Figure 3-23 Inter arrival time histogram for C30902SH

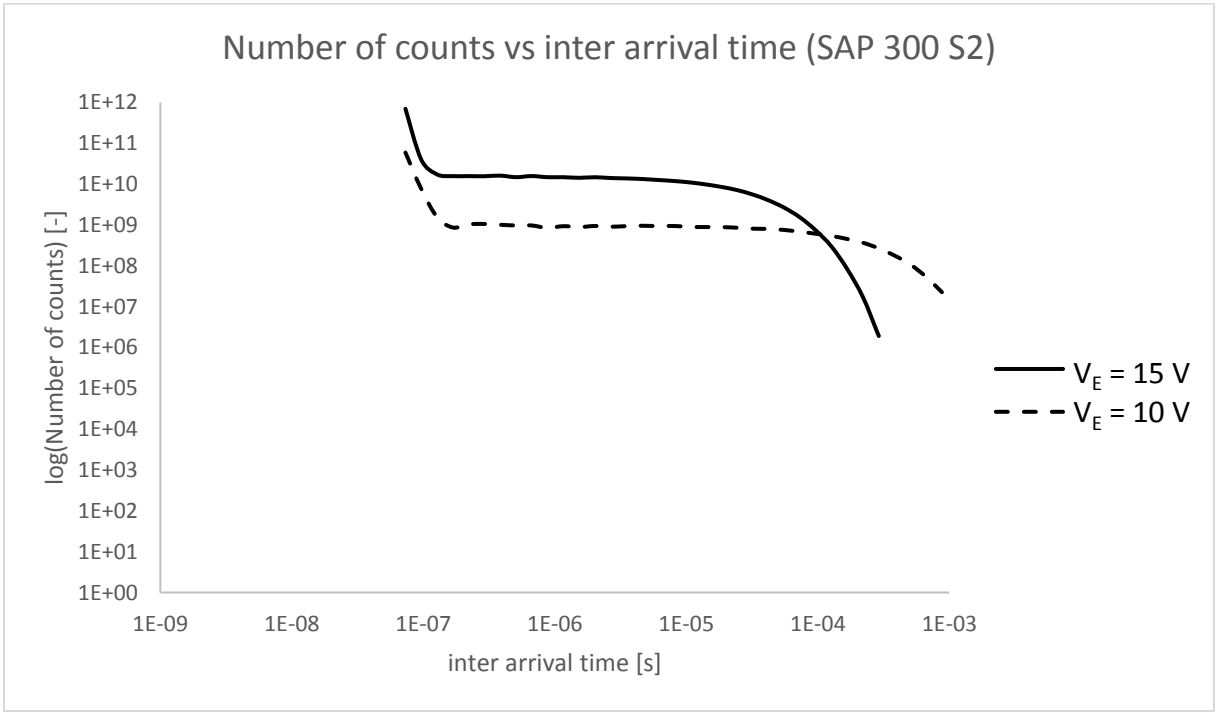

Figure 3-24 Inter arrival time histogram for SAP 300S2

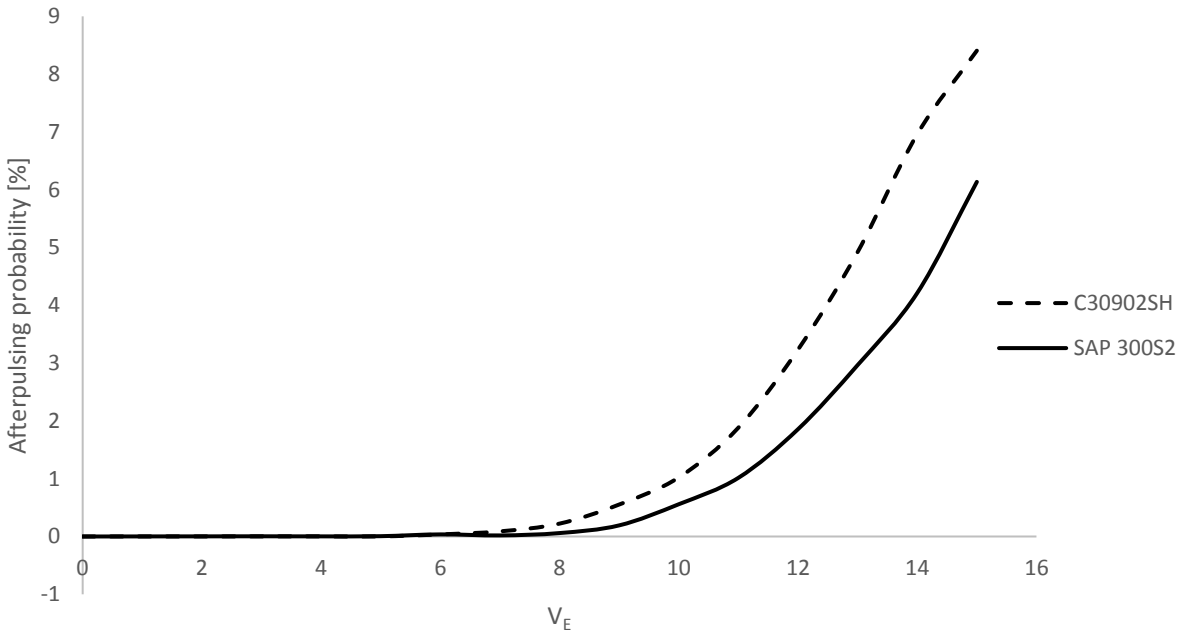

Figure 3-25 Afterpulsing probability in respect to V_E for active quenching circuit

Conclusion

In this work, a summary of available single photon detectors and quenching circuits has been provided. Among the detectors, based on the Table 1-1, single photon avalanche diode has been chosen for its superior performance and availability. Namely, C30902SH from Excelitas and SAP 300S2 from Laser Components. Three quenching circuits, passive quenching circuits with resistors at either cathode or anode and active quenching circuit have been chosen to allow comparison between these two diodes and comparison between the types of quenching circuits as well.

Based on the results from Chapter 3, it has been found out that the SAP 300S2 diode has superior performance in all measured aspects. Compared to C30902SH, it has lower dark count rate at room temperature in the overvoltage range V_E from 0 to 15 V in all three quenching circuits (Figure 3-14, Figure 3-19 and Figure 3-22). At V_E = 5V, measured dark count rate with passive quenching circuit with resistor at the cathode was 11,24 kHz for SAP 300S2 and 19,74 kHz for C30902SH, which is about 43 % higher. Similar differences were measured for the remaining two circuits. Afterpulsing probability was found out to be practically equal to 0 % for both diodes with passive quenching circuits. This was expected, as the afterpulsing in Si diodes ceases to exist after few hundreds of nanoseconds and extremely long dead times of these circuits (almost 1 μs) did not allowed to measure it. As for the active quenching circuit, SAP 300S2 performed better in afterpulsing as well, comparing the value of 6.14 % to 8.41% at V_E = 15V. From Figure 3-13 it can also be seen that SAP 300S2 has a higher avalanche current and produces a higher and narrower voltage pulse at the pick-up resistor.

When the three circuits are compared following can be observed: for applications with low maximal counting rates passive quenching circuit with current limiting resistor at the cathode might be suitable, because it is easy to implement and prevents false counts from afterpulsing. Maximal counting rate of such an application should be kept well below 1 MHz, as the dead time of such a circuit (based on the quenching resistor chosen) was measured to be higher than 700 ns. Passive quenching circuit with quenching resistor at the anode limits the avalanche current, producing a lower voltage peak. This was a problem at V_E = 1V, where the peak could not be detected at all. However, this circuit might be usable with additional logic and a switch that can bypass the resistor and allow the SPAD to be charged much faster, resulting in much smaller dead time. The biggest advantage of the active quenching circuit is the small dead time. A dead time of 87 ns was measured for the circuit that has been realised. It can be further improved by introducing a smaller quenching time and Improving the feedback loop that is used to switch the comparator.

References

[1] M. D. Eisaman, J. Fan, A. Migdall and S. V. Polyakov, “Invited Review Article: Single-photon sources and detectors,” *Review of Scientific Instruments,* Vols. 82, 071101; doi: 10.1063/1.3610677, 2011.

[2] R. H. Hadfield, “Single-photon detectors for optical quantum information applications,” *Nature Photonics,* vol. 230; doi: 10.1038, 2009.

[3] G. Ripamonti and S. Cova, “Carrier diffusion effects in the time-response of a fast photodiode,” *Solid-State Electronics,* vol. 28, no. 9, pp. 925-931, 1985.

[4] D. P. Bertsekas and J. N. Tsitsiklis, Introduction to Probability, Athena Scientific, 2002.

[5] Y. Kang, H. X. Lu, Y. H. Lo, D. S. Bethune and W. P. Risk, “Dark count probability and quantum efficiency of avalanche photodiodes for single-photon detection,” *Applied Physics Letters,* vol. 83, no. 14, pp. 2955-2957, 2003.

[6] S. Cova, A. Lacaita and G. Ripamonti, “Trapping phenomena in avalanche photodiodes on nanosecond scale,” *Electron Device Letters, IEEE,* vol. 12, no. 12, pp. 685-687, 1991.

[7] M. W. Fishburn, Fundamentals of CMOS Single-Photon Avalanche Diodes, Technishe Universiteit Delft, 2012.

[8] B. K. Lubsandorzhiev, “On the history of photomultiplier tube invention,” *Nuclear Instruments and Methods in Physics Research,* vol. 567, pp. 236-238, 2006.

[9] Hamatsu Photonics K. K., Photomultiplier tubes: Basics and applications, Available: https://www.hamamatsu.com/resources/pdf/etd/PMT_handbook_v3aE.pdf, 2007.

[10] Hamatsu Photonics K. K., Photomultiplier tubes, Available: https://www.hamamatsu.com/resources/pdf/etd/PMT_TPMZ0002E.pdf.

[11] R. E. Simon, A. H. Sommer, J. A. Tietjen and B. F. Williams, “New high-gain dynode for photomultipliers,” *Applied Physics Letters,* vol. 13, no. 10, pp. 355-356, 1968.

[12] A. Nevet, A. Hayat and M. Orenstein, “Ultrafast three-photon counting in photomultiplier tube,” *Optics Letters,* vol. 36, no. 5, pp. 725-727, 2011.

[13] G. N. Gol'tsman, O. Okunev, G. Chulkova, A. Lipatov, A. Semenov, K. Smirnov, C. Williams and R. Sobolewski, “Picosecond superconducting single-photon optical detector,” *Applied Physics Letters,* vol. 79, no. 6, pp. 705-708, 2001.

[14] C. M. Natarajan, M. G. Tanner and R. H. Hadfield, “Superconducting nanowire single-photon detectors: physics and applications,” *Superconductor Science and Technology,* vol. 25, 2012.

[15] M. A. Albota and F. N. C. Wong, “Efficient single-photon counting at 1.55 μm by means of frequency upconverison,” *Optics letters,* vol. 29, no. 13, pp. 1449-1451, 2004.

[16] B. E. Kardynal, A. J. Shields, N. S. Beattie, I. Farrer, K. Cooper and D. A. Ritchie, “Low-noise photon counting with a radio-frequency quantum-dot field-effect transistor,” *Applied physics letters,* vol. 84, no. 3, pp. 419-421, 2004.

[17] H. W. Li, B. E. Kardynal, P. See, J. Shields, P. Simmonds, H. E. Beere and D. A. Ritchie, “Quantum dot resonant tunneling diode for telecommunication wavelength single photon detection,” *Applied physics letters,* vol. 91, 2007.

[18] K. F. Brennan, J. I. Haralson, J. W. Parks and A. Salem, “Review of reliability issues of metal-semiconductor-metal and avalanche photodiode photonic detectors,” *Microelectronics Reliability,* vol. 39, pp. 1873-1883, 1999.

[19] M. Teich, K. Matsuo and B. Saleh, “Time and frequency response of the conventional avalanche photodiode,” *IEE Trans Electron Devices,* vol. 33, pp. 1511-1517, 1986.

[20] A. Goetzberger, B. McDonald, R. H. Haitz and R. M. Scarlett, “Avalanche Effects in Silicon p—n Junctions,” *Journal of Applied Physics,* vol. 34, p. 1591, 1963.

[21] A. Lacaita, M. Ghioni and S. Cova, “Double epitaxy improves single-photon avalanche diode performance," *Electronics letters,* vol. 25, no. 13, pp. 841-843, 1989.

[22] H. Dautet, P. Deschamps, B. Dione, A. D. MacGregor, D. MacSween, R. J. McIntyre, C. Trottier and P. Webb, “Photon counting techniques with silicon avalanche photodiodes,” *Applied Optics,* vol. 32, no. 21, pp. 3894-3901, 1993.

[23] A. Lacaita, P. A. Francese, F. Zappa and S. Cova, “Single-photon deteciton beyond 1μm: performance of commercially available germanium photodiodes,” *Applie Optics,* vol. 33, no. 30, pp. 6902-6919, 1994.

[24] A. Lacaita, F. Zappa, S. Cova and P. Lovati, “Single-photon detection beyond 1μm: performance of commercially available InGaAs/InP detectors,” *Applied Optics,* vol. 35, no. 16, pp. 2986-2997, 1996.

[25] S. Cova, M. Ghioni, A. Lotito, I. Rech and F. Zappa, “Evolution and prospects for single-photon avalanche diodes and quenching circuits,” *Journal of Modern Optics,* vol. 51, no. 9-10, pp. 1267-1288, 2004.

[26] S. Donati, Photodetectors: Devices, Circuits and Applications, Prentice Hall, 2000.

[27] “http://jp.hamamatsu.com/resources/products/etd/pdf/m-h7422e.pdf.,” [Online].

[28] “http://jp.hamamatsu.com/resources/products/etd/pdf/NIR-PMT_APPLI_TPMO1040E02.pdf,” [Online].

[29] “http://optoelectronics.perkinelmer.com/content/RelatedLinks/SpecificationSheets/SPC_PhotoDetectors.pdf.,” [Online].

[30] “http://www.microphotondevices.com/products_pdm.asp.,” [Online].

[31] C. Gobby, Z. L. Yuan and Shields, “Quantum key distribution over 122 km of standard telecom fiber,” *Applied Physics Letters,* vol. 84, pp. 3762-3764, 2004.

[32] A. Dixon, Z. L. Yuan, J. F. Dynes, A. W. Sharpe and A. J. Shields, “Gigahertz decoy quantum key distribution with 1Mbit/s secure key rate,” *Optics Express,* vol. 16, pp. 18790-18797, 2008.

[33] H. e. a. Takesue, “Differential phase shift quantum key distribution experiment over 105 km fibre,” *New Journal of Physics,* vol. 7, pp. 232-243, 2005.

[34] W. E. Moerner and D. P. Fromm, “Methods of single-molecule fluorescence spectroscopy and microscopy,” *Reviews of Scientific Instruments,* vol. 74, no. 8, pp. 3597-3620, 2003.

[35] E. B. Shera , N. K. Seitzinger, L. M. Davis, R. A. Keller and S. A. Soper, “Detection of single fluorescent molecules,” *Chemical Physics Letters,* vol. 174, no. 6, pp. 553-557, 1990.

[36] L. Li-Quiang and L. M. Davis, “Single photon avalanche diode for single molecule detection,” *Review of Scientific Instuments,* vol. 64, no. 6, pp. 1524-1531, 1993.

[37] M. Vitali, D. Bronzi, A. J. Krmpot, S. N. Nikolic, F.-J. Schmitt, C. Junghans , S. Tisa, T. Friedrich, V. Vukojevic, L. Terenius , F. Zappa and R. Rigler, “A Single-Photon Avalanche Camera for Fluorescence Lifetime Imaging Microscopy and Correlation Spectroscopy,” *IEEE Journal of Selected Topics in Quantum Electronics,* vol. 20, no. 6, pp. 3804010 - 3804020, 2014.

[38] S. Tisa, F. Villa, A. Giudice, G. Simmerle and F. Zappa, “High-speed quantum random number generation using CMOS photon counting detectors,” *IEEE Journal of Selected Topics in Quantum Electronics,* vol. 21, no. 3, 2015.

[39] A. Gallivanoni , I. Rech and M. Ghioni, “Progress in Quenching Circuits for Single Photon Avalanche Diodes,” *IEEE Transactions on Nuclear Science,* vol. 57, no. 6, pp. 3815-3826, 2010.

[40] C. Niclass, M. Gersbach, R. Henderson, L. Grant and E. Charbon, “A single photon avalanche diode implemented in 130-nm CMOS technology,” *IEEE J. Sel. Topics Quantum Electron,* vol. 13, no. 4, pp. 863-869, 2007.

[41] S. Cova, M. Ghioni, A. Lacaita, C. Samori and F. Zappa, “Avalanche photodiodes and quenching circuits for single-photon detection,” *Applied Optics,* vol. 35, no. 12, pp. 1956-1976, 1996.

[42] A. Rochas , M. Gösch, A. Serov, P. A. Besse, R. S. Popovis, T. Lasser and R. Rigler, “First fully integrated 2-D array of single-photon detectors in standard CMOS Technology,” *IEEE Photonics Technology Letters,* vol. 15, no. 7, pp. 963-966, 2003.

[43] M. Liu, C. Hu, J. C. Campbell, Z. Pan and M. M. Tashima, “Reduce afterpulsing of single photon avalanche diodes using passive quenching with active reset,” *IEEE Journal of quantum electronics,* vol. 44, no. 5, pp. 430-435, 2008.

[44] S. Cova, A. Longoni and G. Ripamonti, “Active-quenching and gating circuits for single-photon avalanche diodes(SPADs),” *IEEE Transactions on Nuclear Science,* vol. 29, no. 1, pp. 599-601, 1982.

[45] M. Stipcevic, “Active quenching circuit for single-photon detection with Geiger mode avalanche photodiodes,” *Applied Optics,* vol. 48, no. 9, pp. 1705-1714, 2009.

[46] G. Acconia, I. Rech, A. Gulinatti and M. Ghioni, “High-voltage integrated active quenching circuit for single photon count rate up to 80 Mcounts/s,” *Optics express,* vol. 24, no. 16, pp. 17819-17831, 2016.

[47] A. Gallivanoni, I. Rech, D. Resnati, M. Ghioni and S. Cova , “Monolithic active quenching and picosecond timing circuit suitable for large-area single-photon avalanche diodes,” *Optics Express,* vol. 14, no. 12, pp. 5021-5030, 2006.

[48] D. Mosconi, D. Stoppa, L. Pancheri, L. Gonyo and A. Simoni, “CMOS single-photon avalanche diode array for time-resolved fluorescence detection,” *Solid-State Circuits Conference,* pp. 564-567, 2006.

[49] S. Bellis, R. Wilcock, C. Jackson, SensL Technologies Ltd and Lee House Riverview Business Park, “Photon counting imaging: the DigitalAPD,” *Proceedings of SPIE-IS&T Electronic Imaging: Sensors, Cameras, and Systems for Scientific Applications,* vol. 6068, 2006.

[50] J. Richardson, R. Henderson and D. Renshaw, “Dynamic Quenching for Single Photon Avalanche Diode Arrays,” *International Image Sensor Workshop,* pp. 258-260, 2007.

[51] R. Mita and G. Palumbo, “High-speed and compact quenching circuit for single-photon avalanceh diodes,” *IEEE Transactions on Instrumentation and Measurement ,* vol. 57, no. 3, pp. 543-548, 2008.

[52] S. Tisa, F. Guerrieri and F. Zappa, “Variable-load quenching circuit for single photon avalanche diodes,” *Optics Express,* vol. 16, no. 3, pp. 2232-2245, 2008.

[53] S. J. Dimler, J. S. Ng, R. C. Tozer, G. J. Rees and J. P. David, “Capacitive quenching measurement circuit for geiger-mode avalanche photodiodes,” *IEEE Journal of Selected Topics in Quentum Electronics,* vol. 13, no. 4, pp. 919-926, 2007.

[54] N. Nakameta, S. Sasamori and S. Inoue, “800 MHz Single photon detection at 1550 nm using InGaAs/InP avalanche photodiode operated with a sine wave gating,” *Optics Express,* vol. 14, no. 21, pp. 10043-10050, 2006.

[55] Excelitas, “C30902 and C309021 Series Datasheet”.

[56] L. Components, “SAP500 Datasheet”.

[57] M. Stipcevic, D. Wang and R. Ursin, “Characterization of a commercially available large area, high detection efficiencz single-photon avalanche diode,” *Journal of Lightwave Technology,* vol. 31, no. 23, pp. 3591-3597, 2013.

[58] S. Tisa, F. Zappa, A. Tosi and S. Cova, “Electronics for single photon avalanche diode arrays,” *Sensors and Actuators,* vol. 140, pp. 113-122, 2007.

[59] F. Zappa, A. Tosi, A. D. Mora and S. Tisa, “SPICE modeling of a single photon avlanche diodes,” *Sensors and Actuators A: Physical,* vol. 153, pp. 197-204, 2009.

[60] M. Stipcevic, B. G. Christensen, P. G. Kwiat and D. J. Gauthier, “Advanced active quenching circuits for single-photon avalanche photodiodes,” *Proc. of SPIE,* vol. 9858, 2016.

[61] M. W. Fishburn, “Fundamentals of CMOS ingle-Photon Avalanche Diodes,” 2012.

[62] J. P. Sprengers and et al, “Waveguide superconducting single-photon detectors for integrated quantum photonic circuits,” *Applied Physics Letters,* vol. 99, no. 11, 2011.

[63] F. Zappa, A. Lotito, A. C. Giudice, S. Cova and M. Ghioni, “Monolithic Active-Quenching and Active-Reset Circuit for Single-Photon Avalanche Detectors,” *IEEE Journal of Solid State Circuits,* vol. 38, no. 7, pp. 1298-1302, 2003.

[64] J. R. Meilink, C. Veerappan, S. Seifert, D. Stoppa, R. Henderson, E. Charbon and D. R. Schaart, “First measurement of scintillation photon arriaval statistics using a high-granularity solid-state photosensor enabling time-stamping of up to 20 480 single photons,” *IEEE Nuclear Science Symposium Conference Record (NSS/MIC),* pp. 2254-2257, 2011.

Appendix A: PCB layout

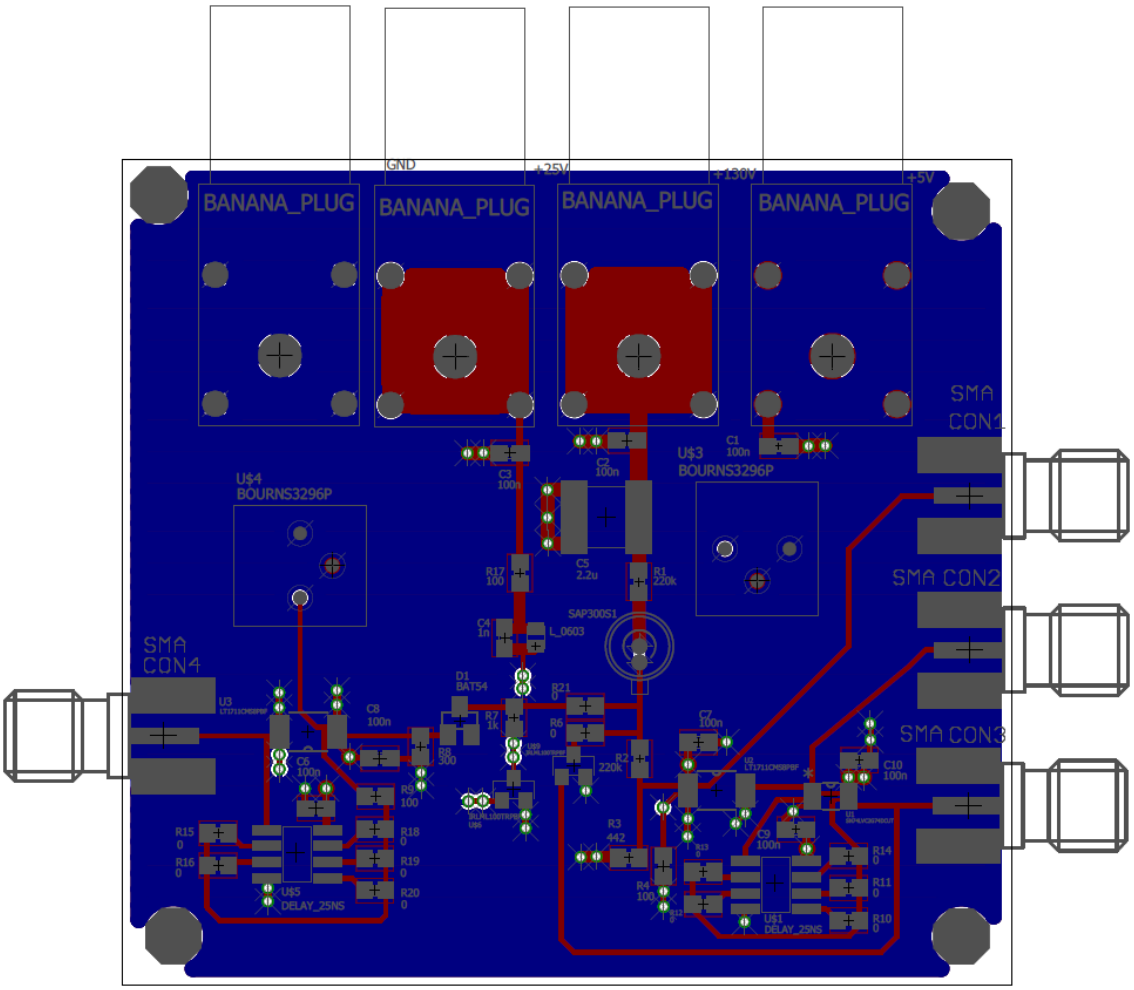

Figure 0-1 Layout of the PCB with all layers